Excitons: From excitations at surfaces to confinement in nanostructures

Gregorio H. Cocoletzi [a,1] and W. Luis Mochán [b,2]

[a] *Instituto de Física, Universidad Autónoma de Puebla, Apartado Postal J-48, Puebla 72570, México*

[b] *Centro de Ciencias Físicas, Univerisdad Nacional Autónoma de México, Apartado Postal 48-3, 62251 Cuernavaca, Morelos, México*

Abstract

We present a review of optical properties of excitonic semiconductors. We consider the interaction of light with surfaces, thin films, multilayered systems, small particles and rough surfaces accounting for excitonic transitions. The first part of the paper is devoted to studies done using classical electrodynamics within the nonlocal dielectric response theory. For the dielectric function we take the Hopfield and Thomas coupled harmonic oscillator model, which yields excitonic modes beyond the usual optical waves. Therefore, studies of the coupling of light to exciton-polaritons in the presence of surfaces require additional boundary conditions (ABC's) to determine the reflected and transmitted electromagnetic field amplitudes within models of abruptly terminated semiconductors. An alternative consisting in solving Maxwell's equations for the electromagnetic field together with an equation for the excitonic polarization derived from the quantum mechanical dynamics of electrons and holes, including a surface potential that accounts for the interaction of excitons with the surface is explored in the latter part of the paper. The surface potential may be modeled by an infinite barrier, or by smooth repulsive exponential potentials and Morse-type potential wells. Surface potential wells may produce entrapped excitonic states, which are explored at surfaces, films and superlattices. Scattering of light from non-ideal rough surfaces is also discussed. Comparison between theory and experiment is emphasized all along the paper. The final section is devoted to a microscopic theory which is ABC independent and explains the experimental measurements of transmission in thin films.

Key words: Excitons, Polaritons, Excitonic Polarization, Additional Boundary Conditions, Surfaces, Films, Multilayers, Superlattices, Dielectric Response, Optical Response, Reflectance, Transmitance, Surface Modes, Surface Potential, Transfer Matrix, Microcavities, Entrapped States, Microscopic Theory.
PACS: pacs, pacs

Preprint submitted to Surface Science Reports *30 November 2004*

Contents

1 Introduction 4

2 Excitons 7

3 Bulk Optical Response 10

3.1 Spatial Dispersion 10

3.2 Non Locality of the Excitonic Response 11

3.3 Exciton-polariton 12

4 Surface Optical Response 15

4.1 Additional Boundary Conditions (ABC) 15

4.2 Reflectance 16

4.3 Surface Modes 20

4.4 Attenuated total reflectivity (ATR) 22

5 Interaction with surfaces 24

5.1 Semiinfinite systems 25

5.2 Surface potential for excitons 26

5.3 Surface potential for the excitonic polarization 27

6 Thin Film 31

6.1 S-polarization 31

6.2 P-polarization 33

7 Entrapped states 35

8 Layered systems 39

8.1 Transfer matrix for S-polarization 39

8.2 Transfer matrix for P-polarization 41

---

[1] Partially supported by SEP-CONACyT PROADU grant No. 2003-01-21-001-051 and CONACyT-VIEP-BUAP grant No. II010G02.

[2] Partially supported by DGAPA-UNAM under grant IN117402

8.3 Transfer matrix collapse 43

8.4 Superlattice normal modes 44

8.5 Entrapped states in superlattices 48

8.6 Optical response of microcavities 49

9 Scaterring of light by small excitonic particles 52

9.1 Spheres 52

9.2 Cylinders 55

10 Scattering of light from non ideal surfaces 59

11 Microscopic theory of optical properties 68

12 Concluding remarks 73

References 75

1 Introduction

Although the study of the optical properties of excitons can be traced back to the 1950's, they form currently an active area of research. The concept of excitons was first introduced by Frenkel [1], Peierls [2] and Wannier [3]. A few years later, Pekar [4] showed that when light waves with frequencies close to those of resonant absorption of light reaches some crystals, unusual refraction takes place. Due to the interaction of light with a crystal, he observed several waves of the same frequency and polarization, but with different index of refraction. This phenomenon differs from double refraction of light and occurs even in isotropically (cubic) polarizing crystals. In addition, strictly longitudinal electric waves were also excited in the crystal.

Pekar introduced [4] the concept of additional boundary conditions (ABC's) in order to arrive at a complete set of equations capable of determining the amplitude of the additional waves transmitted within excitonic media. Hopfield and Thomas [5] developed a formalism to calculate the optical response of semiconductor surfaces, taking Pekar ABC's and allowing for an exciton-free surface layer, known as the dead layer. Pekar ABC's establish that the excitonic polarization vanishes at the semiconductor surface. To deal with excitonic media the classical local dielectric theory was reformulated by introducing a non-local dielectric response. The model proposed by Hopfield and Thomas [5] consists of coupled harmonic oscillators, which yield a dielectric response dependent on the angular frequency of light and the wave vector of the excitonic modes. A system whose dielectric function depends on wavevector besides being frequency dependent is called spatially dispersive or nonlocal.

After Pekar's ABC's, several models have emerged, several of which were summarized by Halevi and Fuchs [6,7] in the so-called generlized ABC's. As particular cases we mention the ABC's of Pekar [4,8], Fuchs-Kliewer [9], Rimbey-Mahan [10], and Agarwal-Pattanayak-Wolf [11]. A long enduring debate has been establish on the question of the correct ABC's, with Pekar's condition being the one that seems to yield better results when compared with experiment. On the other hand, inhomogeneous additional boundary conditions have been suggested by Sel'kin et al. [12], which account for the polarization current at the interface between the excitonic active medium and the surface transition layer or dead layer.

There are many studies of light propagation in semiinfinite systems [4–6,8,13–33] and in multilayered media such as thin films, microcavities and periodic superlattices [34–56], as well as in dielectric spheres and cylinders. Most calculations have employed ABC's, as the boundary conditions of electromagnetic origin are insufficient to solve the problem of reflection and refraction of light.

An alternative to introduction of ABC's in the study of excitons at surfaces is the solution of the equations of motion of the exciton in the presence of an interaction potential [30] . This potential has contributions from the image charges of the electron and hole, produced at the surface of the semiconductor, which lead to a repulsive interaction [7], although impurities and defects at the surface can produce atractive potentials that may even trap excitons at the surface [57,46].

Coupling of light with surface excitons has received considerable attention in the literature [13,18,58,28,33]. Experimentally surface exciton polaritons have been excited and detected using the attenuated total reflection (ATR) arrangement. In the ATR geometry, a prism of constant index of refraction is used to increase the wave vector of the incident light, in order to allow its coupling with surface excitons. The exponential evanescent light wave tunnels through the air gap between the prism and the surface active excitonic medium, and couples with the exciton polariton that propagate along the surface of the semiconductor. Using this technique, Lagois [58] was able to observe the A1, B1 and C1 excitonic transitions using ZnO. Because of spatial dispersion, surface excitons coexist with bulk modes in the frequency region between the transverse and longitudinal resonance frequencies.

Surface excitons have been also investigated on rough surfaces [59–64]. Results of the study of light scattering by non flat surfaces shows the possiblility of roughness coupling of light to surface modes. In this case, the momentum of light is increased by that provided by the rough surface.

Tough most of the exciton polariton studies have used the reflectance of light, other techniques are also available, such as photoluminiscence [65,66], inelastic Raman and Brillouin scattering [67–74], and elastic Rayleigh scattering [75].

In recent years, microscopic theories have emerged for the study of polaritons in semiconductors. Muljarov et al. [76] developed a method based on microscopic boundary conditions, to explore optical properties of exciton polaritons accounting for spatial dispersion. Their approach may be applied to arbitrary electron-hole interaction potential and probed through one-dimensional contact interactions in half-space and slab geometries. Comparisons with ABC based calculations show how crucial the appropiate selection of boundary conditions is for the correct computation of the optical spectra. Electron-hole excitations and optical spectra calculations using first principles were reported [77] recently, describing the excitations of the electronic system through the use of one-, and two-particle Green's function. The computational method combines the local denstiy approximation for the electronic ground state, the single particle spectrum of the electrons and holes as determined according to the GW approximation [78] to the electron self-energy operator, and finally an account of the electron-hole interaction.

First principles studies [79] were developed to investigate optical properties of semiconductors accounting for local-field effect and excitons. Calculations employ Hedin's [78] GW approximation (GWA), based on the all-electron full potential augmented plane wave method. The formalism has been applied to obtain the optical properties of small-, medium-, and large-band gap semiconductors. Comparisons with experiment have been carried out for Si and diamond. When local field effects are neglected the theoretical curves deviate from exeperiment, while good agreement has been found when local field effects are included. Moreover, frequently the local density approximation (LDA) fails to yield good results as compared with experiment. Marini et al. [80] has developed studies of bound excitons using time-dependent density-functional theory (TDDFT). Formulae of the optical and energy-loss spectra were derived using a frequency dependent and non local exchange correlation function within the TDDFT. Theoretical results, including local field effects, have been compared with experiment for LiF, SiO_2 and diamond finding good agreement.

2 Excitons

Consider a transition of an electron from the valence band to the conduction band of a semiconductor, probably induced by the absorption of a photon. The excited electron leaves behind a hole in the valence band, which behaves as a positive charge carrier. The electron interacts with the hole through a screened Coulomb potential and may therefore form bound states. The resulting bound electron-hole pairs are known as *excitons*. The presence of excitons induces strong effects in the optical properties of semiconductors. They manifest themselves as resonant peaks in the absorption, reflection and luminescence spectra correspondig to transitions to or from discrete bound states, and as shifts of the main spectral features due to the electron-hole interaction.

The first theories of excitons were formulated by Frenkel [1], Peierles [81], and Wannier [3] in the decade of 1930's. Since then, two different kinds of excitons have been identified: those where the electron-hole separation is large and those where it is small compared to the lattice parameter. Correspondingly, the studies of optical properties of semiconductors accounting for excitonic transitions have adopted two main approaches known as the Wannier-Mott and Frenkel theories. In this report we will be concerned with the Wannier-Mott excitons, that is, the electron-hole bound states with large effective Bohr radius.

Consider the bulk of a semiconductor and assume that one can approximate its band structure by a two-band model. In this approximation the effective mass Schrödinger equation for the Wannier-Mott excitons has the form [82]

$$\left[\frac{p_e^2}{2m_e} + \frac{p_h^2}{2m_h} - \frac{e^2}{\epsilon r} + E_g\right] \Psi(\vec{r}_e, \vec{r}_h) = E\Psi(\vec{r}_e, \vec{r}_h). \tag{1}$$

The first two terms are the kinetic energy operators of the electron and hole whose effective masses are m_e and m_h in the conduction and valence bands, respectively. The third term represents the Coulomb interaction between the electron and hole, screened by the static dielectric function ϵ, $-e$ is the electron charge, r is the electron-hole separation distance. The fourth term is simply the energy required to create an electron at the bottom of the conduction band and a hole at the top of the valence band, separated from each other by an energy gap E_g. The eigenvalue E is the total energy of an exciton described by the wavefunction $\Psi(\vec{r}_e, \vec{r}_h)$ which depends on the positions $\vec{r}_e$, $\vec{r}_h$ of both the electron and hole. Since the Coulomb term only affects the relative electron-hole coordinates, it is convenient to define the center of mass position,

$$\vec{R} \equiv \frac{m_e\vec{r}_e + m_h\vec{r}_h}{M}, \tag{2}$$

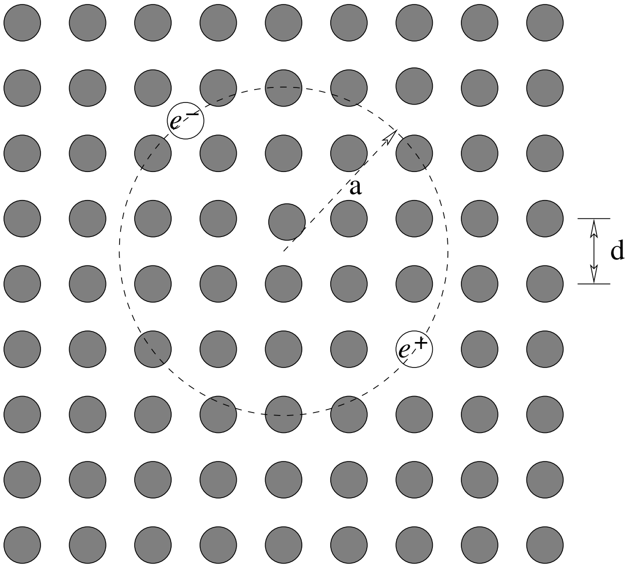

Fig. 1. An exciton is an electron-hole pair (empty circles) bound to each other through their screened Coulomb interacion, but free to move together through the crystal. The exciton shown is a Wannier-Mott exciton, with a radius a larger than the separation between atoms (filled circles).

and relative coordinate,

$$\vec{r} = \vec{r}_e - \vec{r}_h, \tag{3}$$

with $M = m_e + m_h$ the total excitonic mass. The Schrödinger equation can then be rewritten as

$$\left[\frac{P^2}{2M} + \frac{p^2}{2\mu} - \frac{e^2}{\epsilon r}\right]\Psi(\vec{r},\vec{R}) = (E - E_g)\Psi(\vec{r},\vec{R}). \tag{4}$$

Here, $\vec{P} = -i\hbar\nabla_R$ is the total momentum, $\vec{p} = -i\hbar\nabla_r$ is the relative momentum and $\mu = m_e m_h/M$ is the reduced mass of the electron-hole pair. As this modified Schrödinger equation has no dependence on $\vec{R}$, $\vec{P}$ is conserved and $\Psi(\vec{r},\vec{R})$ may be factorized as

$$\Psi(\vec{r},\vec{R}) = \frac{1}{\sqrt{V}} e^{i\vec{q}\cdot\vec{R}}\phi(\vec{r}), \tag{5}$$

where the igenvalue $\hbar\vec{q}$ of $\vec{P}$ is a good quantum number that describes the uniform motion of the center of mass of the exciton and the wavefunction ϕ

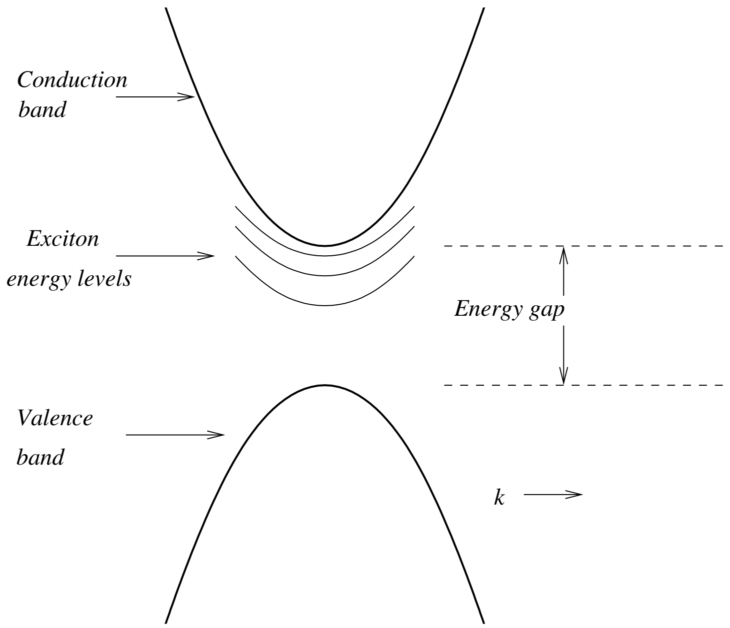

Fig. 2. Exciton levels in relation to the conduction band edge, for a simple band structure with both conduction and valence band edges at $q = 0$. The curvature of the exciton levels is due to their translational kinetic energy.

describes the relative motion of the electron and hole around their center of mass. The substitution of this wave function in the Schrödinger equation (4) yields a hydrogen-like equation

$$\left[\frac{p^2}{2\mu} - \frac{e^2}{\epsilon r}\right] \phi_{nlm}(\vec{r}) = E_n \phi_{nlm}(\vec{r}), \tag{6}$$

whose solutions are hydrogenic functions ϕ_{nlm} with energy levels

$$E_n = -\frac{\mu e^4}{2\hbar^2 \epsilon^2 n^2}, \tag{7}$$

corresponding to the principal quantum number n, the angular momentum l, and its projection m. Therefore we obtain

$$E = E_g + E_n + K, \tag{8}$$

where $K = \hbar^2 q^2/(2M)$ is the kinetic energy associated with the center of mass motion. The effective Bohr radius of the exciton $a_0 = \epsilon\hbar^2/\mu e^2$ is of the order of 100Å for typical semiconductors [83], justifying *a posteriori* the screening of the Coulomb interaction in Eq. (1) through a macroscopic dielectric response ϵ. Correspondingly, the effective Rydberg energy $E_1 \sim 5$meV.

3 Bulk Optical Response

As described above, an exciton is an electron-hole pair bound to each other by Coulomb forces and it displays an hydrogenic spectrum. As the electron and hole are both charged elementary excitations of a semiconductor, the exciton is able to couple strongly to light. This coupling may be described through the dielectric function of the excitonic semiconductor and, together with Maxwell's equations for the electromagnetic field yields excitations which have both an excitonic and a photonic contribution, known as exciton-polaritons. It is known that the dielectric response ϵ of arbitrary quantum systems is well described by a weighted sum of harmonic oscillator response functions, with resonance frequencies corresponding to the transition energies, and oscillator strengths depending on the wavefunctions of the initial and final states involved in the corresponding transitions. For frequencies ω very close to a resonant transition frequency ω_0 the dielectric function may be written as [7]

$$\epsilon(\omega) = \epsilon_\infty + \frac{\omega_p^2}{\omega_0^2 - \omega^2 - i\nu\omega}, \tag{9}$$

where ω_p^2 is a measure of the strength of the transition, ν is a phenomenological damping constant, and ϵ_∞ is a background dielectric constant that accounts for the contribution to the response from the other transitions, farther away from ω than ω_0, and which therefore varies relatively slowly with frequency.

As $\epsilon(\omega)$ depends on frequency, its Fourier transform $\epsilon(t - t')$ depends on the elapsed time between the excitation of the system by an electric field at time t' and the observation of the displacement field at time t, that is,

$$\vec{D}(t) = \int_{-\infty}^{\infty} dt'\, \epsilon(t - t')\vec{E}(t'). \tag{10}$$

Causality implies that $\epsilon(t - t') = 0$ whenever $t < t'$.

3.1 Spatial Dispersion

As the electric and displacement fields vary in general with position $\vec{r}$, as well as varying on time t, it is possible for the response $\vec{D}$ at a position $\vec{r}$ to depend not only on the excitation $\vec{E}$ at $\vec{r}$ but also at nearby positions $\vec{r}'$. In linear response theory and for an isotropic medium, the electric displacement and the electric field are related through

$$\vec{D}(\vec{r},t) = \int d^3r' \int dt' \, \epsilon(\vec{r},\vec{r}';t-t')\vec{E}(\vec{r}',t'), \tag{11}$$

where $\epsilon(\vec{r},\vec{r}';t-t')$ is the non local dielectric response. Notice that the local relation (10) corresponds to Eq. (11) in the limit $\epsilon(\vec{r},\vec{r}';t-t') \propto \delta(\vec{r}-\vec{r}')$, where $\delta(\vec{r}-\vec{r}')$ is Dirac's delta function. In this local limit, the response at $\vec{r}$ depends only on the excitation at $\vec{r}'$. However, there are mechanisms which permit the motion of excitations within a solid. For example, an exciton produced at $\vec{r}'$ at time t' may move so that at a later time t it might arrive and contribute to the polarization at another position $\vec{r}$. Thus, we expect $\epsilon(\vec{r},\vec{r}';t-t')$ to be non null for $\vec{r}'$ within a small neighborhood of $\vec{r}$. The size of this neighborhood is known as the *range of non-locality*. Notice that the response given by Eq. (11) would be undistinguishable from the local response (10) unless the field displays spatial variations on a scale comparable or smaller than the range of non-locality.

For infinite and homogenous media, $\epsilon(\vec{r},\vec{r}';t-t') = \epsilon(\vec{r}-\vec{r}';t-t')$, that is, the response would not depend separately on the excitation and observation points, but only on their relative position $\vec{r}-\vec{r}'$. Thus, Eq. (11) would become a space and time convolution. Taking a Fourier transform with wavevector $\vec{q}$ and frequency ω it becomes the simple product

$$\vec{D}(\vec{q},\omega) = \epsilon(\vec{q},\omega)\vec{E}(\vec{q},\omega). \tag{12}$$

Thus, a dependence of ϵ on $\vec{q}$ implies a non-local response. As the dependence in ω is identified with temporal dispersion, the dependence on $\vec{q}$, and more generally, the non-locality of the response is also known as *spatial dispersion*.

3.2 Non Locality of the Excitonic Response

As shown by Eq. (8), the total energy of an exciton includes the energy E_g required to excite an electron from the valence to the conduction band, the binding energy E_n and the kinetic energy due to the centre of mass motion K. When a photon is absorbed and an exciton is created, the latter takes up the momentum of the former. Thus, the energy $E = \hbar\omega_0$ required to create the exciton depends on the wavevector $\vec{q}$ as

$$E \equiv \hbar\omega_0 = \hbar\omega_T + \hbar^2q^2/2M, \tag{13}$$

where

$$\hbar\omega_T = E_g + E_n, \tag{14}$$

is the energy required to create a motionless exciton with principal quantum number n. Substituting ω_0 into Eq. (9) we obtain

$$\epsilon(\vec{q},\omega) = \epsilon_\infty + \frac{\omega_p^2}{\omega_T^2 + \mathcal{D}q^2 - \omega^2 - i\nu\omega}. \tag{15}$$

Here, $\mathcal{D} = \hbar\omega_T/M$ and we neglected terms of order q^4 as q is a small quantity for light.

We have shown that the center of mass motion of the excitons yields a wavevector dependence of the dielectric function. Therefore, as discussed in section 3.1, the response of an excitonic semiconductor is non-local. The above expression of the dielectric response was introduced by Hopfield and Thomas [5] based on a coupled harmonic oscillator model.

3.3 Exciton-polariton

Within a homogeneous medium, the solution of the field equations can always be written as a superposition of plane waves of the form $e^{i(\vec{q}\cdot\vec{r}-\omega t)}$. For each plane wave, Maxwell's equations yield

$$\vec{q}\times(\vec{q}\times\vec{E}) - \frac{\omega^2}{c^2}\vec{D} = 0, \tag{16}$$

in the absence of external sources. If the system is isotropic, the fields may be separated into longitudinal L and transverse T contributions, parallel and perpendicular to the wavevector $\vec{q}$ respectively, and these components are uncoupled to each other. Thus, Eq. (16) becomes

$$q^2\vec{E}^T - \frac{\omega^2}{c^2}\vec{D}^T = 0, \tag{17}$$

and

$$\frac{\omega^2}{c^2}\vec{D}^L = 0. \tag{18}$$

For a non-local system, $\vec{D}$ is related to $\vec{E}$ through Eq. (12). Thus, $\vec{E}^T$ may be different from zero only if $\vec{q}$ and ω are related through the transverse dispersion

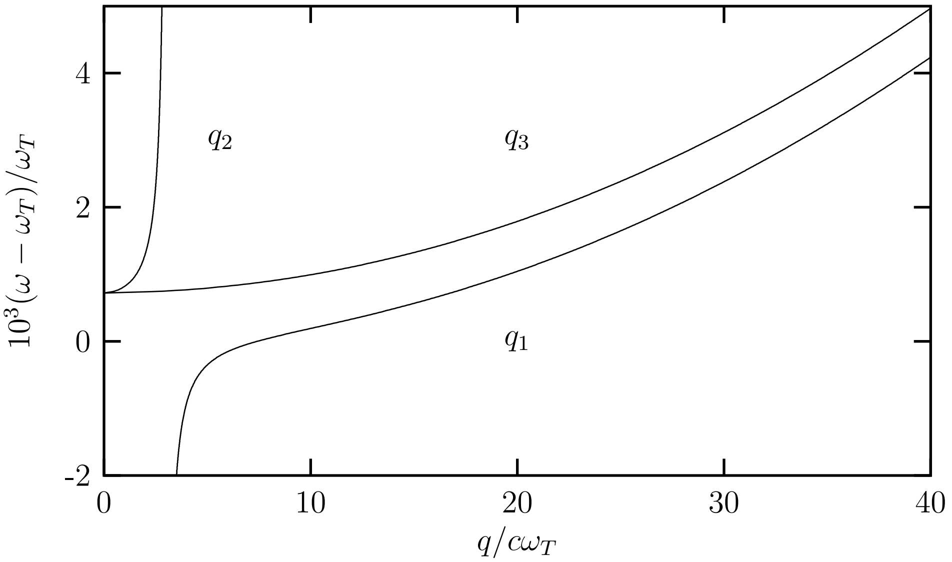

Fig. 3. Schematic dispersion relation ω vs q of the two transverse exciton-polaritons q_1 and q_2 and the longitudinal exciton-polariton q_3 of the an excitonic semiconductor whose dielectric function is given by Eq. (15) in the absence of dissipation $\nu = 0$.

relation, given implicitly by

$$q^2 = \frac{\omega^2}{c^2}\epsilon(\vec{q}, \omega). \tag{19}$$

Similarly, $\vec{E}^L$ may be different from zero but only for wavevectors and frequencies such that

$$\epsilon(\vec{q}, \omega) = 0. \tag{20}$$

We remark that even within an isotropic system, the response of a nonlocal system might depend in the relative direction between the field and the wavevector. Thus, in general, the response ϵ^T to a transverse field need not be the same as the response ϵ^L to a longitudinal field. The dielectric function of Hopfield and Thomas (15) does not distinguish between these two situations. Its substitution into the dispersion relation (19) yields a quadratic equation in q^2. Therefore, there are two transverse modes for each frequency, with wavevectors $\vec{q}$ such that

$$q^2 = \frac{1}{2}\left(\Gamma_0^2 + \epsilon_\infty \frac{\omega^2}{c^2}\right) \pm \frac{1}{2}\left[\left(\Gamma_0^2 - \epsilon_\infty \frac{\omega^2}{c^2}\right)^2 + \frac{4\omega^2\omega_p^2}{\mathcal{D}c^2}\right]^{1/2}, \tag{21}$$

where

$$\Gamma_0^2 \equiv (\omega^2 + i\nu\omega - \omega_T^2)/\mathcal{D}. \tag{22}$$

Furthermore, substituting Eq. (15) into (20) yields a single longitudinal mode for each frequency

$$q^2 = \Gamma_0^2 - \frac{\omega_p^2}{\mathcal{D}\epsilon_\infty}. \tag{23}$$

The resulting dispersion relations are illustrated schematically in Fig. (3) in the case where there is no dissipation $\nu = 0$.

For small wavevectors we can neglect $\mathcal{D}q^2$ and therefore the dispersion relation resembles that of electromagnetic waves in a local system. For small frequencies one of the transverse modes displays a photon-like dispersion corresponding to the propagation of an electromagnetic wave in a medium with index of refraction $n_0 = \sqrt{\epsilon_\infty + \omega_p^2/\omega_T^2}$. This branch shows dispersion as we approach the resonance frequency ω_T, where q would diverge in a local theory. However, when $\omega \approx \omega_T$ and q becomes large, the dispersion relation resembles that of an exciton with kinetic energy $\hbar(\omega - \omega_T) = \hbar^2 q^2/(2M)$. Thus, after a horizontal plateau, the dispersion relation bends upwards, yielding real values of q for arbitrary ω's. This solution is labeled q_1 in Fig. 3. The second transverse mode, labeled q_2 in Fig. 3, starts propagating at the longitudinal frequency,

$$\omega_L = \sqrt{\omega_T^2 + \omega_p^2/\epsilon_\infty} \approx \omega_T + \frac{\omega_p^2}{2\epsilon_\infty \omega_T}, \tag{24}$$

and approaches asymptotically the linear dispersion of a photon propagating within a medium with index of refraction $\sqrt{\epsilon_\infty}$. For frequencies below ω_L, the second transverse mode cannot propagate as its wavevector is imaginary $q \approx i\sqrt{(\omega_T^2 - \omega^2)/\mathcal{D}}$. At ω_L there is a third mode, labeled q_3, which corresponds to the longitudinal solution. Its frequency is shifted from the frequency ω_T of the excitonic resonance due to the long range Coulomb interaction between the charges associated to the longitudinal polarization of this exciton. Spatial dispersion bends the dispersion relation upwards, as in the case of the transverse exciton, and thus, yields a finite group velocity for the longitudinal exciton. Similarly to the transverse case for large wavevectors, the dispersion of the longitudinal exciton is due to its kinetic energy $\hbar\omega = \hbar\omega_L + \hbar^2 q^2/(2M)$. For frequencies below ω_L the longitudinal exciton cannot propagate and its wavevector becomes imaginary $q = i\sqrt{(\omega_L^2 - \omega^2)/\mathcal{D}}$.

Notice that the dispersion relations (19) and (20) yield solutions which resemble excitons for large wavevectors and resemble electromagnetic waves for small wavevectors, with a transition region which interpolates between both behaviors. Thus, these modes, consisting of excitons strongly coupled to the electromagnetic field, are denominated *exciton-polaritons*.

4 Surface Optical Response

In the previous section we showed that there are two transverse and one longitudinal exciton-polaritons that may propagate at any given frequency within an excitonic semiconductor described by the model of Hopfield and Thomas. These modes may be excited at surfaces illuminated by an incoming light beam. To calculate this excitation, we have to investigate the behavior of the exciton polaritons in the neighborhood of the surface. This may be done by adding a surface-exciton interaction potential to the equations that describe the exciton dynamics, such as Eq. (1), as we show in Sec. 5. Here, we present a simplified model of this interaction which was postulated by Hopfield and Thomas [5], in which it is assumed that the sole effect of the surface is to repel the exciton, giving rise to an exciton free region known as the *dead layer*, whose width is of the order of the excitonic radius. In this region the optical response is local and only one kind of mode can propagate, namely, a transverse polariton. The dead layer ends abruptly at the excitonic-active region, where there are additional transverse and longitudinal modes. To find the amplitudes of this multiplicity of modes we need a large enough set of boundary conditions. It turns out that Maxwell's equations are insufficient to determine all of the amplitudes required to solve completely the optical problem in non-local systems with abrupt interfaces, and therefore additional boundary conditions (ABC's) have to be postulated, one for each additional mode.

4.1 Additional Boundary Conditions (ABC)

During the past three decades, since the pioneering work of Pekar [4], several sets of ABC's have been proposed. The non-uniqueness of the ABC's is due to the fact that Eq. (12) is only valid within homogeneous systems and the surface of a semi-infinite semiconductor is necessarily an inhomogeneity. Thus, whenever the excitation point $\vec{r}'$ or the observation $\vec{r}$ point is close to the surface, ϵ depends separately on both $\vec{r}$ and $\vec{r}'$ and not only on its difference, so that $\epsilon(\vec{q},\omega)$ is not a well defined quantity. A detailed model of the surface would be required to calculate the nonlocal response $\epsilon(\vec{r},\vec{r}';t-t')$. Instead of proceeding along this approach, a common alternative has been to assume that beyond the surface, the bulk modes propagate as if Eq. (12) were valid. However, the lack of a model for the surface makes the system of equations that define this approach under-determined. Therefore, the need for ABC's. The multiplicity of ABC's proposed in the literature, their justification, their consequences for the optical properties and the comparison between their predictions and experiment have been addressed in Refs. [84,6].

It is shown in Refs. [84,6] that most ABC's may be included in the *generalized ABC*

$$\alpha_j P_j(z_0^+) + \beta_j \frac{\partial P_j(z_0^+)}{\partial z} = 0 \tag{25}$$

where $P_j = (D_j - \epsilon_\infty E_j)/4\pi$ is the excitonic contribution to the polarization within the active region, j is a cartesian index, z_0 denotes the location of the surface, which we take to be parallel to the $x-y$ plane, we situate the active region at $z > z_0$, so that z_0^+ denotes a position just inside the acitve region, and α_j and β_j are parameters which may depend on the frequency and on the material properties. The Pekar boundary conditions [4] $\vec{P}(z_0^+) = 0$, namely, the continuity of the excitonic polarization at the interface, corresponds to the choice $\beta_x = \beta_y = \beta_z = 0$. The Ting-Frankel-Birman [85] boundary conditions $\partial\vec{P}(z_0^+)/\partial z = 0$, i.e., the continuity of the normal derivative of the excitonic polarization, corresponds to the choice $\alpha_x = \alpha_z = 0$.

The parameters α_j and β_j may be interpreted within the specular reflection model, in which it is assumed that excitons that bump into the interface z_0 may be specularly reflected and that their dipole moment p_j upon reflection becomes $U_j p_j$. The size of the complex parameters U_j is related to the probability of being reflected specularly instead of diffusively. It can be shown [84,6] that

$$\frac{\alpha_j}{\beta_j} = i\Gamma \frac{1-U_j}{1+U_j}, \tag{26}$$

where

$$\Gamma^2 \equiv (\omega^2 + i\nu\omega - \omega_T^2)/\mathcal{D} - Q^2, \tag{27}$$

and $\vec{Q}$ is the projection of the wavevector onto the surface. Notice that Γ_0 in Eq. (22) is simply Γ evaluated at $Q = 0$.

4.2 Reflectance

We consider an electromagnetic wave which impinges at an angle θ on the surface $z = 0$ of an excitonic semiconductor which occupies the region $z > 0$. We assume that $x - z$ is the plane of incidence, so that the incident wavevector $\vec{q} = (Q, 0, q^\perp)$, with $Q = q\sin\theta$, $q^\perp = q\cos\theta$, and $q = \omega/c$. We consider separately the cases of polarization normal to the plane of incidence or S polarization ($\vec{E}_{\text{in}} = (0, E_{\text{in}}, 0)$) and polarization within the plane of incidence or

P polarization ($\vec{E}_{\text{in}} = (q^{\perp}, 0, -Q)B_{\text{in}}/q$), where $\vec{E}_{\text{in}}$ and $\vec{B}_{\text{in}}$ are the amplitudes of the electric and magnetic fields of the incident wave.

In the case of S incoming polarization, the incident field may couple only to S polarized reflected and transmitted fields. We write the wavevector of the transmitted fields as $(Q, 0, q_i^{\perp})$ where we used the conservation of momentum along the interface and where $q_i^{\perp}$, $i = 1, 2$ are obtained from the transverse dispersion relation (21). Therefore, we write the transmitted electric field as

$$E_y = (E_1 e^{iq_1^{\perp} z} + E_2 e^{iq_2^{\perp} z}) e^{i(Qx - \omega t)}, \tag{28}$$

and we obtain the transmitted magnetic field from Maxwell's equations,

$$B_x = -(q_1^{\perp} E_1 e^{iq_1^{\perp} z} + q_2^{\perp} E_2 e^{iq_2^{\perp} z}) e^{i(Qx - \omega t)}/q. \tag{29}$$

For illustrative purposes, we ignore for the moment being the presence of a dead layer at the surface of the semiconductor, and we apply the generalized ABC (25) correponding to the y direction at $z = 0$, obtaining

$$\frac{E_1}{E_2} = -\frac{\alpha_y + \beta_y q_2^{\perp}}{\alpha_y + \beta_y q_1^{\perp}} \frac{\chi_2}{\chi_1}, \tag{30}$$

where $\chi_i \equiv \omega_p^2/\{4\pi\mathcal{D}[(q_i^{\perp})^2 - \Gamma^2]\} \equiv (\epsilon_i - \epsilon_{\infty})/(4\pi)$ is the excitonic susceptibility for the i-th mode. We define the surface impedance for S polarization as

$$Z_s = -\frac{E_y(0)}{B_x(0)}, \tag{31}$$

which may be evaluated indistinctively inside or outside of the semiconductor, as E_y and B_x are continuous quantities. Employing Eqs. (28), (29), and (30), we finally obtain

$$Z_s = q\frac{a_1 - a_2}{q_2^{\perp} a_1 - q_1^{\perp} a_2}, \tag{32}$$

where

$$a_i = \frac{1}{q_i^{\perp} - \Gamma} + \frac{U_y}{q_i^{\perp} + \Gamma}, \qquad (i = 1, 2). \tag{33}$$

Using the general formulae for the reflection amplitudes in terms of the surface impedance, we obtain[84,6]

$$R_s = |r_s|^2 = \left| \frac{Z_s - Z_s^v}{Z_s + Z^v} \right|^2 , \tag{34}$$

where $Z_s^v = 1/\cos\theta = q/q^\perp$ is the surface impedance of vacuum for S polarization.

We proceed in a similar way to obtain the surface impedance and the reflectance for the case of P polarization. In this case, the incoming field may couple to two P polarized transverse transmitted waves with wavevectors $(Q, 0, q_1^\perp)$ and $(Q, 0, q_2^\perp)$ as above, and also to one longitudinal transmitted wave with a wavevector $(Q, 0, q_3^\perp)$ which may be obtained from Eq. (23). Thus, we have two additional waves and we require two additional boundary conditions, namely, the x and z components of Eq. (25). Proceeding as in the S polarized case, we define the surface impedance

$$Z_p = \frac{E_x(0)}{B_y(0)}, \tag{35}$$

for which we obtain the value

$$Z_p = \frac{1}{q} \frac{\Delta_{12} + \Delta_{23} + \Delta_{31}}{\epsilon_1 \Delta_{23}/q_1^\perp + \epsilon_2 \Delta_{31}/q_2^\perp}, \tag{36}$$

where

$$\Delta_{ij} = a_i b_j - a_j b_i, \tag{37}$$

a_i are defined as in Eq. (33) with U_x replacing U_y and $i = 1, \cdots, 3$,

$$b_i = \left(\frac{1}{q_i^\perp - \Gamma} + \frac{U_z}{q_i^\perp + \Gamma} \right) \gamma_i, \tag{38}$$

$\gamma_1 = -Q/q_1^\perp$, $\gamma_2 = -Q/q_2^\perp$, and $\gamma_3 = q_3^\perp/Q$. Finally, we obtain the reflectance [84,6]

$$R_p = |r_p|^2 = \left| \frac{Z_p - Z_p^v}{Z_p + Z_p^v} \right|^2 , \tag{39}$$

with

$$Z_p^v = \cos\theta = q^\perp/q, \tag{40}$$

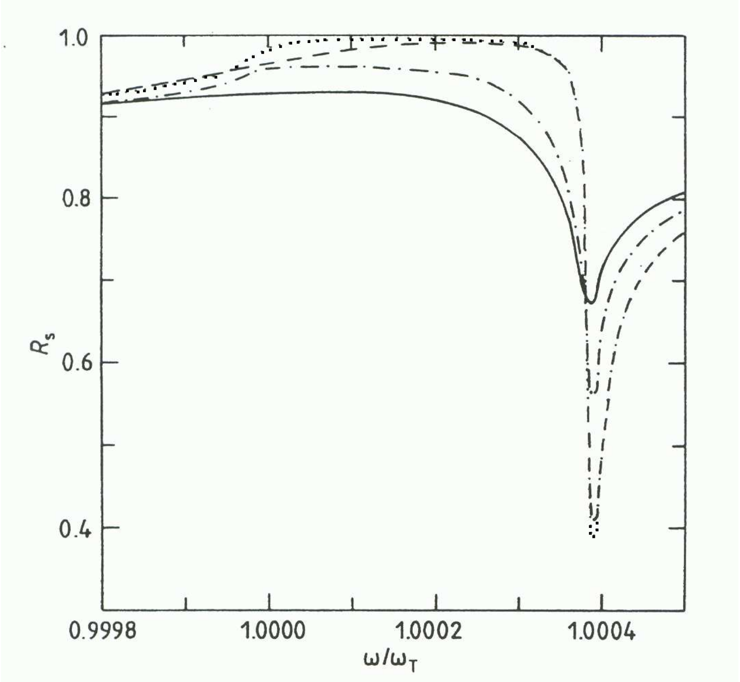

Fig. 4. Reflectance of ZnSe calculated for s polarization with the generalized ABC formalism and employing the ABC of Pekar (solid, $U_y = -1$), Agarwal et al (dashed-dot, $U_y = 0$), Fuchs-Kliewer (dashed, $U_y = 1$) and the results of a local calculation (dots). The parameters are: $\theta = 85°$, $\epsilon_\infty = 8.1$, $\omega_p^2/\omega_T^2 = 5.5 \times 10^{-3}$, $\epsilon_0 \mathcal{D}/c^2 = 5 \times 10^{-5}$, and $\nu/\omega_T = 10^{-5}$. (Taken from [6]).

the surface impedance of vacuum for P polarization [6].

As an example, in Fig. 4 and 5 we show the reflectance of ZnSe for both S and P polarizations and employing different ABC's. Figures were taken from Ref. [6]. For both polarizations the local reflectance is very high between ω_T and $\omega_L \approx 1.0003\omega_T$, and falls abruptly at ω_L. After ω_L there is a sharp minimum in the case of S polarization at the *matching* frequency $\omega_M \approx 1.0004\omega_T$, for which $\epsilon(\vec{q} = 0, \omega) = 1$, while there is a zero at the Brewster frequency $\omega_B \approx \omega_M$ in the case of P polarization corresponding to the Brewster condition $\epsilon(\vec{q} = 0, \omega) = \tan^2\theta$. Non local effects calculated with either of the Agarwal-Pattnayak-Wolf [11], Fuchs-Kliewer [86], or the Pekar [4] ABC's, diminish the reflectance between ω_T and ω_L and soften the fall at ω_L as non local models allow the excitation of the propagating exciton 1, which may take energy away from the interface towards the bulk. We find that the strongest nonlocal effects are predicted by the Pekar model, while the weakest nonlocal manifestations correspond to the Fuchs-Kliewer model.

In the calculations above, we have neglected the exciton-free dead layer, which would be necessary to explain satisfactorily the experimental measurements. The above derivations of R_p and R_s may be easily extended to include a surface dead layer with a local dielectric constant ϵ_∞. An example that describes the

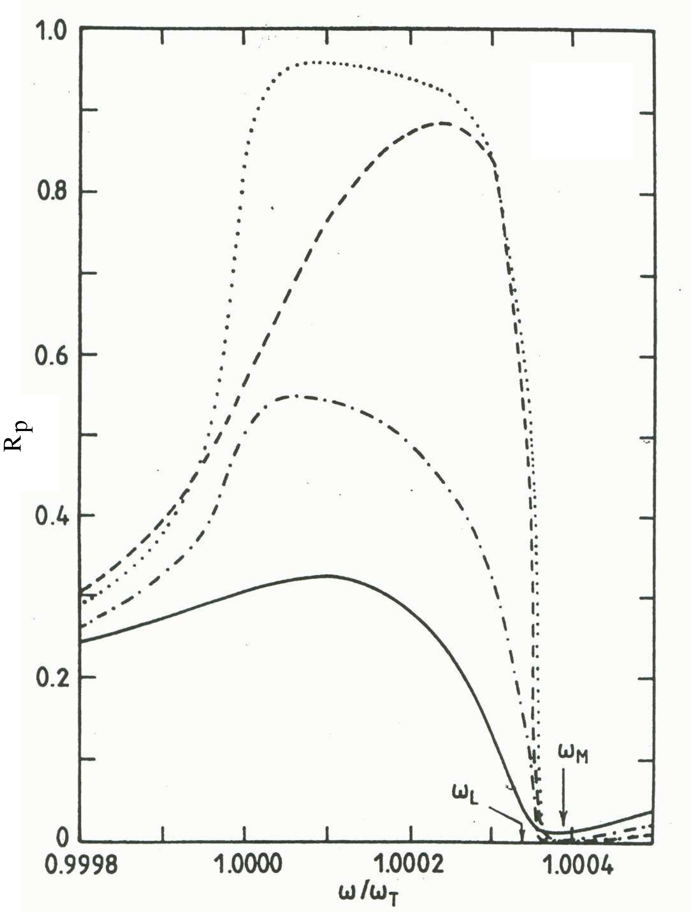

Fig. 5. Reflectance of ZnSe calculated for P polarization with the generalized ABC formalism and employing the ABC's of Pekar (solid, $U_x = -1$, $U_z = -1$), Agarwal et al (dashed-dot, $U_x = 0$, $U_z = 0$), Fuchs-Kliewer (dashed, $U_x = 1$, $U_z = -1$) and the results of local calculation (dots). Parameters are as in Fig. 4 except for the angle of incidence $\theta = 45°$. (Taken from [6]).

dead layer effects in the reflectivity of CdS is given in Figs. 6 calculated for normal incidence using Pekar ABC's and for dead layer thickness in the range from 0 up to 200 Å. Notice that the minimum in the reflectance shifts towards the red as the width of the dead layer increases. A dead layer of width 100 Å yields the best agreement with experiment. In this calcualtion the electric field has to be along a principal direction, as the theory above corresponds to isotropic media while CdS has an hexagonal crystalline structure. For Fig. 6 the field was taken perpendicular to the c axis.

4.3 Surface Modes

Surface polaritons are electromagnetic modes that propagate along a surface and are localized near it. Their amplitudes decay away from the surface in both

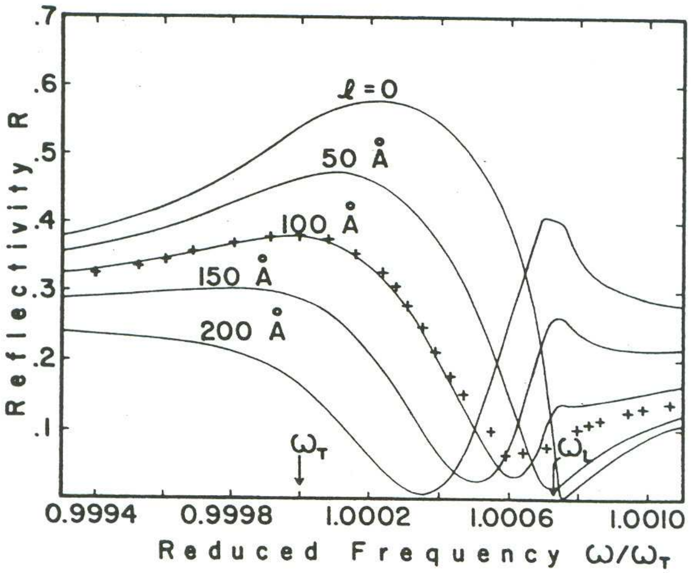

Fig. 6. Normal incidence reflectivity using Pekar ABC's for different dead-layer thicknesses, with parameters correspoding to the $A_{n=1}$ excitonic transition of CdS: $\hbar\omega_T = 2.55273$ eV, $\mathcal{D}/c^2 = 5.543 \times 10^{-6}$, $\hbar\nu = 14$meV, $M = 0.9m_0$ (m_0 is the bare electronic mass) and $\epsilon_\infty = 9.1$. The crosses correspond to experimental results [21]. (Taken from [29]).

directions, within the medium and into vacuum. This decrease of the wave amplitude is not associated with energy loss but is an intrinsic property of the surface polariton modes. On the other hand, their amplitude might diminish with distance along the propagation direction or with time as a consequence of damping mechanisms. In this section we concentrate on surface polaritons in the presence of spatial dispersion in excitonic semiconductors.

Surface modes are free oscillations of the electromagnetic fields and therefore they may be excited even if they are not 'forced' by an external field such as an incident wave. Thus, they may be obtained by analysing the reflectivity of the system. In general, the field in the vacuum side of the surface is the sum of the incident and the reflected field. In the absence of an incident wave, the total field would be null except in the case in which the reflection amplitude has an infinite value. Clearly, the pole of the reflection coefficient has to lie outside of the light cone, $Q > q$, so that the normal component of the wavevector of the reflected wave $-q^\perp$ becomes imaginary. In this region, neither the incident nor the reflected wave carry energy and energy conservation imposes no constriction on the magnitude of the reflection amplitude. Thus, the surface modes may be identified with the poles of the reflection amplitude [87–89]. Using Eq. (39) we may write the dispersion relation of the normal modes for P polarization implicitly as

$$Z_p(Q,\omega) + Z_p^v(Q,\omega) = 0. \qquad (41)$$

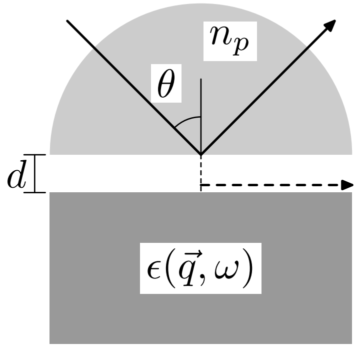

Fig. 7. Schematic drawing showing the principle of the attenuated total reflection (ATR) method: light (solid arrows) is incident on the surface of a prism of index of refaction $n_p = [\epsilon_p]^{1/2}$ separated by a vacuum gap of width d from a semiconductor of dielectric function $\epsilon(\vec{q},\omega)$, exciting surface exciton-polaritons (dashed arrow). The geometry is the Otto [90] experimental array of the excitation and detection of surface polaritons.

Substituting Eq. (36) and (40) we obtain the dispersion relation of the surface polaritons of the semiconductor [32],

$$\begin{aligned} -a_2b_1 + a_1b_2 - \left(1 - \frac{q_0^\perp \epsilon_1}{q_1^\perp}\right)(a_3b_2 - a_2b_3) \\ + \left(1 - \frac{q_0^\perp \epsilon_2}{q_2^\perp}\right)(a_3b_1 - a_1b_3) = 0, \end{aligned} \tag{42}$$

where all the quantities (a_i, b_i, ϵ_i, $q_0^\perp = q_0 \cos(\theta)$, and $q_i^\perp$) are defined in the previous section. We remark that due to spatial dispersion, surface excitons coexist with a bulk propagating mode even for frequencies between ω_T and ω_L, so that they are always of a lossy nature.[58]. A similar development may be attempted for the case of S polarization, but in this case no solution is found.

4.4 Attenuated total reflectivity (ATR)

The surface modes of a flat surface cannot be excited directly by illuminating the surface, as their dispersion relation lies outside of the light cone. Thus, to couple light with surface modes, a mechanism to increase the parallel wavevector Q is required. One method to experimentally excite and detect surface polaritons is that of attenuated total reflectivity (ATR) [90], first proposed and applied by Otto to excite and detect surface plasmons at metallic surfaces. In the Otto arrangement, a prism with a non-dispersive positive dielectric constant $\epsilon_p > 1$ is separated by a thin vacuum gap from the system under study with dielectric function ϵ which supports surface modes. Within the prism, the

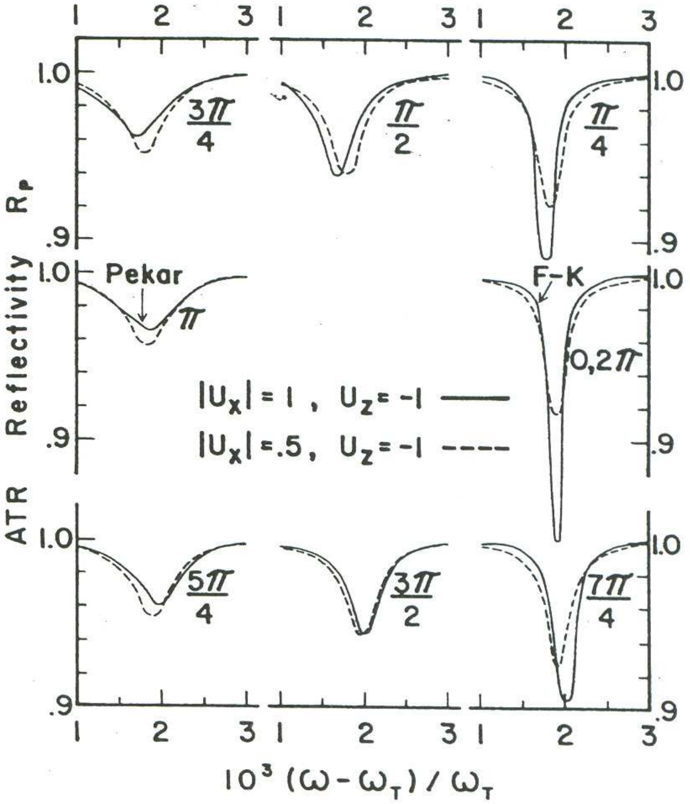

Fig. 8. ATR spectra for the $C_{n=1}$ exciton of ZnO. The angle of incidence in the prism, of index of refraction $n_p = 3.41$, is 50^o. The width of the air-gap is 3600 Å. The ABC's used are of the form $U_z = -1$ and $U_x = |U_x|e^{i\varphi_x}$ and each curve is labeled by the phase φ_x employed in its calculation. (Taken from [29]).

size of the wavevector $\sqrt{\epsilon_p}q$ is larger than q, and thus, for large enough angles of incidence $\theta > \theta_c$ the parallel wavevector $Q = \sqrt{\epsilon_p}q \sin\theta$ may surpass q, where $\theta_c = \sin^{-1}(1/\sqrt{\epsilon_p})$ is the critical angle. In this situation, the field in the vacuum gap becomes evanescent and in the absence of the semiconductor all of the incoming energy would be reflected. This is the well known phenomenon of total internal reflection. By placing the semiconductor close to the face of the prism, the evanescent field may tunnel across the gap and couple with the surface modes, transfering energy resonantly whenever (Q, ω) lies on their dispersion relation, therefore attenuating the total reflectance. Thus, surface modes manifest themselves as minima of the reflectance in the ATR setup. In an alternative arrangement suggested by Kretschmann [91,92], the medium supporting surface modes is deposited as a thin layer on the surface of the prism. As discussed above, only P-polarized light may couple with surface exciton-polaritons at homogeneous semiconducors.

In Fig. 8 we show the ATR spectrum of the $C_{n=1}$ exciton of ZnO calculated with an extension to multiple layers of the non-local theory presented in Sect. 4.2 and for different ABC's [29]. ZnO has a wurtzite structure and therefore possesses three excitonic transitions at about 3.4 eV due to the upper two valence bands (A and B excitons, excited when $\vec{E} \perp \vec{c}$) and to the third valence band (C excitons, excited when $\vec{E} \parallel \vec{c}$). The free C_1 excitons of the ground state are separated by crystal field splitting of about 40 meV from the A_1 and B_1 excitons. Their longitudinal-transverse splittings are about 2 meV (A_1) and 11 meV (B_1 and C_1). The spin-orbit splitting of the A_1 and B_1 excitons is about 5meV [17]. The parameters used for the calculations are: $\epsilon_0 = 6.16$, $\hbar\omega_T = 3.421$ eV, $\hbar\nu = 0.5$ meV and $M = 0.87m_0$ where m_0 is the bare electronic mass. In the calculations the small (30 Å) exciton-free layer was neglected and the parameters corresponding to the experiments of Lagois and Hümmer [17,93] were used. Fig. 8 shows spectra for $U_z = -1$ and $U_x = |U_x|e^{i\varphi_x}$. Two values of $|U_x| = 1.0, 0.5$ were considered, which correspond to specular and to partially diffuse scattering of excitons at the surface, respectively, and several spectra were calculated for different values of the phase φ. Fig. 8 shows that the Pekar ABC's ($|U_x| = 1$, $\varphi_x = \pi$) produces the ATR minimum that is closer to experiment [93] and with the largest width, ≈ 3 meV. However, the experimental linewidth [93] ≈ 6 meV is substantially larger, indicating [29] that a more sophisticated formalism is needed. In particular, in the caculation above, an isotropic response was assumed, while in the experiment, the c axis was oriented along the surface and within the incidence plane, so that the response to P polarized light is necessarily anisotropic. Furthermore, the interaction with the surface might not be well described by a simple exciton-free dead layer. In the following sections we review some microscopic approaches to the surface contributions to the optical properties of excitonic semiconductors.

5 Interaction with surfaces

The potential due to the interaction of an exciton with its image produced at the surface of a clean semiconductor repels the exciton away from the surface and into the bulk [5,94]. However, the presence of impurities produces charges near the surface that gives rise to extrinsic potentials that may either attract or repel the excitons. Thus, the reflectivity of light from semiconductor surfaces may be drastically modified by the presence of impurities near surfaces, within the so-called transition layer, due to interactions of the excitons with the resulting surface potential [84]. Furthermore, absorption processes may take place at the transition layer. Consequently, close to the surface exciton polaritons may exhibit different behavior compared to that in the bulk.

Several theoretical models for semiconductor surfaces have been proposed beyond the primitive model of the *dead layer* in which an inert exciton-free layer is produced at the surface due to an infinite repulsive potential [5]. More realistic continuous surface potential profiles have been proposed, from a simple repulsive linear potential [95] to Morse type potentials which also include an attractive well [41]. The extrinsic contribution to the surface potential may be due to surface treatments such as doping, illumination, electron and ion bombardment. Consequently, a near-surface space-charge region is formed, which may become attractive. The aim of this section is to investigate the motion of excitons near surfaces of semi-infinite media and thin films taking into account continuous potentials.

5.1 Semiinfinite systems

Excitons in semi-infinite semiconductors obey an effective mass Schrödinger equation, as in Eq. (1). However, at the surface, translational invariance is lost, and we have to add the interaction of the electron and the hole with the surface, $V(\vec{r}_e, \vec{r}_h)$. Within the effective mass approximation, Schrödinger's equation becomes

$$\left[\frac{p_e^2}{2m_e} + \frac{p_h^2}{2m_h} - \frac{e^2}{\epsilon r} + V_s(\vec{r}_e, \vec{r}_h)\right]\Psi(\vec{r}_e, \vec{r}_h) = E\Psi(\vec{r}_e, \vec{r}_h), \tag{43}$$

where we measure the energy relative to the gap, i.e., relative to the energy required to create a free electron and a free hole. The solutions are usually obtained by using approximated methods. We now describe briefly a commonly employed adiabatic theory developed by Deigen and Glinchuk [96], Sakoda [97] and Balsev [98], and recently described in Halevi's [7] book, whose approach we will follow.

Assuming that the surface lies parallel to the $x - y$ plane, we make a transformation into relative $\vec{r} = (x, y, z)$ and center of mass $\vec{R} = (X, Y, Z)$ coordinates. Thus,

$$\left[\frac{P^2}{2M} + \frac{p^2}{2\mu} - \frac{e^2}{\epsilon r} + V_s(\vec{r}, Z)\right]\Psi(\vec{r}, \vec{R}) = E\Psi(\vec{r}, \vec{R}), \tag{44}$$

where we employed the translational symmetry along the surface to eliminate X and Y from the potential $V(\vec{r}, Z)$. We propose a solution of the form

$$\Psi(\vec{r}, \vec{R}) = \varphi(\vec{r}, Z)\phi(\vec{R}), \tag{45}$$

which substituted into Eq. (44) yields

$$\left[\frac{p^2}{2\mu} - \frac{e^2}{\epsilon r} + V_s(\vec{r}, Z)\right]\varphi(\vec{r}; Z) = E_r(Z)\varphi(\vec{r}; Z), \tag{46}$$

which defines the binding energy $-E_r(Z)$ of the exciton at a given distance Z of the center of mass from the surface. $E_r(Z)$ may play the role of a potential energy for the center of mass motion,

$$\left[\frac{P^2}{2M} + E_r(Z)\right]\phi(\vec{R}) = E\phi(\vec{R}), \tag{47}$$

whenever the term

$$\frac{-\hbar^2}{2M}\left[\frac{\partial^2\varphi}{\partial Z^2}\phi + 2\frac{\partial\varphi}{\partial Z}\frac{\partial\phi}{\partial Z}\right] \tag{48}$$

is negligible. The neglect of this term amounts to ignoring the kinetic energy of the center of mass in comparison to the binding energy [84]. Eqs. (46) and (47) define the adiabatic approximation.

5.2 Surface potential for excitons

Accounting for image charge forces only, $V_s(\vec{r}_e, \vec{r}_h)$ takes the form [98]

$$V_s(\vec{r}_e, r_h) = \frac{pe^2}{\varepsilon_0}\left[\frac{1}{4z_e} + \frac{1}{4z_h} - \frac{1}{\sqrt{(z_e+z_h)^2 + x^2 + y^2}}\right], \tag{49}$$

where the first two terms account for the interaction of the electron and the hole with their respective image charges, and the last term is the interaction of each particle with the image of the other. Here, $p = (\varepsilon_0 - 1)/(\varepsilon_0 + 1)$ is the image factor from within a semiinfinite medium with static dielectric response ε_0. Using the relative and center of mass coordinate transformation and expanding to lowest order in $1/Z$ we rewrite the potential

$$V_s(r, Z) = \frac{pe^2}{\varepsilon_0 Z^3}\left[\frac{1}{8}z^2 + \frac{1}{16}(x^2+y^2)\right]. \tag{50}$$

With the use of this expression Eq. (46) may be solved subject to the conditions that the electron and the hole must remain in the half-space $z_e > 0$ and $z_h > 0$, or equivalently $-\frac{M}{m_h}Z < z < \frac{M}{m_e}Z$. This could be done through a variational approach using trial variational wave functions such as [98]

$$\varphi(\vec{r}, Z) \propto \sin\left[(\frac{z}{ZM} + \frac{1}{m_h})\mu\pi\right]\left[\psi_{1s}(\vec{r}) + \alpha(Z)\psi_{2p}(\vec{r}) + \beta(Z)\psi_{2s}(\vec{r})\right], \tag{51}$$

or [99]

$$\varphi(\vec{r}, Z) \propto \left[1 - e^{-z_e/a_B}\right] \left[1 - e^{-z_h/a_B}\right] \left[\psi_{1s}(\vec{r}) + \alpha(Z)\psi_{2p}(\vec{r}) + \beta(Z)\psi_{2s}(\vec{r})\right]. \quad (52)$$

The former yields an approximate [98] expression

$$E_r(Z) \simeq -E_b + V_0 e^{-Z/a_B} + \sigma p E_b \frac{a_B^3}{Z^3}, \quad (53)$$

for the eigenvalues of Eq. (46), which is valid for large Z. In Eq. (53) E_b is the electron-hole binding energy far from the surface, a_B is the effective exciton Bohr radius and $V_0 = 12E_b$. It is convenient [84] to rewrite Eq. (53) as

$$E_r(Z) = -E_b + \Delta E(Z), \quad (54)$$

where the correction $\Delta E(Z)$ due to the interaction with the surface contains a repulsive exponential contribution originated in the contact force besides a repulsive dipolar $1/Z^3$ image force. Notice that a photon requires an energy $\hbar\omega = E_g + E$ to create an exciton with energy E with respect to the gap of size E_g, while $\hbar\omega_T = E_g - E_b$ is the minimum energy required to create an exciton within the bulk. Thus, we may write the center of mass equation (47) as

$$\left[\frac{P^2}{2M} + \hbar\omega_T + \Delta E(Z)\right] \phi(\vec{R}) = \hbar\omega\phi(\vec{R}), \quad (55)$$

in which the energy shift $\Delta E(Z)$ plays the role of a potential energy corresponding to the force that acts on the exciton as it approaches the surface, and may be identified with a surface potential $U(Z)$, such as that introduced by Hopfield and Thomas [5] to explain the presence of an exciton-free dead-layer.

We remark that the *potential* (53) contains only repulsive terms due to the contact and the image interactions at a neutral surface. Other terms, both repulsive and attractive, may appear whenever the surface has impurity ions, and frequently, simple model expressions for the surface potential, such as the Morse potential, are employed.

5.3 Surface potential for the excitonic polarization

To deal with the propagation of light close to the surface of excitonic semiconductors it is more accurate to incorporate the continuous surface potential than to assume abruptly terminated homogeneous regions. The continuous potential enters the polarization equation which couples the excitonic polarization to the electromagnetic field, and which has to be solved together with Maxwell's equations.

Let us consider a dielectric occupying the half-space $z > 0$ with a potential $U(z)$ acting on the excitons close to the surface as in the previous section. We can obtain the equation of motion for the polarization by first rewriting Eq. (12) within a homogeneous excitonic semiconductor with response (15) as an equation for the excitonic polarization $4\pi(\omega_T^2 + Dq^2 - \omega^2 - i\nu\omega)\vec{P} = \omega_p^2\vec{E}$. Now we separate q^2 into its parallel and perpendicular components $Q^2 + (q^\perp)^2$ and identify $q^\perp$ with $-i\partial/\partial Z$, which will allow us to incorporate spatial inhomogeneities. Finally we add the surface energy $V(Z)$ to the excitonic energy $\hbar\omega^T + \hbar^2 q^2/2M$ to obtain [100]

$$\left[\frac{\partial^2}{\partial z^2} + \Gamma^2(z)\right]\vec{P}(z) = -\frac{\omega_p^2}{4\pi\mathcal{D}}\vec{E}(z), \tag{56}$$

where

$$\Gamma^2(z) = \left[\omega^2 - \omega_T^2 + i\omega\gamma - \mathcal{D}Q^2 - 2\frac{\omega_T U(z)}{\hbar}\right]/\mathcal{D} = \Gamma_B^2 + \Delta\Gamma^2(z), \tag{57}$$

$$\Delta\Gamma^2(z) = \frac{2\omega_T U(z)}{\hbar\mathcal{D}}, \tag{58}$$

and where we took advantage of the invariance along the xy-plane by assuming a spatial dependence e^{iQx} for all the fields. As $\vec{D} = \varepsilon_\infty\vec{E} + 4\pi\vec{P}$, the electromagnetic wave equation takes the form

$$\nabla \times \nabla \times \vec{E} = \frac{\omega^2}{c^2}\left(\varepsilon_\infty\vec{E} + 4\pi\vec{P}\right). \tag{59}$$

which forms together with Eq. (56) a system of equations that has to be solved for $\vec{P}$ and $\vec{E}$ to obtain the reflection and refraction of electromagnetic waves. This problem shall be addressed below for S and P polarized light incident onto the surface. We will assume $x - z$ is the plane of incidence.

In the case of S-polarization the electric field and the corresponding excitonic polarization have only a y-component. Consequently, Eqs. (56) and (59) reduce to [100]

$$\left[\frac{\partial^2}{\partial z^2} + \Gamma^2(z)\right]P_y(z) = -\frac{\omega_p^2}{4\pi\mathcal{D}}E_y(z), \tag{60}$$

$$\left[Q^2 - \varepsilon_\infty \frac{\omega^2}{c^2} - \frac{\partial^2}{\partial z^2}\right] E_y(z) = 4\pi \frac{\omega^2}{c^2} P_y(z). \tag{61}$$

When the z-dependence of Γ is neglected, the solutions to these coupled equations are plane waves. Their amplitudes may be determined by applying *additional boundary conditions* (ABC's) besides the usual boundary conditions at the surface, as shown in Sec. 4. This is a non-local approach which has been widely studied [101,29,13]. The z-dependence of Γ impedes an analytical solution, requiring a numerical integration [100] $E_y(z)$ and $P_y(z)$. The coupled differential equations may be integrated from a point z_0 deep within the bulk of the dielectric where the surface potential is negligible, and advancing towards the surface. As there are two transverse modes with wave vectors $q_1^\perp$ and $q_2^\perp$ in the bulk, we perform the integration twice, with initial conditions obtained from the asymptotic solutions $E_{y1}(z) = e^{iq_1^\perp z}$ and $E_{y2}(z) = e^{iq_2^\perp z}$. The polarization is a linear combination of the two corresponding solutions $P_y = A_1 P_{y1} + A_2 P_{y2}$. With the aid of the ABC's it is possible to obtain the ratio A_1/A_2 and with the use of the Maxwell boundary conditions the reflectivity may be determined. In the case of P-polarization, Eqs. (56) and (59) yield

$$\left[\frac{\partial^2}{\partial z^2} + \Gamma^2(z)\right] P_j(z) = -\frac{\omega_p^2}{4\pi \mathcal{D}} E_j(z), \quad j = x, z, \tag{62}$$

$$iQ \frac{\partial E_z(z)}{\partial z} - \left[\frac{\partial^2}{\partial z^2} + \varepsilon_\infty \frac{\omega^2}{c^2}\right] E_x(z) = 4\pi \frac{\omega^2}{c^2} P_x(z), \tag{63}$$

$$iQ \frac{\partial E_x(z)}{\partial z} + \left[Q^2 - \varepsilon_\infty \frac{\omega^2}{c^2}\right] E_z(z) = 4\pi \frac{\omega^2}{c^2} P_z(z). \tag{64}$$

As in the previous case, if Γ is z-independent the solution of these equations reduces to the usual non-local problem in which the reflected and transmitted fields are plane waves whose amplitudes are determined from the ABC's (section 4). In the general case a numerical solution may be obtained as for S-polarization, although for P-polarization there is a longitudinal mode in addition to the two transverse modes. In view of this, the differential equations have to be integrated three times with initial conditions $E_{x1}(z) = e^{iq_1^\perp z}$, $E_{x2}(z) = e^{iq_2^\perp z}$, and $E_{x3}(z) = e^{iq_3^\perp z}$, where $q_1^\perp$ and $q_2^\perp$ are the wave vectors of the two transverse modes and $q_3^\perp$ corresponds to the longitudinal mode. The various amplitudes and the reflectivity are obtained by applying boundary conditions at the surface. A detailed procedure may be found in Ref. [100].

As excitons are repeled by the surface potential, the excitonic polarization at the surface is expected to be small, so that the additional boundary conditions are expected to be of little consequence whenever an appropriate surface

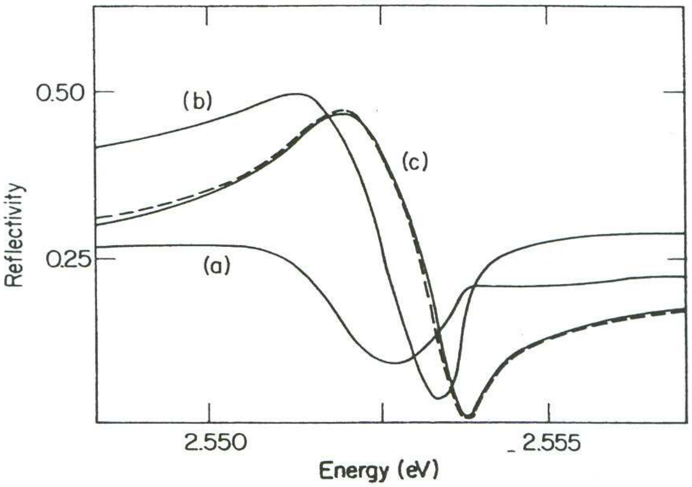

Fig. 9. Reflectivity of a CdS surface calculated for normal incidence according to the theory of Ruppin [100]. An exponential repulsive potential of height $\hbar\omega_B$ and range a was included, with $\omega_B/\omega_T = 0.012$ and a equal to (a) 6 nm; (b) 4 nm; (c) 2 nm. The dashed curve shows the experimental measurements of Lagois et al. [93]. (Taken from [100]).

potential is chosen. This has been demonstrated by numerical studies [100] which show that the refletivity spectra becomes insensitive to the ABC selection. Calculations were done using the Pekar and Fuchs-Kliewer ABC equations, which correspond to opposite extremes. A model repulsive exponential potential of the form $\hbar\omega_B e^{-z/a}$ was considered, where $\hbar\omega_B$ is the height of the potential at the surface and a measures the spatial extent. Numerical results were reported for light with S-polarization incident onto ZnSe, which has a zinc-blende structure and is isotropic, hence, is convenient for theoretical studies of the reflectivity at non-normal incidence of light. Variations of the surface potential height from 0 up to 0.007 $\hbar\omega_T$ with $a = 5$ nm showed that for the largest value of this potential the differences between the reflectivity curves obtained using the Pekar and Fuchs-Kliewer is negligible. Additional studies were done for CdS surfaces and were compared with experimental data for the $A_{n=1}$ exciton, corresponding to a transition from the Γ_7 valence band to the conduction band. In this case, the CdS surface was characterized by a potential height $\omega_B = 0.012\omega_T$ with the spatial extend a being the adjustable parameter. A good agreement of the calculated curve with the experimental result of Lagois et al. [93] was achieved for $a = 2$ nm., as shown in Fig. 9 for normal incidence. The hexagonal axis c was taken along the surface and perpendicular to the electric field.

On the other hand, Halevi et al. [29] studied the same system employing the generalized form of the ABC equations (Eq. (25)) with an abruptly terminated dead layer. This approach also yielded a good agreement with the experimental data of Lagois et al. [93] when the Pekar ABC's were employed. Although calculations with a continuous potential seem to circumvent the problem of defining the appropriate ABC's, the problem reappears as an arbitrariness in the choice of the parameters of the potential, such as its height and range, as long as they are not independently determined.

6 Thin Film

In this section we describe the interaction of exciton polaritons with surface potentials within thin semiconductor films for both S and P polarizations. Realistic models of the surface potentials with both intrinsic and extrinsic contributions are considered. As in the previous section, the optical response is determined by solving the equation of motion of the excitonic polarization coupled with Maxwell's equation for the electromagnetic field subject to appropriate boundary conditions. A coordinate system is chosen such that the semiconductor layer surfaces are parallel to the $x-y$ plane and perpendicular to the z-axis and such that the field propagates on the $x-z$ plane, so that all wave vectors are of the form $\vec{q} = (Q, 0, q^{\perp})$. We will deal separately with S and P polarized waves.

6.1 *S-polarization*

In this case the equations that couple the excitonic polarization and the electric field were given by Eqs. (60) and (61), which may be manipulated to uncouple the polarization, yielding [41]

$$\begin{aligned}\left[\frac{\partial^4}{\partial z^4} + \left(\varepsilon_\infty \frac{\omega^2}{c^2} - Q^2 + \Gamma^2(z)\right)\frac{\partial^2}{\partial z^2} + 2\left(\frac{\partial \Gamma^2}{\partial z}\right)\frac{\partial}{\partial z}\right] P_y(z) \\ + \left[\left(\varepsilon_\infty \frac{\omega^2}{c^2} - Q^2\right)\Gamma^2(z) - \frac{\omega_p^2\omega^2}{c^2\mathcal{D}} + \frac{\partial^2\Gamma^2}{\partial z^2}\right] P_y(z) = 0.\end{aligned} \tag{65}$$

We consider now a surface potential given by a superposition of exponential potentials and infinite barriers,

$$U(z) = \begin{cases} U_1 e^{-z/a} + U_2 e^{-2z/a} & \\ \quad +U_3 e^{-(L-z)/b} + U_4 e^{-2(L-z)/b}, & 0 < z < L, \\ \infty, & z < 0 \text{ or } z > L, \end{cases} \tag{66}$$

one on each surface of the film of width L. Solutions of Eq. (65) may then be obtained from a the series expansion method by writing $P_y(z)$ as a superposition of bulk solutions

$$P_y(z) = \sum_{s=\pm1,\pm2} A_s e^{iq_s^\perp z} F_s(z), \tag{67}$$

modulated at the surfaces by

$$F_s(z) = a_{0s} + \sum_{n=1}^{\infty} \left[a_{ns} e^{-nz/a} + b_{ns} e^{-n(L-z)/b} \right], \tag{68}$$

where $q_s^\perp$ are the z-components of the wave vector corresponding to the four transverse bulk solutions Eq. (21),

$$q_s^\perp = \pm \left\{ \frac{1}{2} \left[\Gamma_B^2 + \varepsilon_\infty \frac{\omega^2}{c^2} - Q^2 \right] \pm \frac{1}{2} \left[\left(\Gamma_B^2 - \varepsilon_\infty \frac{\omega^2}{c^2} + Q^2 \right)^2 + \frac{4\omega^2 \omega_p^2}{c^2 \mathcal{D}} \right]^{1/2} \right\}^{1/2}, \tag{69}$$

two outgoing and two incoming. The coefficients a_{ns} and b_{ns} can be determined by substituting Eqs. (67)-(69) in Eq. (65), obtaining a simple recurrence relation if the interaction between surfaces is negligible, i.e., whenever $e^{-L/a} \ll 1$ and $e^{-L/b} \ll 1$. Using Eq. (67) and (60) we find

$$E_y(z) = -\frac{4\pi\mathcal{D}}{\omega_p^2} \sum_s A_s e^{iq_s^\perp z} \left[\frac{\partial^2 F_s}{\partial z^2} + \left[\Gamma^2(z) - (q_s^\perp)^2 \right] F_s(z) \right]. \tag{70}$$

The amplitudes A_s and the reflection and transmission amplitudes can then be obtained by applying boundary conditions at $z = 0$ and $z = L$.

In Fig. 10 we show the normal incidence reflectance and transmitance of a CdS film calculated with the Pekar ABC's for different widths of the repulsive transition layer. The calculated spectra display a blueshift as the thickness of the transition-layer increases. This blueshift is also present in the dead-layer model [37] where it is simply interpreted in terms of the quantization of the exciton within the effective width $L_{\text{eff}} = L - (a + b)$ of the active excitonic layer. At frequencies above ω_T, the shift can be approximated by $\delta\omega_i \approx 2[\omega_i - \omega_T](\delta a + \delta b)/L_{\text{eff}}$ where $\delta\omega_i$ is the change of the frequency of the i-th resonance ω_i when the width of the transition layers are increased by δa and δb.

Fig. 11 shows the reflectivity of a GaAs film. As in Fig. 10, the reflectivity displays peaks and dips which correspond to Fabry-Perot like oscillations of the multiple transverse exciton polariton modes propagating in the active

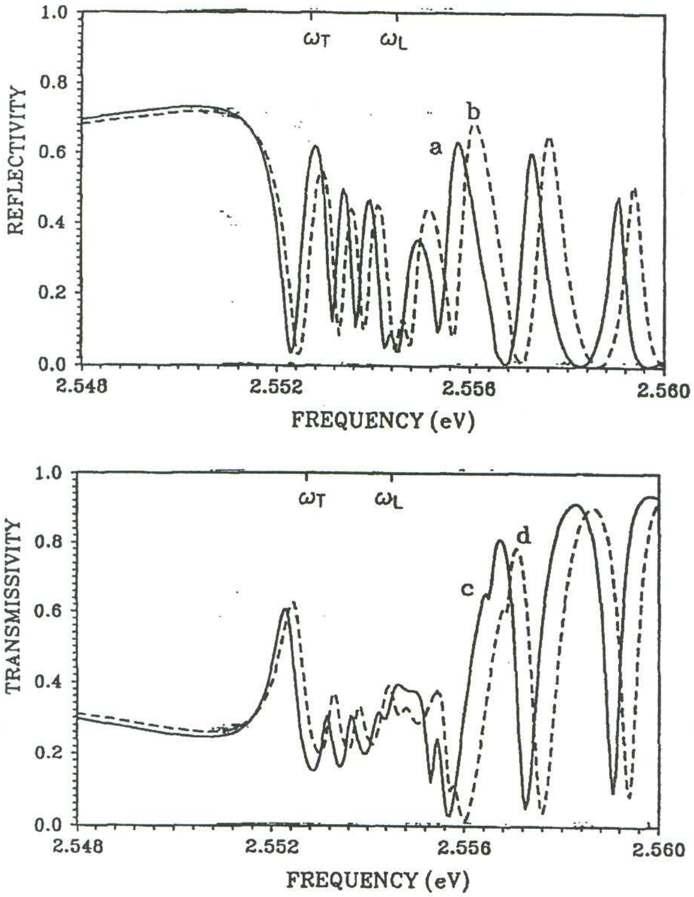

Fig. 10. Normal-incidence reflectance (upper panel) and transmitance (lower panel) of a CdS film of thickness $L = 1000$Å with a repulsive transition layer of thickness $a = b = 60$Å [(a) and (c)] and $a = b = 90$Å [(b) and (d)]. The surface potential heigth is $U_1 = U_3 = 5$ meV and $U_2 = U_4 = 0$ and the material parameters of CdS are $\hbar\omega_T = 2.55272$ eV, $\hbar\omega_p = 0.29396$ eV, $\varepsilon_\infty = 9.1$, $\hbar\nu = 0.124$ meV, and $M = 0.94m_0$. (Taken from [41]).

semiconductor layer. An alternative microscopic formalism due to Cho et al. [102], in which the excitonic wave function is deformed through terms of the form e^{-pz} and $e^{-p(L-z)}$, leads to similar results as the formalism presented above, according to Fig. 11, if we identify the distortion parameter p with $1/a$.

6.2 P-polarization

In this case the equations that couple the excitonic polarization and the electric field were given by Eqs. (62)-(64) which may be combined to eliminate the electric field, yielding

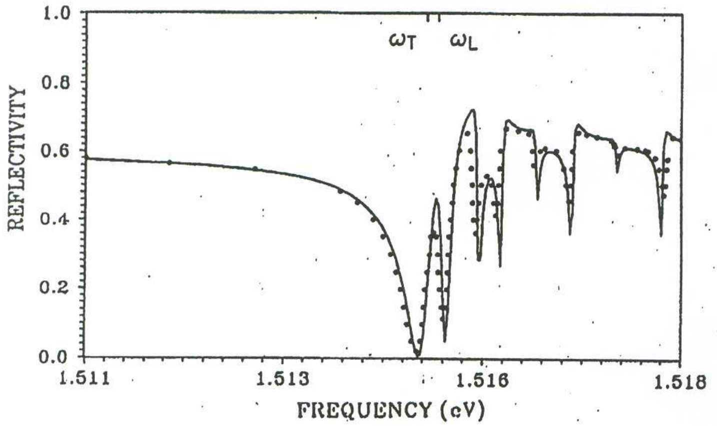

Fig. 11. Normal-incidence reflectance of a GaAs film of thickness $L = 2000$Å calculated with a continuous surface potential with $U_1 = U_3 = 5$ meV, $U_2 = U_4 = 0$ and $a = 65$Å (solid), and calculated with the microscopic theory of Cho et al. [102] with distortion parameter $p = 1/a$. The material parameters of GaAs are $\hbar\omega_T = 1.515$ eV, $\hbar\omega_p = 0.07106$ eV, $\varepsilon_\infty = 12.6$, $\hbar\nu = 0.035$ meV, and $M = 0.298 m_0$. (Taken from [41]).

$$\left(\frac{\partial^2}{\partial z^2} + \varepsilon_\infty \frac{\omega^2}{c^2} - Q^2\right)\left[\left(\frac{\partial^2}{\partial z^2} + \Gamma^2(z)\right) P_x(z)\right] - \frac{\omega_p^2}{\varepsilon_\infty \mathcal{D}}\left(\varepsilon_\infty \frac{\omega^2}{c^2} - Q^2\right) P_x(x) - iQ\frac{\omega_p^2}{\varepsilon_\infty \mathcal{D}}\frac{\partial P_z(z)}{\partial z} = 0, \tag{71}$$

$$iQ\frac{\partial}{\partial z}\left[\left(\frac{\partial^2}{\partial z^2} + \Gamma^2(z)\right) P_x(z)\right] + \frac{\omega^2}{c^2}\frac{\omega_p^2}{\mathcal{D}} P_z(z) - \left(\varepsilon_\infty \frac{\omega^2}{c^2} - Q^2\right)\left(\frac{\partial^2}{\partial z^2} + \Gamma^2(z)\right) P_z(z) = 0. \tag{72}$$

Similar to the S-polarization case, we look for a solution as a superposition of bulk modes

$$\vec{P}(z) = \sum_s A_s e^{iq_s^\perp z} \vec{F}_s(z), \tag{73}$$

modulated by

$$\vec{F}_s(z) = \vec{a}_{0s} + \sum_{n=1}^{\infty}\left[\vec{a}_{ns} e^{-nz/a} + \vec{b}_{ns} e^{-n(L-z)/b}\right], \tag{74}$$

where s takes the values ±1, ±2, and ±3; $q_{\pm3}^\perp = \pm q_3^\perp$ corresponds to the longitudinal solutions which are absent in the case of S-polarization. The coefficients $\vec{a}_{ns}$ and $\vec{b}_{ns}$ in the series (74) are vectors within the incidence plane which may be obtained from the differential equations (71) and (72) assuming that $e^{-L/a} \ll 1$ and $e^{-L/b} \ll 1$. Finally, the amplitudes of the reflected and transmitted fields are determined by applying boundary conditions.

In Fig. 12 we show the reflectance spectra of a $L = 48$ nm thick CuCl film over a MgO substrate for both S- and P-polarization calculated with Pekar's boundary conditions both in the presence of a repulsive exponential potential (Eq. (66)) with $U_1 = U_3 = 10$ meV, $U_2 = U_4 = 0$, and $a = b = 15$Å, and in the absence of a potential. To identify the origin of the abundant structure, the transverse and longitudinal guided mode frequencies, for which $q_1^\perp = n\pi/L$ and $q_3^\perp = l\pi/L$ with integer n and l are indicated. The transverse resonances can be observed near ω_T for both the S and P reflectance spectra. The guided longitudinal resonances are expected to be present in the optical reflectance R_p spectra for P-polarization at frequencies $\hbar\omega_{3,l} \approx \hbar\omega_L + (\hbar^2/2M)(\pi l/L)^2$ ($\omega_L < \omega_{3,l}$). However, due to damping they are not discernible in the reflectivity.

It has been suggested [44] that the coupling to longitudinal exciton polaritons, as well as other surface related effects, might be more readily visible in the quantity [103,104] $\Delta_{45} \equiv R_p - R_s^2$, where both R_s and R_p are obtained at an incidence angle of 45°. The reason for this is that according to Fresnel's formulae for semiinfinite homogeneous local media, $\Delta_{45} = 0$. Thus, when we substract R_s^2 from R_p we eliminate any bulk background contribution to the optical signal, enhancing the relative strength of the surface contributions. Panel (c) of Fig. 12 [57] shows a broad minimum in the Δ_{45} spectra at $\omega > \omega_L$ which results from the coalescence of the first ($l < 5$) longitudinal resonances. It has been found that thinner films allow the separation of the contributions from individual longitudinal resonances.

7 Entrapped states

Similar to electrons trapped in quantum wells, the center of mass of an exciton may be trapped at the surface of a semiconductor if the excitonic potential has a minimum, as would be the case for a Morse potential with both repulsive and attractive components. Although the potential is expected to be narrow and shallow, surface treatment such as intense illumination, electronic and ionic bombardment [105], doping, heating and applying a bias may modify this potential so that it may support a few bound states. In this case, the center-of-mass excitonic spectrum may have discrete energy levels which may manifest themselves in the optical spectra. These have been determined for CdS [106,107] employing a Morse potential

$$U(z) = |U_m| \left[e^{-2(z-z_m)/a} - 2e^{-(z-z_m)/a} \right]. \tag{75}$$

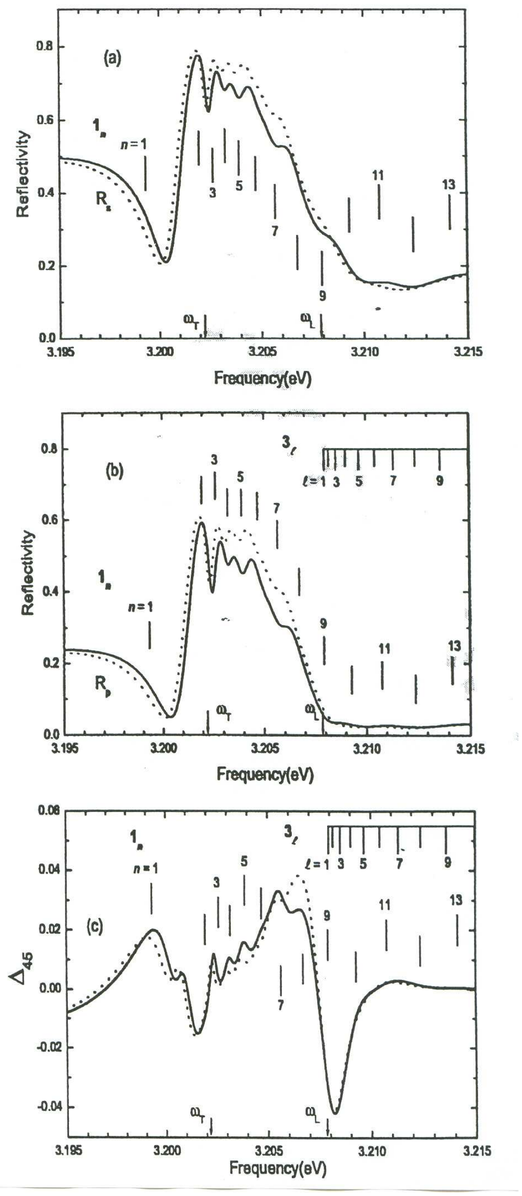

Fig. 12. Reflectivity of S- and P-polarized light (panels (a) and (b) respectively) incident at 45° onto a CuCl film over a MgO substrate. Panel (c) shows the differential reflectance $\Delta_{45} = R_p - R_s^2$. The film thickness is $L = 48$ nm. The solid curve corresponds to a repulsive surface potential (Eq. (66)) with $U_1 = U_3 = 10$ meV, $U_2 = U_4 = 0$, and $a = 15$Å, and the dotted curve correponds to no surface potential. The frequencies for which $q_1^\perp = n\pi/L$ and $q_3^\perp = l\pi/L$ with integer n and l are indicated. The sample parameters are $\varepsilon_\infty = 5.0$, $\hbar\omega_T = 3.2022$ eV, for the Z_3 1s exciton. $\hbar\omega_p = 0.452$ eV, $M = 2.3m_0$, and $\varepsilon_{MgO} = 3.1$. (Taken from [57]).

For example [106], choosing a minimum energy $U_m = -5$ meV, with $z_m = 60$Å and $a = 60$Å yields two bound modes which correspond to the two transverse frequencies (14) $\hbar\omega_{T1} = 2.54990$ eV and $\hbar\omega_{T2} = 2.55237$ eV, slightly below the bulk excitonic transition at $\hbar\omega_T = 2.5527$eV, and similarly, the two

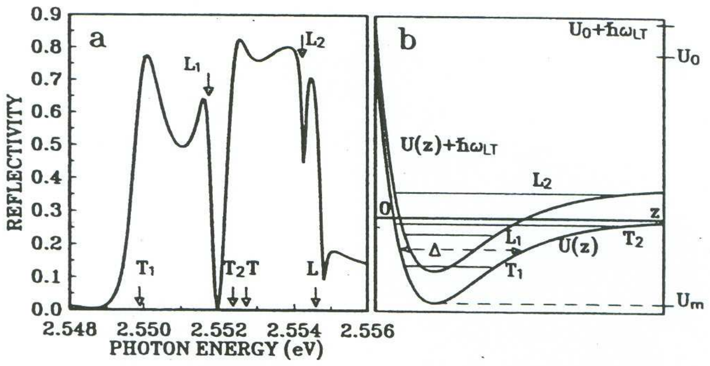

Fig. 13. We display in (a) the reflectivity spectrum of the $A_{n=1}$ exciton of CdS. The interaction of the exciton with the surface is modeled according the potential well depicted in (b). We consider that P-polarized light is incident at an angle of 80°. The parameters are $\hbar\omega_T = 2.55272$ eV, $\hbar\omega_{LT} = 1.86$ meV, $\hbar\nu = 0.124$ meV, $\epsilon_\infty = 9.1$, $M = 0.94m_e$. Taken from Ref. [106]

longitudinal frequencies (24) $\hbar\omega_{L1} = 2.55176$ eV and $\hbar\omega_{L2} = 2.55423$ eV. Fig. 13 shows that the reflection spectra for P-polarized light displays peaks due to the excitation of all of the entrapped states.

The confinement of exciton states at the surface of $\mathrm{CdS}_{1-x}\mathrm{Se}_x$ with a small quantity of Se, and at the surface of CdSe would lead to a very rich reflectance spectra for P polarized light [108,109]. Unfortunately, the exciton damping at the surfaces inhibits the detailed experimental observation of this structure, as the peaks corresponding to different entrapped states overlap each other. Nevertheless, the lineshape depends strongly on the exciton confinement and quantization in the near-surface region. An excelent agreement between theory and experiment was obtained by adjusting the parameters of a complex potential of the form

$$U(z) = U_1 e^{-(z-z_1)/a_1} - U_2 e^{-(z-z_2)/a_2} + iU_3 e^{-(z-z_3)/a_3}. \qquad (76)$$

As discussed in Sec. 6, the $\Delta_{45} = R_p - R_s^2$ spectra at an incidence angle of 45° is very sensitive to the surface, as its value would be null according to Fresnel's formulae. It has very recently been suggested [57] that this sensitivity might permit observation of the individual resonances due to the excitation of both transverse and longitudinal excitons entrapped at surfaces. Fig. 14 shows the Δ_{45} spectra calculated for a thin CuCl film of width $d = 48$nm wih a Morse complex surface potential that is able to sustain two transverse bound states [57]. Fig. 14 shows that the contributions of the transverse entrapped states to the S and P reflectivity is barely visible, while the contribution of the longitudinal entrapped states to the P polarized reflectance seems negligible, and their contribution for the S polarized reflectance is null. However, both kinds of resonances are clearly visible in the Δ_{45} spectrum. Other experimental and theoretical studies of the optical manifestation of excitons trapped at

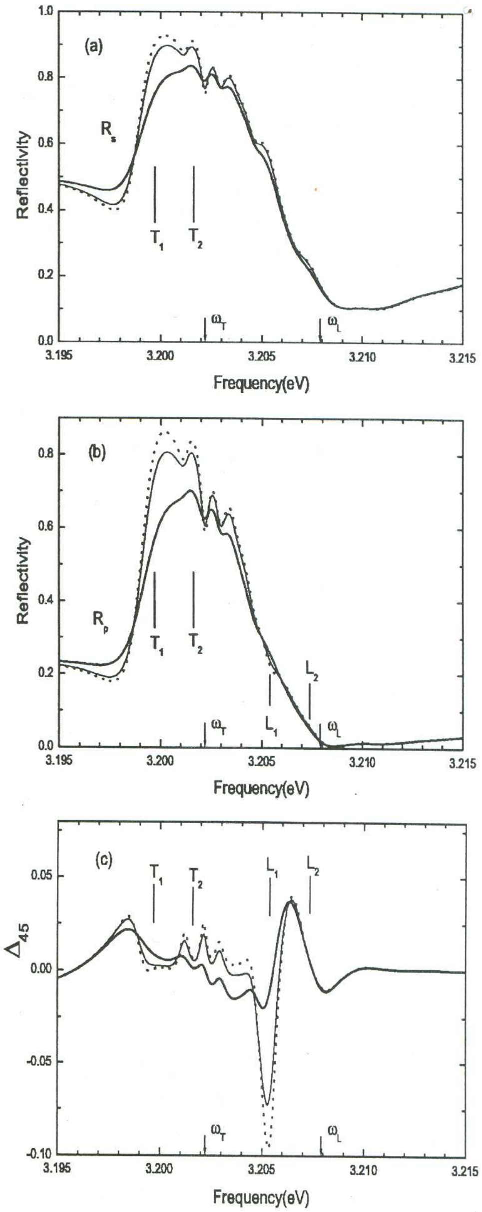

Fig. 14. We display spectra of R_s in (a), R_p in (b) calculated at an angle of incidence of 45° and Δ_{45} in (c) for CuCl film of thickness $d = 48$ nm deposited on a MgO substrate. An intrinsic surface-potential well has been considered with parameters $U_m = 0.4$ meV, $z_m = 50$ Å, $a = 50$ Å, $U_d = 10$ meV and $b = 15$ Å. Three values of the damping factor $\hbar\Delta\nu(0)$ are included; 0 (dotted curve), 0.4 (thin solid line) and 2.0 (thick solid line). Taken from Ref. [57]

surfaces are presented in Refs. [108,109,105].

8 Layered systems

We have shown above that when the polarization equation accounts for a continuous surface potential, the polarization and wave equations may be solved numerically (Sec. (5.3)), or using a series expansion (Sec. (6)). Here we describe a multistep method, which is an alternative method to solve differential equations, and we apply it to the study of single films, superlattices and microcavities.

To describe the multistep method we consider a semiconductor layer. We have seen that the interaction of excitons with the surface may be modeled with a continuous surface potential, and the optical response is then determined by solving the coupled equations (56) and (59), subject to appropriate boundary conditions. The surfaces of the layer are assumed parallel to the $x-y$ plane and perpendicular to the z-axis and the plane of incidence is taken to be the $x-z$ plane. As S and P polarized waves are uncoupled, we study them separately.

8.1 Transfer matrix for S-polarization

For S polarized light $\vec{P}(\vec{r},t) = (0, P_y(z)e^{i(Qx-\omega t)}, 0)$ and $\vec{P}_y(z)$ obeys the differential equation (65), which we solve following Kiselev's [110] multistep method. We divide the z axis into intervals $\mathcal{I}_i = (z_{i-1}, z_i)$ of width $d_i = z_i - z_{i-1}$ so small that the continuous potential may be assumed to be constant within each of them, and we construct a transfer matrix for each step. Within $\mathcal{I}_i$, $P_y(z)$ can be written as a superposition of terms with the form $e^{\pm i q^{\perp}_{ni} z}$, with

$$\begin{aligned}\left(q^{\perp}_{ni}\right)^2 = &\frac{1}{2}\left[\Gamma^2(\overline{z}_i) + \varepsilon_0\frac{\omega^2}{c^2} - Q^2\right] \\ &\pm\frac{1}{2}\left[\left(\Gamma^2(\overline{z}_i) - \varepsilon_0\frac{\omega^2}{c^2} + Q^2\right)^2 + \frac{4\omega^2\omega_p^2}{cD}\right]^{1/2},\end{aligned} \tag{77}$$

where $n = 1, 2$ denote the two transverse exciton-polariton modes corresponding to the i-th step, $\overline{z}_i = (z_i + z_{i-1})/2$ and the surface potential at $\mathcal{I}_i$ is accounted for through $\Gamma^2(\overline{z}_i)$. Since there are four propagating modes at each step, we require four independent fields to construct the transfer matrix. We chose the tangential components of the electric field E_y, of the magnetic field H_x, the excitonic polarization P_y and its normal derivative $\partial P_y/\partial z$, all of which are continuous quantities according to Maxwell's equations and Eq. (60). Each field is expressed in terms of the amplitudes of the modes traveling to the right (increasing z) $(+)$ and left $(-)$. Thus we write for $z \in \mathcal{I}_i$

$$E_y(z) = \sum_{n=1}^{2} \left[E_{ni}^{+} e^{iq_{ni}^{\perp} z} + E_{ni}^{-} e^{-iq_{ni}^{\perp} z} \right], \qquad H_x(z) = \frac{i}{\omega} \frac{\partial E_y}{\partial z}, \tag{78}$$

$$P_y(z) = \sum_{n=1}^{2} \chi_{ni} \left[E_{ni}^{+} e^{iq_{ni}^{\perp} z} + E_{ni}^{-} e^{-iq_{ni}^{\perp} z} \right], \qquad P_y'(z) = \frac{\partial P_y(z)}{\partial z}, \tag{79}$$

where

$$\chi_{ni} = \frac{\omega_p^2}{4\pi \mathcal{D}} \frac{1}{(q_{ni}^{\perp})^2 - \Gamma^2}. \tag{80}$$

Eqs. (78) and (79) may be summarized in matrix form as

$$\begin{bmatrix} \mathcal{F} \\ \mathcal{P} \end{bmatrix}_z = G_i \begin{bmatrix} \mathcal{A}_{1i} \\ \mathcal{A}_{2i} \end{bmatrix}_z, \tag{81}$$

where

$$\mathcal{F} = \begin{bmatrix} E_y \\ H_x \end{bmatrix}, \qquad \mathcal{P} = \begin{bmatrix} P_y \\ P_y' \end{bmatrix}, \qquad \mathcal{A}_{ni}(z) = \begin{bmatrix} E_{ni}^{+} e^{+iq_{ni}^{\perp} z} \\ E_{ni}^{-} e^{-iq_{ni}^{\perp} z} \end{bmatrix}, \tag{82}$$

$$G_i = \begin{bmatrix} 1 & 1 & 1 & 1 \\ -Y_{1i} & Y_{1i} & -Y_{2i} & Y_{2i} \\ \chi_{1i} & \chi_{1i} & \chi_{2i} & \chi_{2i} \\ iq_{1i}^{\perp}\chi_{1i} & -iq_{1i}^{\perp}\chi_{1i} & iq_{2i}^{\perp}\chi_{2i} & -iq_{2i}^{\perp}\chi_{2i} \end{bmatrix}, \tag{83}$$

with surface admittance $Y_{ni} = q_{ni}^{\perp}/q_0$. Evaluating Eq. (81) at z_{i-1} and z_i we may eliminate the amplitudes E_{ni}^{+} and E_{ni}^{-} to write [43]

$$\begin{bmatrix} \mathcal{F} \\ \mathcal{P} \end{bmatrix}_{z_i} = M_i \begin{bmatrix} \mathcal{F} \\ \mathcal{P} \end{bmatrix}_{z_{i-1}}, \tag{84}$$

where

$$M_i = G_i T_i G_i^{-1} \tag{85}$$

is the transfer matrix of the interval $\mathcal{I}_i$, with

$$T_i = \mathrm{diag}(e^{iq_{1i}^{\perp} d_i}, e^{-iq_{1i}^{\perp} d_i}, e^{iq_{2i}^{\perp} d_i}, e^{-iq_{2i}^{\perp} d_i}) \tag{86}$$

a diagonal translation matrix of dimension 4×4.

As M_i transfers continuous quantities $\mathcal{F}$ and $\mathcal{P}$, to build the transfer matrix M of a finite layer, such that

$$\begin{bmatrix} \mathcal{F} \\ \mathcal{P} \end{bmatrix}_{z_R} = M \begin{bmatrix} \mathcal{F} \\ \mathcal{P} \end{bmatrix}_{z_L}, \tag{87}$$

we simply multiply

$$M = M_N \cdots M_2 M_1, \tag{88}$$

where N is number of intervals, $z_L = z_0$ and $z_R = z_N$ are the leftmost and rightmost positions within the finite layer. Notice that for any thin interval $\det M_i = 1$ and therefore, for any layer $\det M = 1$.

8.2 Transfer matrix for P-polarization

The polarization vector for P polarized light has the form $\vec{P}(\vec{r},t) = (P_x, 0, P_z)e^{i(Qx-\omega t)}$ and obeys equations (71) and (72). We employ a multistep method similar to that introduced above for S polarization. Now we have to account at each interval $\mathcal{I}_i$ for a longitudinal mode with wavevector

$$(q_{3i}^{\perp})^2 = \Gamma^2(\overline{z}_i) - \frac{\omega_p^2}{\varepsilon_0 \mathcal{D}}. \tag{89}$$

besides the two transverse modes which appear for S polarization, with wavevectors given by Eq. (77). At each interval the fields are given by a superposition of three waves propagating in the z direction and other three waves propagating in the $-z$ direction. Consequently, six independent fields are required to construct the transfer matrix. We chose the continuous fields E_x, H_y, P_x, P_z, $\partial P_x/\partial z$, and $\partial P_x/\partial z$, which in analogy to Eqs. (78) and (79) have the following form

$$E_x(z) = \sum_{n=1}^{3} \left[E_{ni}^{+} e^{iq_{ni}^{\perp} z} + a_n E_{ni}^{-} e^{-iq_{ni}^{\perp} z} \right], \tag{90}$$

$$H_y(z) = \sum_{n=1}^{2} Y_{ni} \left[E_{ni}^{+} e^{iq_{ni}^{\perp} z} + E_{ni}^{-} e^{-iq_{ni}^{\perp} z} \right], \tag{91}$$

$$P_x(z) = \frac{\omega_p^2}{4\pi \mathcal{D}} \sum_{n=1}^{3} \chi_{ni} \left[E_{ni}^{+} e^{iq_{ni}^{\perp} z} + a_n E_{ni}^{-} e^{-iq_{ni}^{\perp} z} \right], \tag{92}$$

$$P_z(z) = \frac{\omega_p^2}{4\pi\mathcal{D}} \sum_{n=1}^{3} \chi_{ni} D_{ni} \left[-E_{ni}^{+} e^{iq_{ni}^{\perp} z} + a_n E_{ni}^{-} e^{-iq_{ni}^{\perp} z} \right], \tag{93}$$

where for the transverse modes $n = 1, 2$, $Z_{ni} = (q_{ni}^{\perp} c)/(\varepsilon_{ni}\omega)$ is the surface impedance, $Y_{ni} = 1/Z_{ni}$ is the surface admittance, $\varepsilon_{ni} = \epsilon_\infty + 4\pi\chi_{ni}$ is the dielectric response evaluated at the n-th mode of the i-th interval, χ_{ni} is the corresponding susceptibility given by Eq. (80), $D_{ni} = Q/q_{ni}^{\perp}$, and $a_n = -1$, while for the longitudinal mode $D_{3i} = -q_{3i}/Q$, and $a_3 = 1$. In matrix notation, we write

$$\begin{bmatrix} \mathcal{F} \\ \mathcal{P} \end{bmatrix}_z = G_i \begin{bmatrix} \mathcal{A}_{1i} \\ \mathcal{A}_{2i} \\ \mathcal{A}_{3i} \end{bmatrix}_z , \tag{94}$$

where

$$\mathcal{F} = \begin{bmatrix} E_x \\ H_y \end{bmatrix}, \qquad \mathcal{P} = \begin{bmatrix} P_x \\ P_z \\ \partial P_x/\partial z \\ \partial P_z/\partial z \end{bmatrix} \qquad \mathcal{A}_{ni}(z) = \begin{bmatrix} E_{ni}^{+} e^{+iq_{ni}^{\perp} z} \\ E_{ni}^{-} e^{-iq_{ni}^{\perp} z} \end{bmatrix}, \tag{95}$$

$$G_i = \begin{bmatrix} 1 & -1 & 1 & -1 & 1 & 1 \\ Y_{1i} & Y_{1i} & Y_{2i} & Y_{2i} & 0 & 0 \\ \chi_{1i} & -\chi_{1i} & \chi_{2i} & -\chi_{2i} & \chi_{3i} & \chi_{3i} \\ -D_{1i}\chi_{1i} & -D_{1i}\chi_{1i} & -D_{2i}\chi_{2i} & -D_{2i}\chi_{2i} & D_{3i}\chi_{3i} & -D_{3i}\chi_{3i} \\ iq_{1i}^{\perp}\chi_{1i} & iq_{1i}^{\perp}\chi_{1i} & iq_{2i}^{\perp}\chi_{2i} & iq_{2i}^{\perp}\chi_{2i} & iq_{3i}^{\perp}\chi_{3i} & iq_{3i}^{\perp}\chi_{3i} \\ -iq_{1i}^{\perp}D_{1i}\chi_{1i} & iq_{1i}^{\perp}D_{1i}\chi_{1i} & -iq_{2i}^{\perp}D_{2i}\chi_{2i} & iq_{2i}^{\perp}D_{2i}\chi_{2i} & iq_{3i}^{\perp}D_{3i}\chi_{3i} & iq_{3i}^{\perp}D_{3i}\chi_{3i} \end{bmatrix}. \tag{96}$$

The field and polarization at the edges of $\mathcal{I}_i$ are related again by Eq. (84), where the transfer matrix M_i is given by Eq. (85) but where G_i is now the 6×6 matrix given by Eq. (96) instead of the 4×4 matrix (83), and where

$$T_i = \mathrm{diag}(e^{iq_{1i}^{\perp} d_i}, e^{-iq_{1i}^{\perp} d_i}, e^{iq_{2i}^{\perp} d_i}, e^{-iq_{2i}^{\perp} d_i}, e^{iq_{3i}^{\perp} d_i}, e^{-iq_{3i}^{\perp} d_i}), \tag{97}$$

is a diagonal translation matrix of dimension 6×6 instead of the 4×4 matrix (86). In analogy to the S-polarization case, we use the continuity of $\mathcal{F}$ and $\mathcal{P}$ to obtain the total transfer matrix of a finite layer. The result is again given by Eqs. (87) and (88), but in this case, the transfer matrix of each interval is of dimension 6 × 6. As in the previous case, $\det M = 1$.

8.3 Transfer matrix collapse

We have shown above that the transfer matrix of a single layer is of dimension $m \times m$, where m is the number of modes, including those moving in the z and in the $-z$ direction. For S and P-polarization the corresponding matrices are of dimension 4×4 and 6×6, respectively. The usual optical transfer matrix [111] of an insulator layer is of dimension 2×2. Therefore, at the interface between a nonlocal semiconductor and a local insulator we should account for this difference. To match the matrix of a semiconductor with that of the insulator, it is necessary to reduce the dimension of the semiconductor matrix. To that end, we apply ABC's at the interface to collapse the $n \times n$ matrices to 2×2 matrices. We use the generalized form for the ABC's given by Eq. (25).

In the case of S polarization the additional boundary conditions at the two interfaces of the semiconductor layer yield two equations which, together with the third and fourth rows of Eq. (87) allow us to eliminate the two components of $\mathcal{P}(z_L)$ and the two components of $\mathcal{P}(z_R)$, and to obtain a relation [43]

$$\mathcal{F}(z_R) = N\mathcal{F}(z_L), \tag{98}$$

which involves only the two compnents E_y and H_x of the field $\mathcal{F}$ at z_L and z_R. The matrix

$$N = M_{ff} - (M_{fp} + M_{fp'}\alpha)S^{-1}(\alpha M_{pf} + M_{p'f}) \tag{99}$$

plays then the role of an optical 2×2 transfer matrix which may be simply multiplied with the transfer matrices

$$M_I = \begin{bmatrix} \cos(q_I^{\perp} d_I) & -iY_I \sin(q_I^{\perp} d_I) \\ -iZ_I \sin(q_I^{\perp} d_I) & \cos(q_I^{\perp} d_I) \end{bmatrix}, \tag{100}$$

of the adjacent insulating layers, where $Z_I = q_0/q_I^{\perp} = 1/Y_I$ is the surface impedance of the insulator of width d_I, Y_I is its surface admittance, and $q_I^{\perp}$ is the normal component of the wavevector within the insulator. Here, we wrote the transfer matrix of the semiconductor in block form

$$M = \begin{pmatrix} M_{ff} & M_{fp} & M_{fp'} \\ M_{pf} & M_{pp} & M_{pp'} \\ M_{p'f} & M_{p'p} & M_{p'p'} \end{pmatrix}, \tag{101}$$

where M_{ff} is 2×2 block that connects $\mathcal{F}(z_L)$ directly to $\mathcal{F}(z_R)$, M_{fp} is the 2×1 block that connects $\mathcal{P}(z_L)$ to $\mathcal{F}(z_R)$, while $M_{fp'}$ is the block that connects $(\partial/\partial z)\mathcal{P}(z_L)$ to $\mathcal{F}(z_R)$, and so on, and

$$S = \alpha M_{pp} + \alpha M_{pp'} \alpha + M_{p'p} + M_{p'p'} \alpha \tag{102}$$

is a 1×1 block. To arrive at Eq. (99) we normalized the coefficient $\beta_y \to 1$ in the generalized ABC (25) and we renamed $\alpha_y \to \alpha$.

In the P-polarization case, we apply the ABC's (25) at both interfaces, obtaining 4 equations, which together with rows 3-6 of Eq. (87) permits the elimination of the four components of $\mathcal{P}(z_L)$, and the four components of $\mathcal{P}(z_R)$, and to find a relation of the form (98) between the two components E_x and H_y of the field $\mathcal{F}$ at z_L and z_R, through another 2×2 transfer matrix N, appropriate for P-polarization [38], which may be simply multiplied by the transfer matrices

$$M_I = \begin{bmatrix} \cos(q_I^{\perp} d_I) & iY_I \sin(q_I^{\perp} d_I) \\ iZ_I \sin(q_I^{\perp} d_I) & \cos(q_I^{\perp} d_I) \end{bmatrix}, \tag{103}$$

of the adjacent insulating layers. The expression for N is identical to that for S polarization given in Eqs. (99) and (102), but now M_{fp}, $M_{fp'}$, M_{pf}, M_{pp}, $M_{pp'}$, $M_{p'f}$, $M_{p'p}$, and $M_{p'p'}$, are 2×2 block submatrices, we normalized the ABC coefficients $\beta_x = \beta_z = 1$ (Eq. (25)) and we introduced the 2×2 ABC matrix $\alpha = \mathrm{diag}(\alpha_x, \alpha_z)$.

8.4 Superlattice normal modes

We consider the superlattice depicted in Fig. 15, which is a bilayer periodic system. The insulator layers (I) have dielectric constant ϵ_i and thickness d_i, while the semiconductor layers (S) have dielectric function $\epsilon(\omega, \vec{q})$ and thickness d_S. For S-polarization the transfer matrix of the semiconductor is of dimension 4×4, while that for P-polarization is of dimension 6×6. To match these matrices with those of the insulator, the matrices are first collapsed into

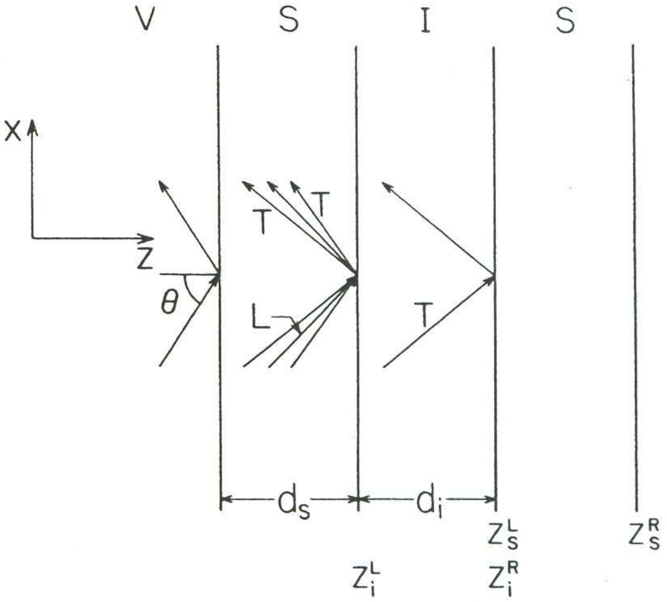

Fig. 15. Superlattice made up of alternating excitonic semiconductor layers (S) of thickness d_s and isulator layers (I) of thickness d_i. We illustrate the transverse (T) modes that may propagate within insulating layers and the manyfold transverse (T) and longitudinal (L) modes that may propagate within semiconductor layers. We also show a wave incident from vacuum (V) incident at an angle θ and the corresponding reflected wave. Taken from Ref. [38]

2×2 matrices N, so that the optical transfer matrix of a period is $M = M_I N$, as described in the previous section.

According to Bloch's theorem, the field at a periodic system may be written as a superposition of Bloch waves, whose amplitude is simply multiplied by a *phase* factor e^{ipd} whenever we apply a translation of one period $d = d_s + d_i$. Thus, e^{ipd} is an eigenvalue of the transfer matrix M, and we may write [38]

$$\left[M - I e^{ipd}\right] \mathcal{F}(0) = 0. \tag{104}$$

As $\det M = 1$, the dispersion relation of the normal modes becomes simply

$$2\cos(pd) = \mathrm{tr}(M). \tag{105}$$

Here p is the one-dimensional Bloch's wavevector and tr stands for the trace of the matrix. Eq. (104) is valid for both S and P polarizations.

Eq. (104) allows us to obtain the surface impedances $Z_s \equiv -E_y(0)/H_x(0)$ and

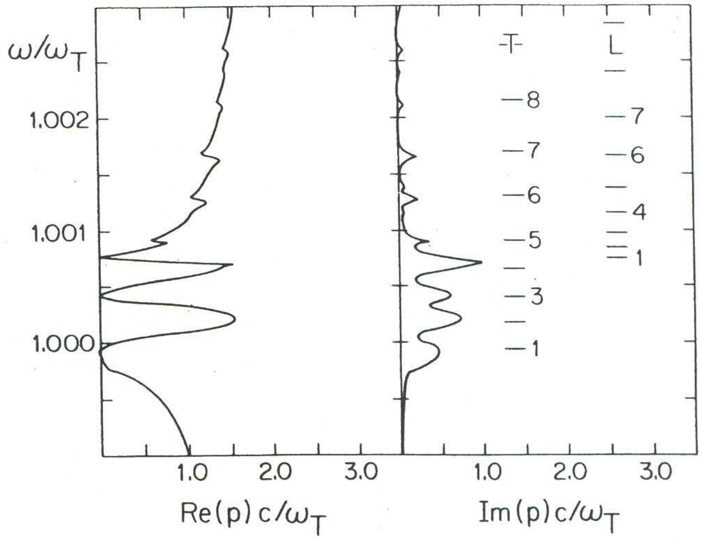

Fig. 16. Disperison relation ω vs. $p = \mathrm{Re}\,p + i\mathrm{Im}\,p$ of the electromagnetic normal modes of a periodic superlattice made up of alternating CdS and vacuum layers of width $d_s = d_i = 773$Å. The parallel component of the wavevector Q is chosen so that coupling with light incident at and angle of $\theta = 60°$ is possible. The frequencies of the transverse (T) and longitudinal (L) resonances are indicated. Taken from Ref. [38]

$Z_p \equiv E_x(0)/H_y(0)$ of a truncated semiinfinite superlattice, which has the form

$$Z_\alpha = \pm\frac{M_{12}}{M_{11} - e^{ipd}} = \pm\frac{M_{22} - e^{ipd}}{M_{21}}, \tag{106}$$

where the upper sign (+) corresponds to S polarization and the lower sign (−) corresponds to P polarization. The optical reflectance for a semiinfinite superlattice can be obtained from the surface impedance using Eq. (34) for S and Eq. (39) for P polarized light.

In Fig. 16 we show the dispersion relation of the P polarized normal modes of a superlattice made up of alternating CdS and insulator layers, with parameters corresponding to the $A_{n=1}$ excitonic transition [38], as obtained from Eq. (105). For simplicity, we assumed a constant excitonic potential up to the interface and we considered a vacuum gap as the insulator layer. At frequencies near the excitonic transition, the one-dimensional Bloch's wavevector p shows a structure which is produced by the multiple Fabry-Perot resonances of the transverse and longitudinal modes excited within the excitonic layer. To understand these resonances, in Fig. 17 we show the dispersion relation of the modes of a homogeneous semiconductor. At frequencies below ω_T there are no longitudinal waves, only one long-wavelength transverse mode propagates. The resonances apparent in Fig. 16 below ω_L appear when this mode

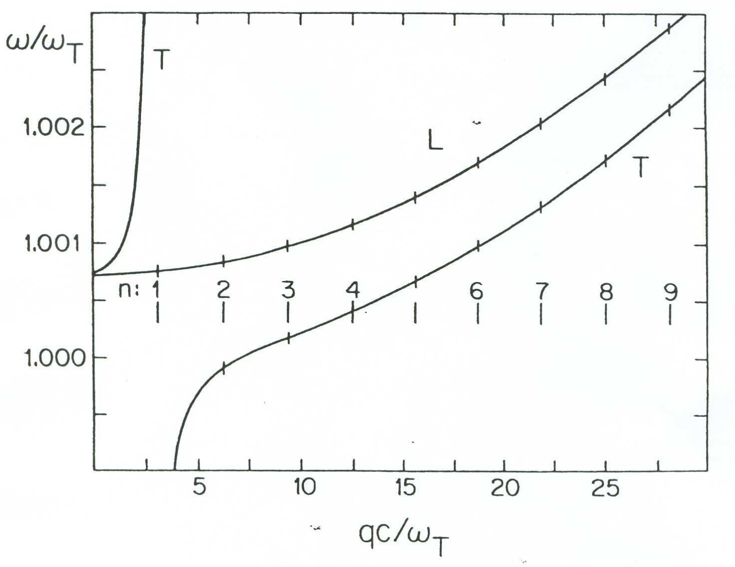

Fig. 17. Dispersion relation ω vs. q of the two transverse (T) and the longitudinal (L) exciton polariton modes of CdS, close to its $A_{n=1}$ excitonic resonance, which may couple to light incident at an angle $\theta = 60°$. The wavevectors $n\pi/d_s$ which lead to resonant behavior in the semiconductor layer of thickness $d_s = 773$Å are indicated. Taken from Ref. [38]

satisfies approximately the guided mode resonance condition $q_1^\perp = n\pi/d_s$. At $\omega > \omega_L$ one additional longitudinal wave emerges, with a wavevector that grows rapidly with ω and originates resonances whenever $q_3^\perp = n\pi/d_s$. The longitudinal field is confined within the semiconductor layers since there is no longitudinal mode propagating in the local media, so the corresponding resonances may be regarded as guided longitudinal modes.

Above the critical frequency $\omega_c = \left[\omega_T^2 + \omega_p^2/(\varepsilon_0 - \sin^2(\theta))\right]^{1/2}$ a second transverse mode propagates in the semiconductor; it has a long wavelength and its dispersion follows closely that obtained with the local model. Consequently, the structure of the Bloch wave vector becomes somewhat complex, as it is produced by the resonances of one longitudinal and two transverse modes. In our example, no resonances due to the second transverse waves are visible.

In Fig. 18 we show the optical reflectance for P polarization of a semiinfinite superlattice corresponding to that presented above. The reflectance exhibits peaks which correspond to the longitudinal and transverse guided modes discussed above, both of which may couple at the surface with the incoming and reflected transverse waves in vacuum. The reflectance of a superlattice has also been calculated with other ABC's as well. As expected, the Ting et al. ABC leads to a smaller coupling between modes at the surfaces and therefore to a smother structure in the reflectance [38]. When surface dead layers are accounted for, the active excitonic layer thickness decreases and therefore the resonance condition of the excitonic waves is met at higher energies.

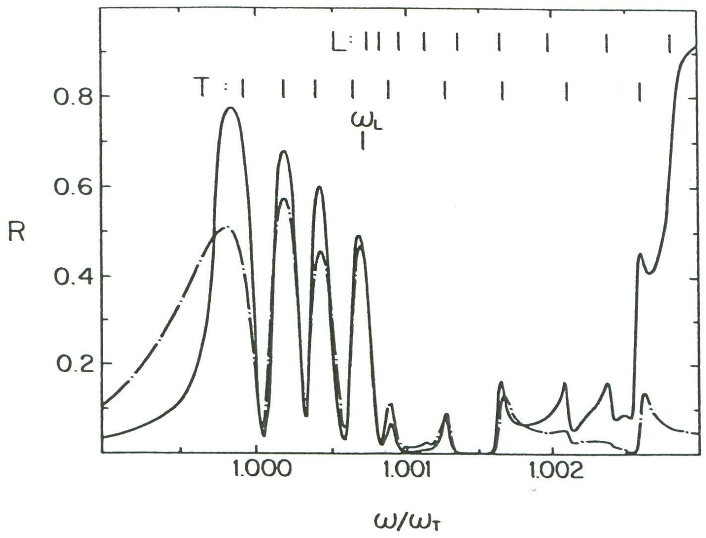

Fig. 18. Reflectivity spectra of a semi-infinite superlattice (solid) and of a single CdS film (dashed) calculated with the Pekar ABC.The frequencies of the transverse (T) and longitudinal resonances are indicated, as well as ω_L. Taken from Ref. [38] .

Consequently, the resonances of the reflectivity suffer a blue shift [39].

8.5 Entrapped states in superlattices

In Sec. 7 we have shown the possibility of trapping longitudinal and transverse exciton states near surfaces of semiconductors subject to potentials with an attractive well. The longitudinal trapped states manifest themselves as structures in the reflectance for P polarized light below ω_L, while the transverse states appear as structures below ω_T for both S and P polarization. Using the transfer matrix formalism presented above, the optical spectra of superlattices with continuous potentials capable of trapping excitons at their surfaces can be calculated. Fig. 19 shows the reflectivity spectra calculated for both S and P polarizations for a semiinfinite two-layer periodic system with one layer being of a semiconductor of thickness $d_s = 620$ Å and the other layer being an insulator of thickness $d_i = 480$ Å. The excitons are trapped by a Morse potential well (75) with the same parameters as in Sec. 7. The coupling of light to the localized transverse modes manifest themselves as broad maxima for S and P polarization, while longitudinal entrapped modes yield sharp dips for P polarization only, somewhat shifted from the calculated energy eigenvalues. Notice that these structures are enhanced in the superlattice (Fig. 19) as compared to the corresponding structures in semiinfinite semiconductors (Fig. 13) simply due to their large surface to volume ratio. Notice also that the entrapped states produce an abundant structure below ω_T and ω_L, where only one transverse wave may propagate across the semiconductor layers.

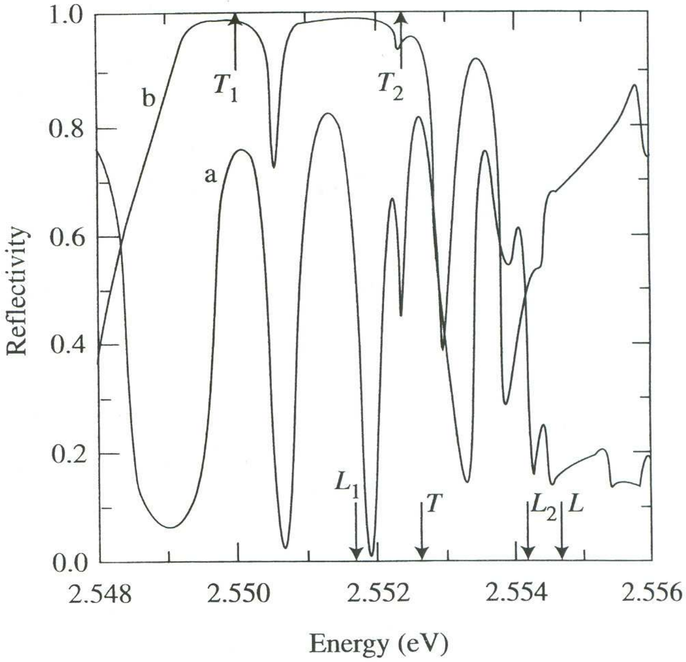

Fig. 19. P-polarized (a) and S-polarized (b) reflectivities of a semiinfinite superlattice made up of aleternating CdS and vacuum layers of widths $d_s = 620$ Å and $d_I = 480$Årespectively for frequencies close to the $A_{n=1}$ excitonic transition. The interaction of the excitons with the surfaces are modeled with a truncated Morse potential of depth $U_m = -5$ meV, range $a = 60$Åand centered at $z_m = 60$Åfrom each surface. The angle of incidence is $\theta = 80°$. We indicate the energy eigenvlaues of the bound states in the potential well as T_i and L_i for the transverse and longitudinal modes, respectively. Taken from Ref. [112]

8.6 Optical response of microcavities

The transfer matrix method presented in Secs. 8.1, 8.2, and 8.3 may be used to study novel optical devices such as microcavities. These consist of Fabry-Perot resonators in whose interior a quantum system is placed. By tuning the resonance frequency of the cavity to a transition energy of the system, interesting effects such as Rabi splitting may be explored. Solid state microcavities may be built by growing dielectric mirrors made up of superlattices, as in the previous sections, and the quantum system may be a quantum well or an excitonic semiconductor. In this section we describe the optical response of excitons in semiconductor microcavities [113,5,114,115,48,53,49,47,116]. As an illustrative example we describe the work of Tredicucci et al. [53,113], who grew several samples by MBE. Full-cavity samples were made of two Bragg reflectors composed of $\sim$ 20 bilayers of $Al_{0.18}Ga_{0.82}As/AlAs$, with corresponding dielectric functions $\varepsilon_1 = 11.7$ and $\varepsilon_2 = 9.8$ and thicknesses of 595 and 696Årespectively. The reflectors were separated by an active layer made up of GaAs. Different cavity widths close to $\lambda/2$ were explored, i.e., the cavity was tuned close to the

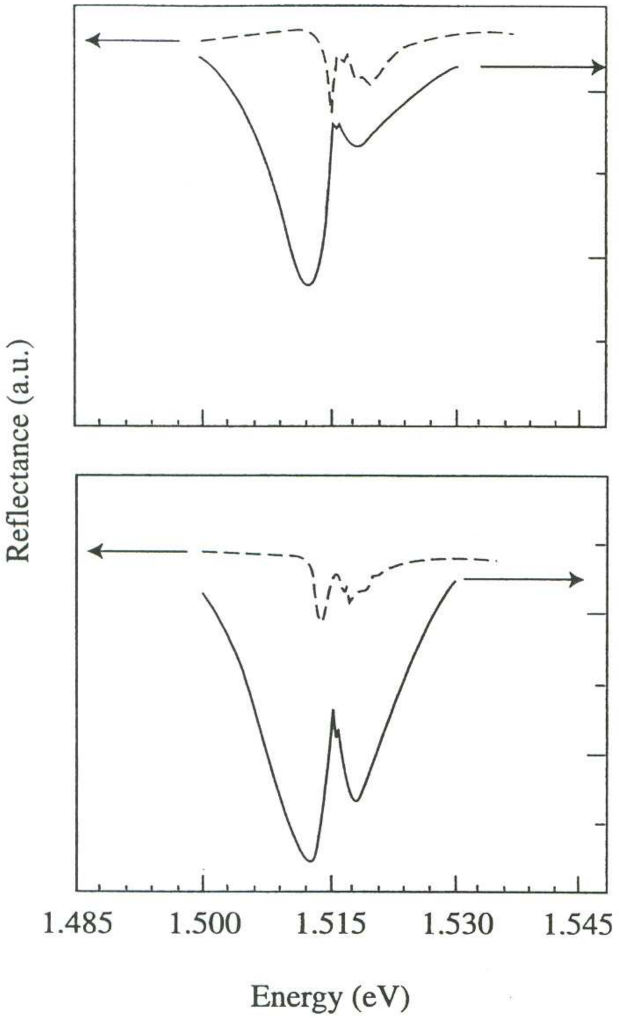

Fig. 20. Normal incidence calculated (solid curve) and the experimental (dashed curve) reflectivities for full microcavities. The cavity width was taken as 1148 Å and 1160 Å for the upper and lower panels, respectively. The scaling of the experimental data is unspecified. Taken from Ref. [112]

the excitonic transition of $GaAs$ and the optical reflectance and luminiscence were measured as the optical energy was scanned close to the resonance. Two main peaks and several secondary peaks were observed and ascribed to the Rabi-splitted excitonic transition, with the secondary structure arising from the center of mass quantization. Qualitative agreement (Fig. 20) was obtained between experiment [5] and a calculation [112] in which the active excitonic layer of GaAs is described according to Hopfield and Thomas model (Eq. (15)) with no surface potential, with parameters $\hbar\omega_T = 1.515$ eV, $\hbar\omega_p = 0.07106$ eV, $h\nu = 4 \times 10^{-4}$ eV, $\varepsilon_\infty = 12.53$, and $M = 0.2 m_0$, and with active layer widths 1148 and 1160 Å.

Similar features have been observed in the luminescence spectra of open and

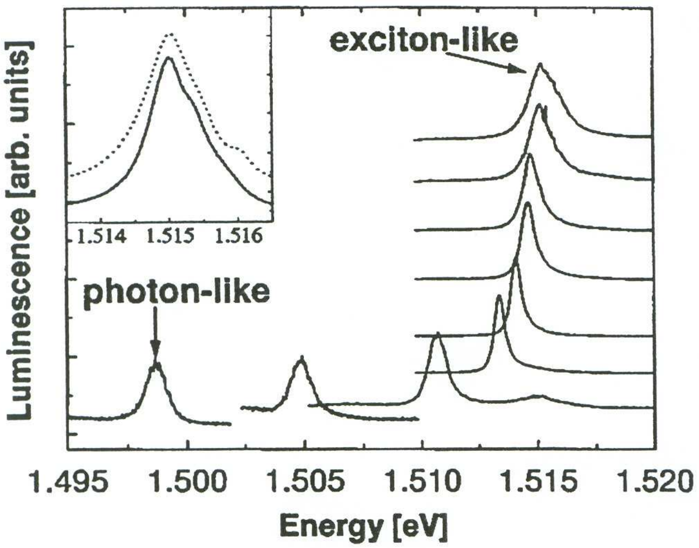

Fig. 21. Low temperature luminescence spectra of an open wedge shaped GaAs microcavity taken for different spot positions over the wedge, so that different spectra correspond to different cavity thickness, increasing from top to bottom. The inset shows an experimental (solid curve) and calculated (dashed curve) luminescence spectra for the half cavity. Taken from Ref. [114].

closed microcavities [114] of continuosly varying width, which can be accomplished by growing a wedge shaped cavity and varying the lateral position at which it is excited (Fig. 21). For very wide open cavities a peak below the excitonic transition is observed, corresponding to a photon-like exciton-polariton (Fig. 3) which becomes exciton-like for narrower cavities as the luminiscence line approaches the excitonic transition energy 1.515 eV. For closed cavities, additional peaks are observed above the excitonic transition [108] corresponding to the Rabi-splitted exciton with a discrete positive shift due to the kinetic energy of the center of mass motion quantized due to the boundary conditions at the cavity edges [48,53,49,47]. Only odd modes appear due to a parity selection rule, obtained from the overlap integral of the exciton and the cavity photon wave functions [108].

9 Scaterring of light by small excitonic particles

In this section we apply the formalism developed in Sec. 4 to the study of the optical properties of small particles made of excitonic semiconductors with simple shapes.

9.1 Spheres

We extend here the classical Mie theory [117] of the optical properties of spherical particles, incorporating excitonic effects [118]. As in Mie theory, the incident and scattered electromagnetic fields are expanded in terms of vector spherical wave functions [117], and we apply both elecctromagnetic and additional boundary conditions at the surface of the sphere to determine the amplitudes of the scattered fields. These amplitudes can then be employed to calculate the scattering and extinction cross sections. The formalism is applied to the study of the optical properties ZnSe spheres [118] and CuCl micro-crystals [119]. In the case of micro-crystals, we compare the calculated excitonic absorption with the experimental measurements.

Let us consider a sphere of radius R and bulk dielectric response function $\epsilon(\vec{q},\omega)$ given by Eq. (15), and let it be irradiated by plane waves. The electromagnetic fields may be expanded in terms of the following spherical vector wave functions [118]

$$\vec{M}_{\sigma mn}(kr,\theta,\phi) = \frac{1}{k}\nabla\times[k\vec{r}Y_{\sigma mn}(\theta,\phi)z_n(kr)], \tag{107}$$

$$\vec{N}_{\sigma mn}(kr,\theta,\phi) = \frac{1}{k}\nabla\times\vec{M}_{\sigma mn}(kr,\theta,\phi), \tag{108}$$

$$\vec{L}_{\sigma mn}(kr,\theta,\phi) = \frac{1}{k}\nabla\left[Y_{\sigma mn}(\theta,\varphi)z_n(kr)\right], \tag{109}$$

where $\sigma = e$ (even) or o (odd) according to whether the associated Legendre polynomial $P_n^m(\cos\theta)$ is multiplied by $\cos(m\phi)$ or $\sin(m\phi)$ to obtain the real spherical harmonic $Y_{\sigma mn}(\theta,\phi)$, z_n represents a spherical Bessel function j_n when we expand the incident wave or the field inside the sphere, or a spherical Hankel function h_n when we expand the outgoing scattered waves outside the sphere. The wavevector k takes the value $k_0 = \sqrt{\epsilon_M}\omega/c$ outside of the sphere, within the host of dielectric response ϵ_M, and it runs over the values k_1 and k_2 corresponding to the $+$ and $-$ signs of Eq. (21), respectively, for the transverse waves (107) and (108) within the sphere, and the value k_3 given by Eq. (23) for the longitudinal waves (109). Thus, outside the sphere the electric field has the form

$$\vec{E}^{\nu}(r,\theta,\phi) = \sum_{n=1}^{\infty} i^n \frac{2n+1}{n(n+1)} [a_n^{\nu} \vec{M}_{o1n}(k_0 r,\theta,\phi) - i b_n^{\nu} \vec{N}_{e1n}(k_0 r,\theta,\phi)], \quad (110)$$

with corresponding magnetic field

$$\begin{aligned}\vec{H}^{\nu}(r,\theta,\phi) = &-\sqrt{\epsilon_M} \sum_{n=1}^{\infty} i^n \frac{2n+1}{n(n+1)} \\ &\times [b_n^{\nu} \vec{M}_{e1n}(k_0 r,\theta,\phi) + i a_n^{\nu} \vec{N}_{o1n}(k_0 r,\theta,\phi)],\end{aligned} \quad (111)$$

where $\nu = i$ denotes the incident wave and $\nu = s$ stands for the scattered wave. We have assumed that the incident wave is linearly polarized along the x direction and propagates along the z direction, so that $a_n^i = b_n^i = 1$.

Within the sphere there are two transverse modes and one longitudinal mode. The electric fields of the transverse modes are

$$\vec{E}^{\alpha}(r,\theta,\phi) = \sum_{n=1}^{\infty} i^n \frac{2n+1}{n(n+1)} \left[a_n^{\alpha} \vec{M}_{o1n}(k_{\alpha} r,\theta,\phi) - i b_n^{\alpha} \vec{N}_{e1n}(k_{\alpha} r,\theta,\phi)\right], \quad (112)$$

and the corresponding magnetic fields are

$$\begin{aligned}\vec{H}^{\alpha}(r,\theta,\phi) = &-\sqrt{\epsilon_M} \sum_{n=1}^{\infty} i^n \frac{2n+1}{n(n+1)} \\ &\times [b_n^{\alpha} \vec{M}_{o1n}(k_{\alpha} r,\theta,\phi) - i a_n^{\alpha} \vec{N}_{e1n}(k_{\alpha} r,\theta,\phi)],\end{aligned} \quad (113)$$

where $\alpha = 1, 2$. The electric field of the longitudinal mode is

$$\vec{E}^{3}(r,\theta,\phi) = \sum_{n=1}^{\infty} i^n \frac{2n+1}{n(n+1)} c_n^3 \vec{L}_{e1n}(k_3 r,\theta,\phi), \quad (114)$$

and there is no corresponding magnetic field.

The coefficients a_n^s, b_n^s, a_n^{α}, b_n^{α} ($\alpha = 1, 2$), and c_n^3 may be determined by applying electromagnetic and additional boundary conditions at the surface $r = R$ and using the orthogonality of the basis function set $\{\vec{M}_{\sigma mn},\ \vec{N}_{\sigma mn},\ \vec{L}_{\sigma mn}\}$. From the scattered field coefficients a_n^s and b_n^s we can calculate the total scattering cross section

$$\sigma_s = \frac{2\pi}{k_0^2} \sum_{n=1}^{\infty} (2n+1) \left[|a_n^s|^2 + |b_n^s|^2\right], \quad (115)$$

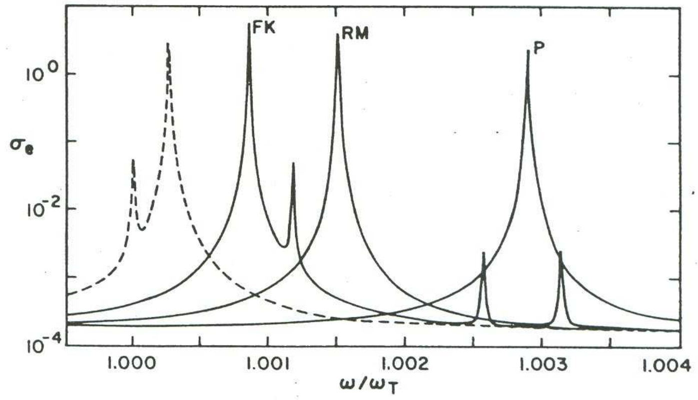

Fig. 22. Calculated extinction cross section of a ZnSe sphere of radius 75 Å using the ABC's of Pekar (P), Rimbey-Mahan (RM), and Fuchs-Kliewer (FK). The local case is also shown (dashed curve). Taken from Ref. [118].

and the extinction cross section

$$\sigma_e = -\frac{2\pi}{k_0^2}\sum_{n=1}^{\infty}(2n+1)\mathrm{Re}\left[a_n^s + b_n^s\right], \tag{116}$$

where Re stands for the real part.

Fig. 22 shows the extinction cross section calculated [118] for a 75 Å sphere of ZnSe as a function of the frequency. The results display different structures for different ABC's. The principal extintion peak is blue shifted in the non-local calculations with respect to the local result. The shift is smaller for the Fuchs-Kliewer (FK) ABCs [9] than for the Rimbey Mahan (RM) ABCs [10], and is largest for the Pekar ABCs [4]. Near the energy of the excitonic transition the FK curve exhibits four peaks, associated with resonances of the different scattering amplitudes a_n^s and b_n^s, the strongest of which corresponds to b_1^s. The latter resonance is the only one present for the other ABCs considered.

In Fig. 23 we show the position of the excitonic absorption peak measured for a system of small CuCl microcrystals embedded within a glass matrix [121]. The theory above yielded a good agreement for the dependence of the peak position on the size of the particles [119] when Pekar ABCs were employed. Similar agreement was obtained for the experimental absorption of CuCl particles within an NaCl matrix [122] and for CdS particles within glass [123].

Similar techniques have been employed to calculate the response of more elaborate spherically symmetric geometries. For example, in Ref [124], the normal modes and the absorption of an excitonic spherical quantum dot at the center of a spherical microcavity made up of alternating dielectric shells were calculated. The nonlocality of the excitonic dot was accounted for through an approximate separable susceptibility, and the electromagnetic field produced

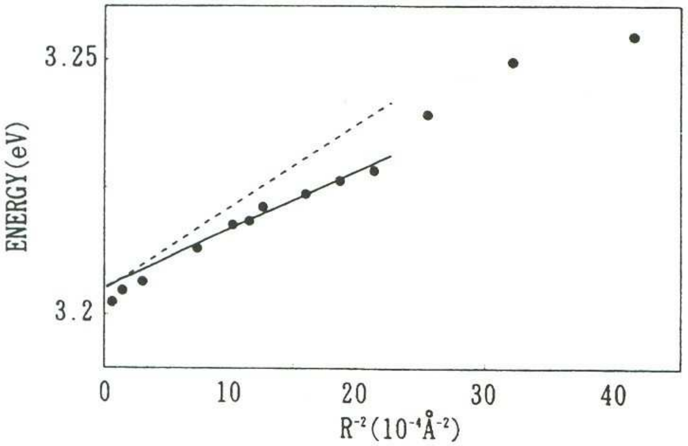

Fig. 23. We show the size dependence of the excitonic absorption peak of CuCl spheres in a glass matrix. The full curve corresponds to a Lifshitz-Slezov poly-dispersed size distribution, while the dashed curve corresponds to a monodispersed distribution. Circles represent the experimental data of Ekimob et al. [120]. Taken form Ref. [119].

by the excitonic polarization was obtained through a Green's function technique. The resonant excitonic absorption displayed a Rabi splitting when the cavity was tuned to the zero-dimensional polariton modes of the dot.

9.2 Cylinders

We study now an excitonic infinite cylinder of radius a and bulk dielectric constant $\epsilon(\vec{q},\omega)$, given by Eq. (15), irradiated by a normally incident plane wave. Similar to the sphere problem, the fields are expanded [125] in terms of cylindrical vector wave functions,

$$\vec{M}_n(kr,\theta) = \frac{1}{k}\nabla \times \left[\hat{z} Z_n(kr) e^{in\theta}\right], \tag{117}$$

$$\vec{N}_n(kr,\theta) = \frac{1}{k}\nabla \times \vec{M}_n, \tag{118}$$

$$\vec{L}_n(kr,\theta) = \frac{1}{k}\nabla \left[Z_n(kr) e^{in\theta}\right], \tag{119}$$

where cylindrical coordinates (r,θ,z) are used, $\hat{z}$ is a unit vector in the z direction, Z_n represents a cylindrical Bessel function J_n when we expand the incident wave or the field inside the sphere, or a cylindrical Hankel function H_n when we expand the outgoing scattered waves outside the cylinder. As in the case of the sphere, the wavevector k takes the value $k_0 = \sqrt{\epsilon_M}\omega/c$ outside of the sphere, within the host of dielectric response ϵ_M, and it runs over the values k_1 and k_2 corresponding to the $+$ and $-$ signs of Eq. (21), respectively, for the transverse waves (107) and (108) within the sphere, and the value k_3 given by Eq. (23) for the longitudinal waves (109). Notice that there is no z dependence in Eqs. (117)-(119), since we assumed normal incidence and translationally invariant infinite cylinders. We study separately the cases when the incident electric field points along the axis of the cylinder and when it points across the axis.

Parallel polarization

In this case electromagnetic fields for the incident and scattered waves have the form

$$\vec{E}^{\nu}(r,\theta) = \sum_{n=-\infty}^{\infty} i^n b_n^{\nu} \vec{N}_n(k_0 r, \theta), \tag{120}$$

$$\vec{H}^{\nu}(r,\theta) = -i\sqrt{\epsilon_M} \sum_{n=-\infty}^{\infty} i^n b_n^{\nu} \vec{M}_n(k_0 r, \theta), \tag{121}$$

where $\nu = i$ stands for the incident fields, with $b_n^i = 1$, and $\nu = s$ is for the scattered fields, with amplitudes b_n^s. Within the cylinder there are two transverse modes $\alpha = 1, 2$ with corresponding fields

$$\vec{E}^{\alpha}(r,\theta) = \sum_{n=-\infty}^{\infty} i^n b_n^{\alpha} \vec{N}_n(k_\alpha r, \theta), \tag{122}$$

$$H^{\alpha}(r,\theta) = -i\frac{k_\alpha c}{\omega} \sum_{n=-\infty}^{\infty} i^n b_n^{\alpha} \vec{M}_n(k_\alpha r, \theta), \tag{123}$$

and no longitudinal field. The unknown coefficients, b_n^s and b_n^α are determined using the usual boundary conditions and the Pekar ABC. We only write the result for the scattered amplitudes

$$b_n^s = -R_s/S_n, \tag{124}$$

where

$$\begin{aligned} R_n = {} & J_n(k_0 a)\left[(\epsilon_1 - \epsilon_\infty)\sqrt{\epsilon_2} J_n(k_1 a) J_n'(k_2 a)\right] \\ & - J_n(k_0 a)\left[(\epsilon_2 - \epsilon_\infty)\sqrt{\epsilon_2} J_n'(k_1 a) J_n(k_2 a)\right] \\ & + \sqrt{\epsilon_M} J_n'(k_0 a) J_n(k_1 a) J_n(k_2 a)(\epsilon_2 - \epsilon_1), \end{aligned} \tag{125}$$

$$\begin{aligned} R_n = & H_n(k_0a)\left[(\epsilon_1-\epsilon_\infty)\sqrt{\epsilon_2}J_n(k_1a)J_n^{'}(k_2a)\right] \\ & -H_n(k_0a)\left[(\epsilon_2-\epsilon_\infty)\sqrt{\epsilon_2}J_n^{'}(k_1a)J_n(k_2a)\right] \\ & +\sqrt{\epsilon_m}H_n^{'}(k_0a)J_n(k_1a)J_n(k_2a)(\epsilon_2-\epsilon_1). \end{aligned} \tag{126}$$

Here we introduced the quantities $\epsilon_\alpha = (k_\alpha c/\omega)^2$. The extinction width of the cylinder, analogous in this essentially 2D problem to the extinction cross section of 3D scattering, is given by

$$C_e = -\frac{4}{k_0}\sum_{n=\infty}^{\infty} Re(b_n^s). \tag{127}$$

Perpendicular polarization

For this polarization we write

$$\vec{E}^\nu(r,\theta) = \sum_{n=-\infty}^{\infty} i^n a_n^\nu \vec{M}_n(k_0r,\theta), \tag{128}$$

$$\vec{H}^\nu(r,\theta) = -i\sqrt{\epsilon_M}\sum_{n=-\infty}^{\infty} i^n a_n^\nu \vec{N}_n(k_0r,\theta), \tag{129}$$

where $\nu = i$ stands for the incident light, with amplitude $a_n^i = 1$, and $\nu = s$ is for the scattered light of amplitudes a_n^s. Inside the cylinder there are two transverse modes $\alpha = 1,2$ with corresponding fields

$$\vec{E}^\alpha(r,\theta) = \sum_{n=-\infty}^{\infty} i^n a_n^\alpha \vec{M}_n(k_\alpha r,\theta), \tag{130}$$

$$H^\alpha(r,\theta) = -i\frac{k_\alpha c}{\omega}\sum_{n=-\infty}^{\infty} i^n a_n^\alpha \vec{N}_n(k_\alpha r,\theta), \tag{131}$$

and a longitudinal mode, with electric field

$$\vec{E}^3(r,\theta) = \sum i^n c_n^3 \vec{L}_n(k_3r,\theta). \tag{132}$$

As in the previous case geometry, the boundary conditions of electromagnetic origin and the Pekar ABC's allow us to determine the expansion coefficients a_n^s, a_n^α and c_n^3. For a_n^s we obtain

$$a_n^s = -P_n/Q_n, \tag{133}$$

where

$$P_n = \alpha_n J_n^{'}(k_0 a) - \beta_n J_n(k_0 a), \tag{134}$$

$$Q_n = \alpha_n H^{'}(k_0 a) - \beta_n H_n(k_0 a), \tag{135}$$

$$\begin{aligned}\alpha_n = & \frac{k_1}{k_0}(\epsilon_2 - \epsilon_\infty)\epsilon_\infty J_n(k_1 a) \\ & \times \left[J_n^{'}(k_2 a) \frac{k_3}{k_0} J_n^{'}(k_3 a) - \frac{n^2}{k_2 a} J_n(k_2 a) \frac{J_n(k_3 a)}{k_0 a} \right] \\ & + \frac{k_2}{k_0}(\epsilon_1 - \epsilon_\infty)\epsilon_\infty J_n(k_2 a) \\ & \times \left[J_n^{'}(k_1 a) \frac{k_3}{k_0} J_n^{'}(k_3 a) - \frac{n^2}{k_1 a} J_n(k_1 a) \frac{J_n(k_3 a)}{k_0 a} \right],\end{aligned} \tag{136}$$

$$\begin{aligned}\beta_n = & (\epsilon_2 - \epsilon_\infty)\epsilon_\infty J_n^{'}(k_1 a) \\ & \times \left[J_n^{'}(k_2 a) \frac{k_3}{k_0} J_n^{'}(k_3 a) - \frac{n^2}{k_2 a} J_n(k_2 a) \frac{J_n(k_3 a)}{k_0 a} \right] \\ & + (\epsilon_1 - \epsilon_\infty)\epsilon_\infty J_n^{'}(k_2 a) \\ & \times \left[J_n^{'}(k_1 a) \frac{k_3}{k_0} J_n^{'}(k_3 a) - \frac{n^2}{k_1 a} J_n(k_1 a) \frac{J_n(k_3 a)}{k_0 a} \right] \\ & - \frac{n^2}{k_0 a}(\epsilon_1 - \epsilon_\infty)(\epsilon_2 - \epsilon_\infty) J_n(k_3 a) \\ & \times \left[J_n^{'}(k_1 a) \frac{J_n(k_2 a)}{k_2 a} - J_n^{'}(k_2 a) \frac{J_n(k_1 a)}{k_1 a} \right].\end{aligned} \tag{137}$$

The extinction width of the cylinder is

$$C_e = -\frac{4}{k_0} \sum_{n=-\infty}^{\infty} Re(a_n^s). \tag{138}$$

In Fig. 24 we show the extinction width C_e calculated for CuCl nanocrystals with radius 100 Å for both $\vec{E}^i \parallel \hat{z}$ and $\vec{E}^i \perp \hat{z}$ polarizations [125]. Both curves show a peak close to the excitonic transition energy. The extintion width is smaller for perpendicular polarization than for parallel polarization and is blue shifted. Non-local effects diminish C_e with respect to the local result. As the radius of the cylinder takes smaller values, the non-local peaks approach each other. Similar behavior is observed for the local curves.

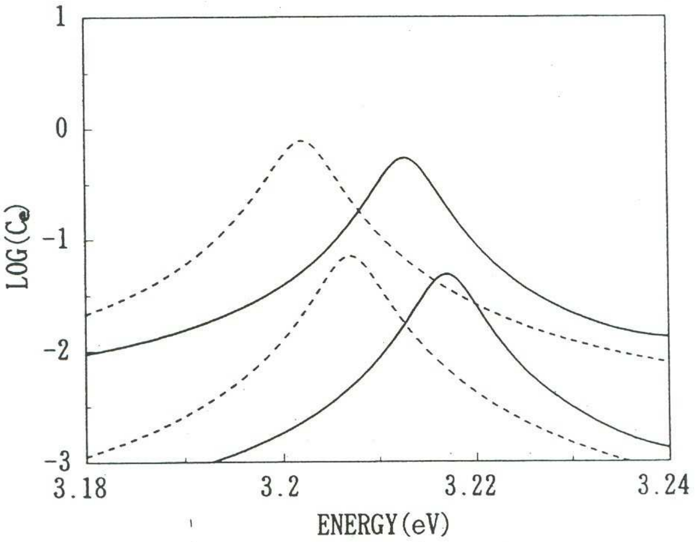

Fig. 24. Extinction width C_e calculated for a CuCl cylinder of radius 30 Å, normalized to the geometrical width $2a$. Upper curves are for $\vec{E} \parallel \vec{z}$ and lower curves for $\vec{E} \perp z$. Dashed curves are calculated within the local theory. Taken from Ref. [125].

10 Scattering of light from non ideal surfaces

Until now we have dealt with smooth surfaces of semiconductors. In this Section we describe the interaction of light with non ideal, random slightly rough surfaces. Consider a semiconductor occupying the region $z > \zeta_r(\vec{r}_\parallel)$, where $\vec{r}_\parallel = (x, y, 0)$ and $\zeta_r(\vec{r}_\parallel)$ represents the deviation of the surface from the nominal surface at $z = 0$. We assume that ζ_r is a random function of $\vec{r}_\parallel$ with null average $\langle \zeta_r \rangle = 0$. We identify its second moment $\delta_r^2 = \langle \zeta_r^2 \rangle$ with the characteriztic size δ_r of the roughness, which we assume much smaller than wavelength of light, and we assume that the two point correlation function is given by

$$\langle \zeta_r(\vec{r}_\parallel)\zeta_r(\vec{r'}_\parallel)\rangle = \delta_r^2 e^{-|\vec{r}_\parallel - \vec{r'}_\parallel|^2/L_r^2}, \tag{139}$$

i.e., ζ_r is a zero-mean, stationary, Gaussian random process, with correlation distance L_r which we assume to be much larger than δ_r, so that the slope of the surface is small.

We choose $x - z$ as the plane of incidence, and write the incident electric field as [64]

$$\vec{E}_i(\vec{r}, t) = E_i \left[\cos\sigma(\hat{x}\cos\theta_i - \hat{z}\sin\theta_i) + \hat{y}\sin\sigma\right] e^{i(k_x x + k_z z - wt)}, \tag{140}$$

where $k_x = k\sin\theta_i$, $k_z = k\cos\theta_i$, $k = \omega/c$, θ_i the angle of incidence, and σ is the polarization. P polarization corresponds to $\sigma = 0$, while S polarization corresponds to $\sigma = \pi/2$. As the height and slope of the surface are small, we expand the scattered fields up to first order in the quantities $k\delta_r \ll 1$ and $|\nabla\zeta_r| \sim \delta_r/L_r \ll 1$, and we write the field as $\vec{E}_{sc} = \vec{E}^{(0)}_{sc} + \vec{E}^{(1)}_{sc}$, where the zeroth-order term is the field specularly reflected by the nominal flat surface

$$\vec{E}^{(0)}_{sc}(\vec{r},t) = \left[E^{(0)}_p(k_x)(\hat{x}\cos\theta_i + \hat{z}\sin\theta_i) + E^{(0)}_s(k_x)\hat{y}\right] e^{i(k_x x - k_z z - wt)}, \quad (141)$$

and the first-order field is given by the Rayleigh expansion

$$\vec{E}^{(1)}_{sc}(\vec{r},t) = \int \frac{d^2k'_\parallel}{(2\pi)^2}\vec{E}^{(1)}_{sc}(\vec{k}'_\parallel)e^{i(\vec{k}'_\parallel\cdot\vec{r}_\parallel - k'_z z - \omega t)}, \quad (142)$$

where

$$\vec{E}^{(1)}_{sc}(\vec{k}'_\parallel) = \hat{T}\left[E^{(1)}_p(\vec{k}'_\parallel)(\hat{x}'\cos\theta' + \hat{z}'\sin\theta') + E^{(1)}_s(\vec{k}'_\parallel)\hat{y}'\right]. \quad (143)$$

Here $\hat{x}' = \vec{k}'_\parallel/k'_\parallel$, $k'_\parallel =\mid \vec{k}'_x \mid$, $\hat{z}' = \hat{z}$, $\hat{y}' = \hat{z}' \times \hat{x}'$, so that $x' - z'$ is the scattering plane with respect to which S and P scattered waves are defined, θ' is the scattering angle, which may take complex values, $k'_{x'} = k\sin\theta'$, $k'_{z'} = (k^2 - (k'_{x'})^2)^{1/2} = k\cos\theta'$ and

$$\hat{T} = \begin{pmatrix} k'_x/k'_\parallel & k'_y/k'_\parallel & 0 \\ -k'_y/k'_\parallel & k'_x/k'_\parallel & 0 \\ 0 & 0 & 1 \end{pmatrix} \quad (144)$$

is a rotation matrix,

As in Sect. 5, we introduce a potential $U_r(\vec{r})$ that describes the interaction of excitons with the rough surface. As the roughness is small, we assume that locally the potential is given by the interaction with a flat surface, $U_r(\vec{r}) = U(z - \zeta_f(\vec{r}_\parallel))$, where $U(z)$ represents the interaction of excitons with the nominal flat surface, and $\zeta_f(\vec{r}_\parallel)$ is a local shift in the reference position of the surface. In a pure system, we might expect that ζ_f coincides with ζ_r. However, the presence of impurities and defects which modify locally the potential introduce additional randomness, so that we keep ζ_f as another random function which we expect to be highly correlated to the geometrical surface profile ζ_r. We assume that ζ_f is also a Gaussian correlated random process, so that

$$\langle\zeta_f(\vec{r}_\parallel)\zeta_f(\vec{r}'_\parallel)\rangle = \delta^2_f e^{-|\vec{r}_\parallel - \vec{r}'_\parallel|^2/L^2_f}, \quad (145)$$

$$\langle\zeta_r(\vec{r}_\parallel)\zeta_f(\vec{r}'_\parallel)\rangle = \delta_r\delta_f k_{rf} e^{-|\vec{r}_\parallel - \vec{r}'_\parallel|^2/L^2_{rf}}, \quad (146)$$

where L_f is the correlation length of $\zeta_f(\vec{r}_\parallel)$, L_{rf} is the mutual correlation length of $\zeta_r(\vec{r}_\parallel)$, δ_f is the height of the fluctuations in the reference position of the surface, and $k_{rf} = \langle\zeta_r(0)\zeta_f(0)\rangle/(\delta_r\delta_f)$. We further assume $\langle\zeta_f(\vec{r}_\parallel)\rangle = 0$.

Assuming ζ_f is very small, i.e., $\delta_f \ll a \ll \min\{L_f, L_r, L_{rf}\}$, we expand

$$U_r(\vec{r}) = U(z) - U'(z)\zeta_f(\vec{r}_\parallel). \tag{147}$$

Here we introduced the width a of the surface transition layer, and we denoted dU/dz by U'. We notice that $U_r(\vec{r}_\parallel, z)$ has a random dependence on $\vec{r}_\parallel$ and a deterministic dependence on z.

The zeroth order field $\vec{E}^{(0)}$ and polarization $\vec{P}^{(0)}$ obey a set of coupled equations which may be obtained immediately from Eqs. (56) and (59) by replacing $\vec{E} \to \vec{E}^{(0)}$ and $\vec{P} \to \vec{P}^{(0)}$. The first order field $\vec{E}^{(1)}$ and polarization $\vec{P}^{(1)}$ obey an equation which can also be obtained from Eqs. (56) and (59) by first generalizing the arbitrary x and y dependence, i.e., replacing $i\vec{Q}$ by $\nabla_\parallel$, and then performing a power expansion and identifying the first order contribution, yielding

$$4\pi k^2\vec{P}^{(1)} + \nabla^2\vec{E}^{(1)} - \nabla(\nabla\cdot\vec{E}^{(1)}) + \epsilon_\infty k^2\vec{E}^{(1)} = 0 \tag{148}$$

$$\left[\frac{-\hbar\omega}{M}\nabla^2 + \omega_T^2 - \omega^2 - i\nu\omega + \frac{2\omega_T}{\hbar}U\right]\vec{P}^{(1)} - \frac{\omega_p^2}{4\pi}\vec{E}^{(1)} = \frac{2\omega_T}{\hbar}\zeta_f(\vec{r}_\parallel)U'\vec{P}^{(0)}. \tag{149}$$

As in sections 6.1 and 6.2, we may eliminate the electric field to obtain fourth order differential equations for the polarization, similar to Eqs. (65), (71), and (72). In the case of a Morse potential $U(z) = U_1e^{-z/a} + U_2e^{-2z/a}$, we may seek solutions for the *zero*-th polarization similar to Eqs. (68) and (74),

$$\vec{P}^{(0)}(x, z) = e^{ik_xx}\sum_{\alpha=1}^{3} A_\alpha^{(0)}\hat{e}_\alpha e^{ik_\alpha z}\sum_{n=0}^{\infty} a_{n\alpha}e^{-nz/a} \tag{150}$$

where k_α (with $\alpha = 1, 2, 3$) are the z-components of the wave vectors of the two transverse ($\alpha = 1, 2$) and the longitudinal $\alpha = 3$ modes, and $\hat{e}_\alpha$ are corresponding polarization vectors, either perpendicular to the wavevector ($\alpha = 1, 2$) or pararllel ($\alpha = 3$). Substitution into the differential equation for the polarization yields recursion relations from which we may obtain the coefficients $a_{n\alpha}$. The coefficients $A_m^{(0)}$ and $B_m^{(0)}$ are then determined from the boundary condition equations. Explicit expressions are given in Ref. [64].

The first order fields may be obtained in a similar fashion. First we construct a fourth order differential equation for the polarization from Eqs. (148) and (149). This is an inhomogeneous equation forced by the zeroth order polarization (150). For each value of the scattered wavevector $\vec{k}'_\parallel$, the solution is similar to the zeroth order solution, i.e., a combination of decaying exponentials $e^{-nz/a}$ modulating the bulk-like solutions $\propto e^{ik'_\alpha z}$. The coefficients of the decaying exponentials may be obtained by substituting the proposed solution back into the differential equation for the polarization and iterating over the resulting recursion relations. Next, the first order field may be obtained from the polarization, which still contains unknown coefficients, by applying Eq. (149). Finally, the remaining coefficients and the fields scattered away from the surface may be obtained by matching the resulting fields to the Rayleigh expansion (142) by imposing boundary conditions at the rough surface $z = \zeta_r$. The details are given in Ref. [64].

To calculate the first order amplitudes it is convenient to factorize out of the Rayleigh coefficients

$$E_p^{(1)}(\vec{k'}_\parallel) = E_{p,r}(\vec{k'}_\parallel)\zeta_r(\vec{k'}_\parallel - \vec{k}_\parallel) + E_{p,f}(\vec{k'}_\parallel)\zeta_f(\vec{k'}_\parallel - \vec{k}_\parallel), \tag{151}$$

$$E_s^{(1)}(\vec{k'}_\parallel) = E_{s,r}(\vec{k'}_\parallel)\zeta_r(\vec{k'}_\parallel - \vec{k}_\parallel) + E_{s,f}(\vec{k'}_\parallel)\zeta_f(\vec{k'}_\parallel - \vec{k}_\parallel), \tag{152}$$

the Fourier transforms of the surface profile $\zeta_r(\vec{r}_\parallel)$ and the surface potential reference position $\zeta_f(\vec{r}_\parallel)$. The scattering cross section is obtained from the time and ensemble averaged Poynting vector of the first order fields

$$\begin{aligned}\langle\vec{S}_{sc}\rangle &= \frac{c}{8\pi}\mathrm{Re}\langle\Big[\vec{E}_{sc}^{(1)}(\vec{r},t)^\star \times \vec{H}_{sc}^{(1)}(\vec{r},t)\Big]\rangle \\ &= \frac{c^2}{128\pi^5\omega}\int\limits_{<} d^2k'_\parallel \int\limits_{<} d^2k''_\parallel \langle\vec{E}_{sc}^{(1)}(\vec{k}''_\parallel)^\star \times [\vec{k'} \times \vec{E}_{sc}^{(1)}(\vec{k}'_\parallel)]\rangle,\end{aligned} \tag{153}$$

where $\vec{k'} = \vec{k'}_\parallel - k'_z\hat{z}$, the $\star$ denotes the complex conjugate, and the symbol $<$ in the integral indicates that this should be evaluated within the light cone $k'_\parallel < \omega/c$, where k'_z is real, and energy propagates away from the surface. Using Eqs. (151) and (152) the average Poynting vector may be cast into the form

$$\begin{aligned}\langle\vec{S}_{sc}\rangle &= \frac{c^2}{32\pi^2\omega}\int\limits_{<} d^2k'_\parallel\vec{k'}\left[\mid \vec{E}_{sc,r}\mid^2 \delta_r^2 L_r^2 e^{-|\vec{k'}_\parallel - \vec{k}_\parallel|^2 L_r^2/4}\right] + \\ &\quad \frac{c^2}{32\pi^2\omega}\overset{<}{\int} d^2k'_\parallel\vec{k'}\left[\mid \vec{E}_{sc,f}\mid^2 \delta_f^2 L_f^2 e^{-|\vec{k'}_\parallel - \vec{k}_\parallel|^2 L_f^2/4}\right] +\end{aligned} \tag{154}$$

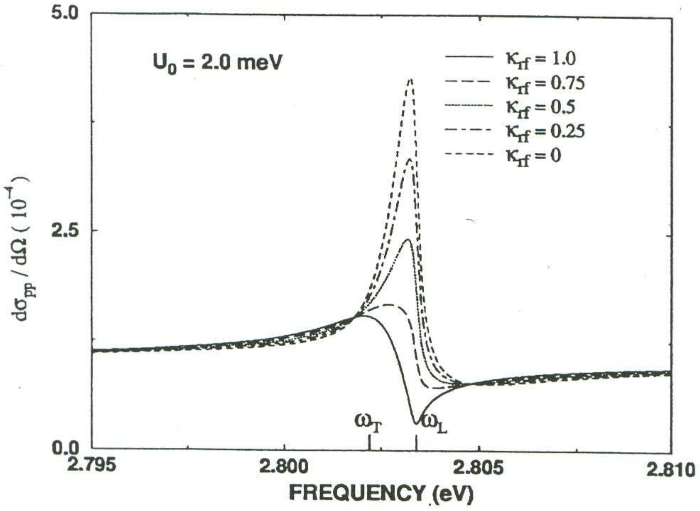

Fig. 25. Dimensionless cross section $d\sigma_{pp}/d\Omega$ of P polarized light scattered from a ZnSe surface for P polarized incident light at an angle $\theta_i = 15^o$ and scattering angle $\theta' = 3^o$ in the plane of incidence for different cross correlation coefficients. The excitonic potential is a repulsive exponential whose value at the surface is $U_0 = 2.0$meV, the roughness and potential heights are $\delta_r = \delta_f = 8$Å, and the autocorrelation distances are $L_r = L_f = L_{rf} = 2500$Å. Taken from Ref. [64].

$$\frac{c^2}{32\pi^2\omega}\int_{<} d^2k'_{\parallel}\vec{k}'[2\delta_r\delta_f k_{rf}L_{rf}^2\mathrm{Re}(\vec{E}^*_{sc,r}\cdot\vec{E}_{sc,f})e^{-|\vec{k}'_\parallel-\vec{k}_\parallel|^2L_r^2/4}],$$

where we made use of the stationarity and Gaussian correlations (139), (145), and (146) of ζ_r and ζ_f to evaluate the averages $\langle\ldots\rangle$.

Finally, we define the dimensionless scattering cross section $d\sigma/d\Omega$, as the ratio of the energy flux density of light scattered into the direction of $\vec{k}' = k'(\cos\theta'\cos\phi', \cos\theta', \sin\phi', \sin\theta')$ to the incident energy flux density. From Eq. (154) we identify

$$\begin{aligned}\frac{d\sigma}{d\Omega} = \frac{\omega^2}{4\pi c^2}\frac{\cos\theta'}{\cos\theta_i}\frac{1}{\mid\vec{E}_i\mid^2}\{&\left[\mid E_{p,r}(\vec{k'}_\parallel)\mid^2 + \mid E_{s,r}(\vec{k'}_\parallel)\mid^2\right]\delta_r^2L_r^2e^{-|\vec{k'}_\parallel-\vec{k}_\parallel|L_r^2/4} \\ &\left[\mid E_{p,f}(\vec{k'}_\parallel)\mid^2 + \mid E_{s,f}(\vec{k'}_\parallel)\mid^2\right]\delta_f^2L_f^2e^{-|\vec{k'}_\parallel-\vec{k}_\parallel|L_r^2/4} + \\ &2\delta_r\delta_f k_{rf}^2L_{rf}^2\left[E_{p,r}(\vec{k'}_\parallel)^\star E_{p,f}(\vec{k'}_\parallel) + E_{s,r}(\vec{k'}_\parallel)^\star E_{s,f}(\vec{k'}_\parallel)e^{-|\vec{k'}_\parallel-\vec{k}_\parallel|L_r^2/4}\right]\}.\end{aligned}\tag{155}$$

The terms with δ_r^2 and δ_f^2 describe the power scattered from roughness and potential fluctuations, respectively, and k_{rf} determines the scattered associated with the cross-correlations between the functions $\zeta_r(\vec{r}_\parallel)$ and $\zeta_f(\vec{r}_\parallel)$.

In Fig. 25 we display the P incoming and P outgoing cross section $d\sigma_{pp}/d\Omega$ for light scattering from a ZnSe rough surface. P-polarized light is incident at $\theta_i =$

15° and scattered at $\theta' = 3°$. The structural parameters for the calculations are; $\epsilon_\infty = 8.1$, $\hbar\omega_T = 2.8022eV$, $\hbar\omega_p = 0.2334eV$, (longitudinal-transverse splitting $\hbar\omega_{LT} \approx \hbar\omega_p/2\omega_T\epsilon_\infty = 1.2meV$), and bulk damping $\hbar\nu = 0.2meV$. For a single exciton branch the total mass takes the value $M = 0.57m_0$. The transition layer was modeled with an exponential potential with parameters $U_1 = U_0 = 2.0$meV, $U_2 = 0$, $a = 50$ Å. U_0 denotes average height of the potential at $z = 0$. The correlation parameters are $\delta_r = \delta_f \equiv \delta = 8$ Å, and $L_r = L_f = L_{rf} \equiv L = 2500$ Å. According to the first order formulae, for P- (S-) polarized incident light, there is only P- (S-) scattered light in the plane of incidence. For complete cross-correlation the cross section is similar to the P polarized reflectance, with a maximum at ω_T and a minimum at ω_L. As the cross-correlation diminishes, the minima dissapears and the maximum increases its height and is blue shifted.

Fig. 26 shows the $P \rightarrow P$ and $S \rightarrow S$ cross sections $(d\sigma_{pp}/d\Omega)$ and $(d\sigma_{ss}/d\Omega)$ as functions of the scattering angle in the plane of incidence for a fixed photon energy $\omega = \omega_L$. Total cross correlation $(k_{rf} = 1)$ is assumed and different values are given to the angle of incidence θ_i. In the $S - S$ case, the scattering is maximum close to the specular direction. However, in the $P - P$ case a minimum appears close to the specular direction for large incidence angles. This peculiar behavior is only observed close to ω_L and is due to the excitation of the longitudinal mode. At other frequencies and/or at small angles, the $P - P$ scattering looks qualitatively similar to the $S - S$ scattering.

In Fig. 27 (a) we show experimental spectra [62] of $d\sigma_{pp}/d\Omega$ for the $A_{n=1}$ excitonic transition of CdS. Data were taken at different areas of the same sample crystal with a fixed angle of incidence $\theta_i = 14°$ and scattering angle $\theta' = 4°$ within the plane of incidence. Fig. 27 (b) corresponds to calculated spectra. Four experimental curves are shown. Curve 1 displays a maximum at the longitudinal frequency ω_L. Similar structures have been observed in different high quality samples. However, in some cases the shape is quite different as it may exhibit a broad shoulder or even a peak at the excitonic transition energy ω_T , as exemplified by curves 3 and 4 of the same figure. Curve 2 lies between 1 and 3 and represents a transition from curves with no resonance to curves with a resonance at ω_T. Theoretical curves were obtained assuming a repulsive exciton potential of width 70 Åand strength $U_0 = 4$ meV. Since different experimental behavior was observed from assorted sample areas, it was assumed that the discrepancy originated from distinctness in the parameters that characterize the surface roughness, while the parameters that characterize the material were assumed invariant. The parameters of CdS are $\hbar\omega_p = 0.29396eV$, $\epsilon_\infty = 9.1$, $M = 0.94m$, $\hbar\nu = 0.124meV$, and $\hbar\omega_T = 2.55225eV$ was obtained from the best global fitting. The correlation distances were assumed equal $L_r = L_f = L_{rf} = 0.5\,\mu$m and the amplitudes δ_r, δ_f, and κ_{rf} were fitted to each experimental curve. For example, curve 4 was obtained using the following set of parameters; $\delta_r = 17.8$ Å, $\delta_f = 26.2$ Å,

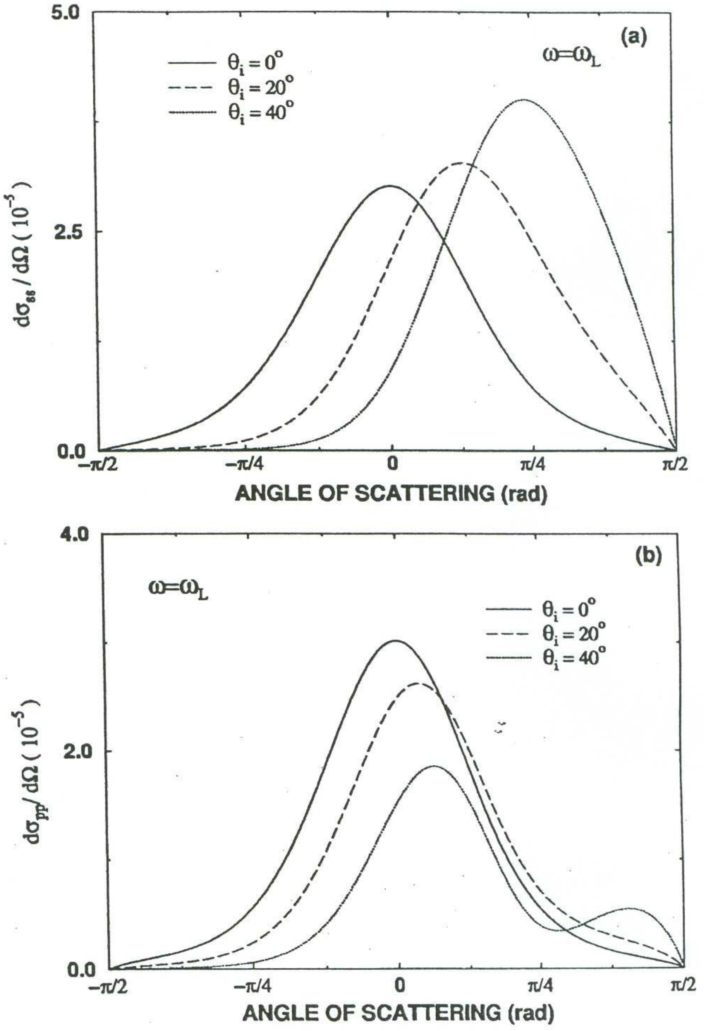

Fig. 26. Angular dependence of the dimensionless cross sections (a) $d\sigma_{ss}/d\Omega$ and (b) $d\sigma_{pp}/d\Omega$ for ZnSe calculated with the parameters of Fig. 25, except for the surface potential $U_0 = 1$ meV. THe frequency is fixed at $\omega = \omega_L$, the cross correlation at $k_{rf} = 1$ and different angles of incidence $\theta_i = 0, 20, 40$ degrees are considered. Taken from Ref. [64].

and $k_{rf} = 0.915$. In all four curves the agreement found between theory and experiment was excellent.

Theories similar to the one outlined above have been applied to other excitonic systems with rough surfaces. For example, in Ref. [126] it was used to study the scattering of light by nonlocal semiconductor thin films deposited above metallic substrates. The scattering cross section displayed a series of peaks due to the resonant coupling into the guided wave modes of the film.

Alternative simplified calculations for slightly rough surfaces have been performed by generalizing the Rayleigh-Fano method, incorporating into it the two transverse modes and the longitudinal mode that may be excited within

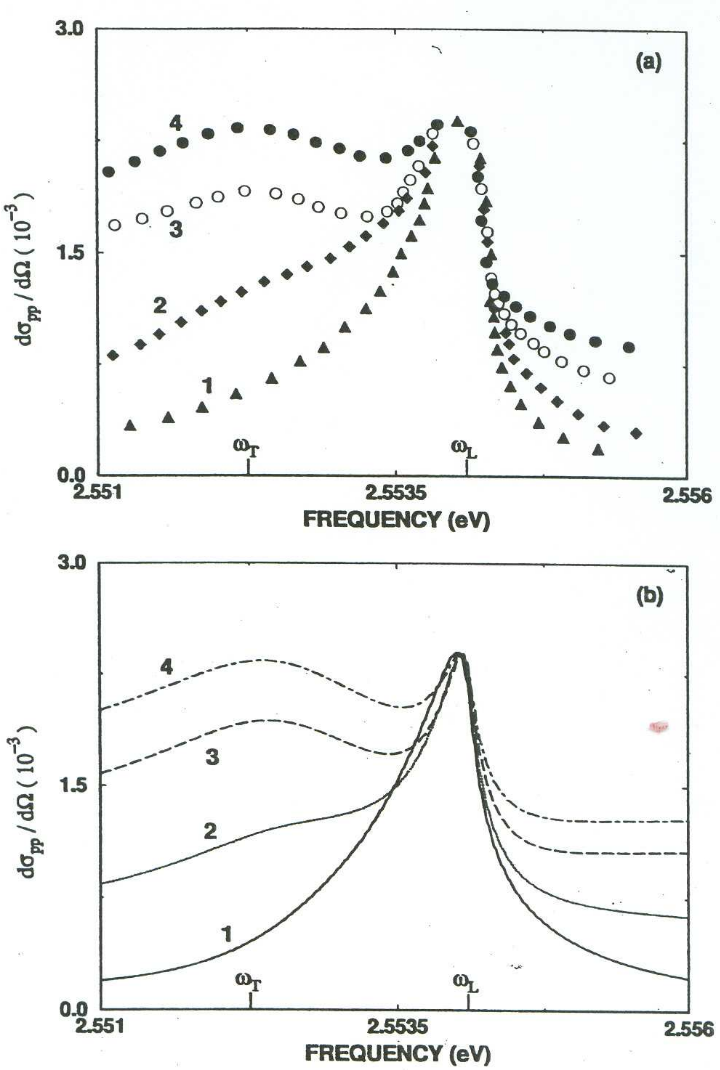

Fig. 27. Comparisons between theorical and measured dimensionless cross section, $d\sigma_{pp}/d\Omega$. In (a) we show the experimental data of CdS taken from Ref. [62], which correspond to light incident at an angle $\theta_i = 14^o$ and scattered at an angle $\theta' = 4^\circ$ from different areas of the same sample surface. The hexagonal $\vec{c}$ axis lies along the surface. Panel (b) displays the cross section calculated for an exponential excitonic potential. The parameters of the rough surface and the fluctuations of the surface potential are: $\delta_r = 5.05$ Å, $\delta_f = 13.35$ Å $(\eta = 0.38)$, $k_{rf} = 0.39$ Å (curve 1); $\delta_r = 10.45$ Å, $\delta_f = 21.55$ Å $(\eta = 0.34)$, $k_{rf} = 0.917$ Å (curve 2); $\delta_r = 15.1$ Å, $\delta_f = 26.05$ Å $(\eta = 0.27)$, $k_{rf} = 0.931$ Å (curve 3); $\delta_r = 17.8$ Å, $\delta_f = 26.2$ Å $(\eta = 0.19)$, $k_{rf} = 0.915$ Å (curve 4); and $L_r = L_f = L_{rf} = 0.5$ μm. Taken from Ref. [64].

the semiconductor. This method was employed in Ref. [127], where the roughness mediated coupling of a P polarized wave incident on a surface of CdS to the surface exciton-polaritons was shown to manifest itself as resonant structures in the specular and the diffuse scattered light. Non-locality diminishes the size of these structures, and as usual, the Pekar ABC yields the largest nonlocal effect.

11 Microscopic theory of optical properties

Since the macroscopic approach of Pekar [4] to the optical properties of non-local excitonic semiconductors, several developments have emerged. Most of them introduce ABC's in order to determine the reflected and transmitted amplitudes of the electromagnetic fields. However, microscopic theories [4] which do not require the concept of ABC's have appeared recently in the literature.

Consider a two band system and let $\Psi(\vec{r}_e, \vec{r}_h)$ be the off-diagonal part of the density matrix in the position respresentation[128], commonly designated as the electron-hole transition amplitude. Let $\vec{d}(\vec{\rho})$ be the dipole matrix element between the two bands corresponding to a separation $\vec{\rho} = \vec{r}_e - \vec{r}_h$ between the electron (at $\vec{r}_e$) and the hole (at $\vec{r}_h$). Then, the polarization may be written as [4]

$$\vec{P}(\vec{r}) = \int d^3\rho \, \vec{d}^*(\vec{\rho}) \Psi(\vec{r}_e, \vec{r}_h), \tag{156}$$

where $\vec{r} = \vec{r}_e + \vec{r}_h$. The electron-hole transition amplitude obeys the two-particle effective mass Schrödinger equation[4]

$$\begin{aligned}\left[i\hbar \frac{\partial}{\partial t} - E_g + \frac{\hbar^2}{2m_e}\nabla_e^2 + \frac{\hbar^2}{2m_h}\nabla_h^2 + V_C \right] \Psi(\vec{r}_e, \vec{r}_h, t) = \\ -\vec{d}(\vec{\rho}) \cdot \vec{E}(\vec{r}, t),\end{aligned} \tag{157}$$

with E_g being the energy gap between valence and conduction bands, $-V_C$ the Coulomb interaction potential between electrons and holes, and $\vec{E}$ the external electric field. Although the equation for Ψ is translationally invariant, the boundary conditions ($\Psi = 0$ at the surface) introduce the geometry of the system into the problem. In a slab geometry where the surfaces are perpendicular to the z-direction and parallel to the $x-y$ plane, and the electromagnetic field propagates along the z-direction as a plane wave, it is useful to take the in-plane two dimensional Fourier transform of Ψ,

$$\Psi(\vec{K}; z_e, z_h) = \int d^2R e^{i\vec{K}\cdot\vec{R}} \Psi(\vec{r}_e, \vec{r}_h), \tag{158}$$

where we have written $\vec{r}_e = (\vec{R}_e, z_e)$, $\vec{r}_h = (\vec{R}_h, z_h)$, in terms of the projections parallel to the surface $\vec{R}_e$ and $\vec{R}_h$ and the normal to the surface components z_e, z_h, we defined $\vec{R} = \vec{R}_e - \vec{R}_h$, and $\vec{K}$ is the in-plane wavevector. In Eq. (158) it has further been assumed that the wavefunction is independent of the center of mass position along the $x - y$ plane, i.e., there is no center-of-mass motion along $x - y$. Because of the translational and rotational invariance of the $x-y$ plane, Ψ depends only on the modulus of $\vec{K}$. A two-dimensional Fourier transform of the Schrödinger equation yields

$$\begin{aligned}\left[E_g + i\gamma + \frac{\hbar^2}{2\mu}K^2 - \frac{\hbar^2}{2m_e}\frac{\partial^2}{\partial z_e^2} - \frac{\hbar^2}{2m_e}\frac{\partial^2}{\partial z_h^2}\right]\Psi(K;z_e,z_h) \qquad (159)\\ -\frac{1}{(2\pi)^2}\int_0^\infty dK'\,K' V_C(\vec{K},\vec{K}',|z_e-z_h|)\Psi(K';z_e,z_h)\\ -\vec{d}\cdot\vec{E}(z,t)\delta(z_e-z_h) = i\hbar\frac{\partial}{\partial t}\Psi(K;z_e,z_h),\end{aligned}$$

where μ is the effective mass. This equation has also been generalized for the case of anisotropic crystals subject to strain in Ref. [4]. The transformed Coulomb matrix element is

$$V_C(\vec{K},\vec{K}',|z_e-z_h|) = \frac{e^2}{2\varepsilon_\infty}\int_0^{2\pi} d\phi \frac{e^{-|\vec{K}-\vec{K}'||z_e-z_h|}}{|\vec{K}-\vec{K}'|}. \qquad (160)$$

Here, ϕ is the angle between $\vec{K}$ and $\vec{K}'$ so that $|\vec{K}-\vec{K}'| = \sqrt{K^2+(k')^2-KK'\cos\phi}$.

The electromagnetic field is determined by Maxwell equations, which for transverse fields travelling in the z direction yield [129]

$$\frac{\epsilon_\infty}{c}\frac{\partial}{\partial t}E(z,t) = -\frac{\partial}{\partial z}B(z,t) - \frac{4\pi}{c}\frac{\partial}{\partial t}P(z,t), \qquad (161)$$

$$\frac{1}{c}\frac{\partial}{\partial t}B(z,t) = -\frac{\partial}{\partial z}E(z,t). \qquad (162)$$

The electromagnetic field is coupled through the source term in Eq. (161) to the polarization given by Eq. (156). Since no analytical solution may be obtained for the coupled time dependent Schrödinger and Maxwell equations, numerical solutions have been pursued [4].

For comparative purposes we consider the phenomenological work of Ref. [130], which studies the optical response of surfaces and slabs in terms of the non-local bulk dielectric function, presumably without introducing ABC's. The reflection amplitude is calculated by solving the wave equation assuming the response within the slab is given by the same non-local response as that of a homogeneous infinite fictitious system with a singular source at the positions occupied by the surfaces of the slab, and whose strength is obtained by matching the resulting fields within the slab to the fields outside of the semiconductor by applying Maxwell's boundary conditions [86].

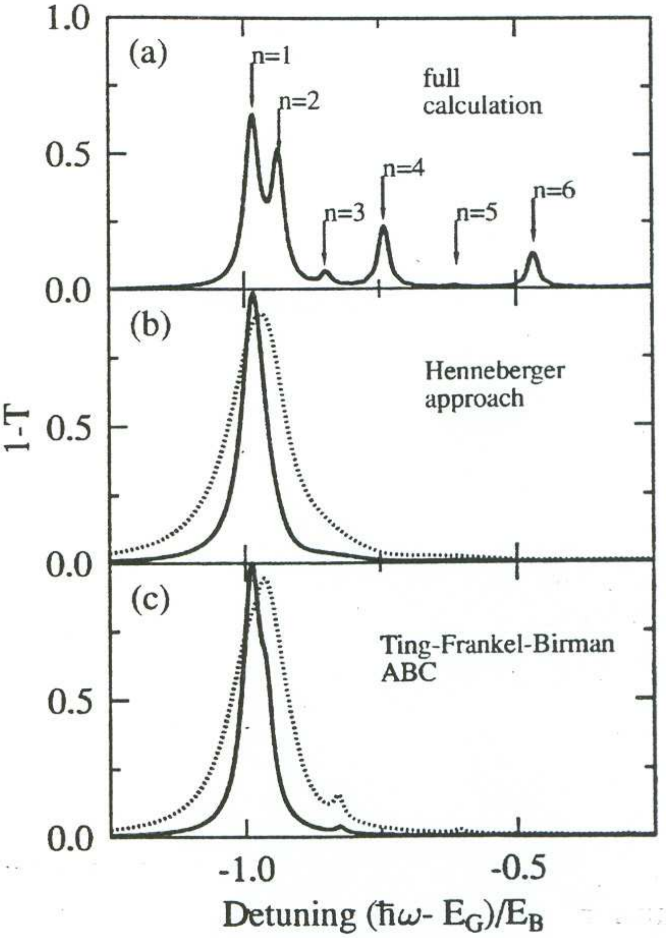

Fig. 28. Calculated transmission T for a GaAs film of thickness $L = 10a_B$ within a two band model. In panel (a) we present results of the calculations using the microscopic theory of Ref. [4], in panel (b) the calculations were done applying the phenomenological approach of Ref. [130], and in panel (c) the curves were obtained [131] using the Ting, Frankel, Birman ABC's. The detuning is relative to bulk semiconductor band-gap egergy E_g in units of the three dimensional exciton Rydberg energy E_B. Solid lines correspond to the dipole strength $d = 5$ Å of GaAs. The dotted lines in panels (b) and (c) correspond to a larger value $d = 10$ Å. Taken from Ref. [132].

In Fig. 28 we display the calculated transmission spectra of a GaAs film [132] calculated for a two band model with the microscopic and the phenomenological models described above, and with the ABC's of of Ting, Frankel, and Birman [85] (TFB). The microscopic calculation shows a series of peaks (labeled $n = 1, 2, \ldots$) corresponding to the quantization of the 1-s center-of-mass (COM) motion along z; for a sample of thickness L, the corresponding kinetic energies are approximately $K_n = \frac{\hbar}{2M}[\frac{\pi}{L}]n^2$. The phenomenological results show only the $n = 1$ peak, of which the TFB results show only a very small replica. On the other hand, a calculation employing Pekar's ABC's has s better agreement with the microscopic results [132].

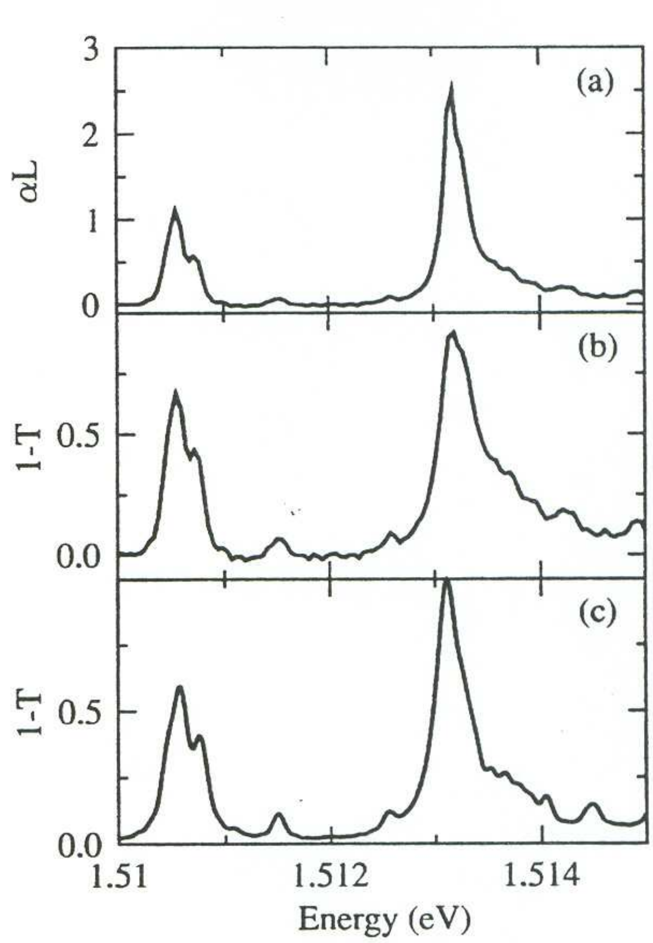

Fig. 29. Experimental absorption (a) and transmitance (b) of a high quality GaAs film of thickness 0.25 μm, and transmitance (c) calculated with the microscopic theory including light and heavy holes. Taken from Ref. [132].

Fig. 29 shows experimental results for GaAs films. The transmitance and absortance display non Lorentzian excitonic lines, with an asymmetric heavy hole (HH) transition at 1.5132 eV, and a light hole (LH) transition at 1.5105 eV that exhibits a fine structure: it is split into two components, and it is followed by secondary peaks of smaller magnitude at higher energy. Microscopic theoretical calculations [132] were performed including transitions from both light and heavy hole bands to the electron bands and employing parameters corresponding to GaAs. The calculated spectrum (Fig. 29) agrees remarkably well with experiment. The characteristic splitting of the light hole (LH) exciton resonance and the asymmetric line shape of the heavy hole (HH) exciton are well reproduced. These features are explained in terms of the interplay of polaritonic effects and quantization of the COM motion. Calculations reproduce also the secondary peaks. In contrast, when the approach of Ref. [130] is used, results show that neither reproduce the characteristic features of HH and LH excitonic line shapes nor the COM replicas. The spectrum calculated using the TFB formalism displays the characteristic double peak structure of the LH exciton line, but the HH line shape remains symmetrical and no COM replicas are obtained [132].

12 Concluding remarks

Our aim has been to bring forth the importance of the optical properties of excitonic semiconductors. We have provided a review of the excitations of exciton polaritons at surfaces, films, layered systems, superlattices, microcavities and small particles. In the first part of the report we have shown solutions of Maxwell wave equation within the nonlocal dielectric theory. Spatially dispersive or nonlocal media allow the propagation of excitonic waves beyond the usual light waves. Consequently, Maxwell boundary conditions are insufficient to determine all of the electromagnetic field amplitudes in abruptly terminated finite media, and additional boundary conditions (ABC's) are required to complement the electromagnetic boundary conditions and produced a closed system of equations. A generlized form of the ABC's has been used to demonstrate that the nonlocal theory together with an appropriate dead layer free of excitons colse to the surface may explain several reflectance experiments.

It is well established that the properties of semiconductor surfaces may be modified by intense illumination, electronic or ionic bombardment, heating, doping or applying a bias. As a consequence, excitons may be repelled by or trapped at the surface, as has been confirmed experimentally. The interaction of excitons with the surface may be described by a continuous potential. An approach beyond that of the classical nonlocal theory have been employed to solve the dynamical equations of motion for the exciton coupled to the electromagnetic equations. Theory for both semiinfinite media and films show that appropriate surface potential wells yield entrapped exciton states as experimentally observed. The optical contribution of entrapped states may be enhanced using novel surface sensitive spectroscopies beyond the usual reflectance spectroscopy, such as reflectometry at 45°. In the former technique damping effects preclude the observation of entrapped exciton states. In contrast, as discussed in Sec. 7, the latter spectroscopy is highly sensitive and may discern the entrapped states.

Studies of optical properties of excitonic films and multilayered systems have been done using a transfer matrix approach. The transfer matrix can be applied together with a multistep approach in the case where the interaction of excitons with the surfaces is modeled by continuous potentials. The transfer matrix was also used to the study of superlattices and microcavities. In particular, the method was proven to be useful to calculate collective normal modes in periodic superlattices.

Small particles with spherical and cylindrical geometries were studied by applying a non-local extension of Mie theory. The extinction coefficients display the excitonic resonances of the small particle.

Excitonic effects at non-ideal surfaces have been discussed in the context of rough surfaces. For small roughness with a large correlation length an extension of the Rayleigh-Fano method may be applied, expanding the fields to first order on the roughness height. The calculated scattering cross section was very successfully fitted to experimental spectra taken at different regions of a CdS surface, using only few parameters that characterize locally the surface roughness and the near surface defects.

Finally, we have included a microscopic theory of the calculations of the optical response. The theory was formulated within a linear response approach using a four band model. The transmissivity of very thin films displays a series of peaks at the excitonic transition and at frequencies that correspond to the quantization of the motion of the excitonic center of mass, and the theory has a very good agreement with experiment.

References

[1] J. Frenkel, Phys. Rev. 37 (1931) 17; J. Frenkel, Phys. Rev. 37 (1931) 1276; J. Frenkel, Physik. Z. Sowjetunion 9 (1936) 158.

[2] R. E. Peierls, Ann. Physik 13 (1936) 905.

[3] G. H. Wannier, Phys. Rev. 52 (1937) 191.

[4] S. I. Pekar, Zh. Eksp. Teor. Fiz. 33 (1957) 1022 [Sov. Phys.-JETP 6 (1958) 785]; 34 (1958) 1176 [7 (1958) 813]

[5] J. J. Hopfield and D. G. Thomas, Phys. Rev. 132 (1963) 563.

[6] P. Halevi and R. Fuchs, J. Phys. C: Solid State Phys. 17 (1984) 3869.

[7] P. Halevi, Editor, *Spatial Dispersion in Solids and Plasmas* (Electromagnetic Waves, Recent Developments in Research) Vol. 1, North Holland, Amsterdam 1992).

[8] S. I. Pekar, Sov. Phys. JETP 47 (1978) 762. [Z. I. Pekar, Zh. Eksp. Teor. 74 (1978) 1458].

[9] Fuchs Kliewer ABC.***

[10] P. R. Rimbey and G. D. Mahan, Solid State Commun. 15 (1974) 35.

[11] G. S. Agarwal, D. N. Pattanayak, and E. Wolf, Phys. Rev. Lett. 27 (1971) 1002 *** o 1022?.

[12] N. N. Akhmediev, M. I. Sazhin, and A. V. Sel'kin, Sov. Phys. JETP 69 (1989) 408, [Zh. Eksp. Teor. Fiz. 96 (1989) 720].

[13] A. A. Maradudin and D. L. Mills, Phys. Rev. B, 7 (1973) 2787.

[14] G. S. Agarwal, D. N. Pattanayak, and E. Wolf, Phys. Rev. 10 (1974) 1447.

[15] F. Evangelisti, A. Frova, and F. Patella, Phys. Rev. B 10 (1974) 4253.

[16] S. I. Pekar and M. I. Strashnikova, Sov. Phys. JETP, 41 (1975) 1024. [Zh. Eksp. Teor. Fiz. 68 (1975) 2047].

[17] J. Lagois and K. Hümmer, Phys. Stat. Sol. (b) 72 (1975) 393.

[18] B. Fischer and H. J. Queisser, Solid State Commun. 16 (1975) 1125.

[19] U. Ratsch, Phys. Stat. Sol. 69 (1975) 459.

[20] V. A. Kiselev, B. S. Rasbirin, and I. N. Uraltsev, Phys. Stat. Sol. 72 (1975) 161.

[21] F. Patella, E. Evangelisti, and M. Capizzi, Solid State Commun. 20 (1976) 23.

[22] D. L. Johnson and P. R. Rimbey, Phys. Rev. 14 (1976) 2398.

[23] F. Garía-Moliner and F. Flores, J. phys. 38 (1977) 851.

[24] I. Broser, M. Rosenzweig, R. Broser, M. Richard, and E. Birkicht, Phys. Stat. Sol. 90 (1978) 77.

[25] N. N. Akhmediev and V. V. Yatsishen, Solid State Commun. 27 (1978) 357.

[26] A. V. Komarov, S. M. Ryabchenko, and M. I. Strashnikova, Sov. Phys.JETP 47 (1978) 128.

[27] D. L. Johnson, Phys. Rev. B 18 (1978) 1942.

[28] L. Schultheis and J. Lagois, Solid State Commun., 44 (1982) 1557..

[29] P. Halevi and G. Hernández-Cocoletzi, Phys. Rev. Lett. 48 (1982) 1500.

[30] R. Ruppin and R. Englmann, Phys. Rev. Lett. 53 (1984) 1688.

[31] R.Ruppin, Phys. Rev. B, 29 (1984) 2232.

[32] P. Halevi and R. Fuchs, J. Phys. C: Solid State Phys. 17 (1984) 3889.

[33] P. Halevi, G. Hernández-Cocoletzi, and F. Ramos, in *Excitons in Confined Systems, Proceedings of the International Meeting*, Editors: R. Del Sole, A. D'Andrea, and A. Lapiccirella, (1987) 35.

[34] P. Halevi, G. Hernández-Cocoletzi, and J. A. Gaspar-Armenta, Thin Solid Films, 89 (1982) 271.

[35] V. M. Agranovich, V. E. Kravtsov, T. A. Leskova, A. G. Mal'shukov, G. Hernández-Cocoletzi, and A. A. Maradudin, Phys. Rev. B, 29 (1984) 976.

[36] V. M. Agranovich and V. E. Kravtsov, Solid State Commun. 55 (1985) 85

[37] J. A. Gaspar-Armenta and P. Halevi, Rev. Mex. Fis., 33 (1988) 599.

[38] G. H. Cocoletzi and W. L. Mochán, Phys. Rev. B, 39 (1989) 8403.

[39] G. H. Cocoletzi, A. Ramírez-perucho, and W. L. Mochán, Phys. Rev. B, 44 (1991) 11514.

[40] L. C. Andreani. Phys. Lett A 192 (1994) 99.

[41] B. Flores-Desirena, F. Pérez-Rodriguez, and P. Halevi, Phys. Rev. B, 50 (1994) 5404.

[42] M. Palomino-Ovando, P. H. Hernández, and G. H. Cocoletzi, Solid State Commun. 100 (1996) 111.

[43] H. A. Coyotécatl and G. H. Cocoletzi, J. Phys.: Condens. Matter 10 (1998) 79.

[44] A. Silva-Castillo and F. Pérez-Rodríguez, J. App. Phys. 90 (2001) 3662.

[45] B. Flores-Desirena and F. Pérez-Rodríguez, Appl. Surf. Sci. ??? (2003) ????

[46] B. Flores-Desirena, A. Silva-Castillo, and F. Pérez-Rodríguez, J. Appl. Phys. 93 (2003) ???.

[47] A. Tredicucci, Y. Chen, F. Bassani, Phys. Rev. B, 47 (1993) 10348.

[48] Y. Chen, A. Tredicucci and F. Bassani, Phys. Rev. B, 52 (1995) 1800.

[49] A. Tredicucci, Y. Chen, V. Pellegrini, M. Börger, L. Sorba, F. Beltram, and F. Bassani, Phys. Rev. Lett. 75 (1995) 3906.

[50] M. R. Vladimirova, A. V. Kavokin, and M. A. Kaliteevski, Phys. Rev. B, 54 (1996) 14566.

[51] J. H. Dickerson, E. E. Mendez, A. A. Allerman, S. Manotas, F. Agulló-Rueda, and C. Pecharromán, Phys. Rev. B, 64 (2001) 155302.

[52] R. Houdré, R. P. Stanley, U. Oesterle, M. Ilegems, and C. Weisbuch, Phys. Rev. B, 49 (1994) 16761.

[53] A. Tredicucci, Y. Chen, V. Pellegrini, and C. Deparis, Appl. Phys. Lett. 66 (1995) 2388.

[54] C. Pecharromán, J. K. Son, I. W. Tao, and E. E. Mendez, Phys. Rev. B 64 (2001) 245331.

[55] G. Malpuech, A. Kavokin, A. Di Carlo, and J. J. Baumberg, Phys. Rev. B, 65 (2002) 153310.

[56] R. Huang, Y. Yamamoto, R. André, J. Bleuse, M. Muller, and H. Ulmer-Tuffigo, Phys. Rev. B, 65 (2002) 165314.

[57] B. Flores-Desirena, A. Silva-Castillo, and F. Pérez-Rodríguez, J. Appl. Phys., 93 (2003) 3308.

[58] J. Lagois and B. Fischer Phys. Rev. Lett. 36 (1976) 680.

[59] K. V. Sobha and G. S. Agarwal, Solid State Commun., 43 (1982) 99.

[60] A. B. Petsov and A. V. Sel'kin, Sov. Phys. Solid State 26 (1984) 1741 (Fiz. Tverd. Tela 26 (1984) 2875).

[61] V. A. Kosobukin and A. V. Sel'kin, JETP Lett. 44 (1986) 484.

[62] V. A. Kosobukin and A. V. Sel'kin, Solid State Commun. 66 (1988) 313.

[63] V. A. Kosobukin, M. I. Sazhin and A. V. Sel'kin, Solid State Commun. 94 (1995) 947.

[64] J. Madrigal-Melchor, H. Azucena-Coyotécatl, A. Silva-Castillo, and F. Pérez-Rodríguez, Phys. Rev. B, 61 (2000) 15993.

[65] D. D. Sell, S. E. Stokowski, R. Dingle, and J. V. DiLorenzo, Phys. Rev. B, 7 (1973) 4568.

[66] T. Mozume and J. Kasai, J. Appl. Phys. 95 (2004) 1050.

[67] W. Brenig, R. Zeyher, J. L. Birman, Phys. Rev. B, 6 (1972) 4617.

[68] G. Winterling and E. Koteles, Solid State Commun., 23 (1977) 95.

[69] R. G. Ulbrich and C. Weisbuch, Phys. Rev. Lett. 38 (1977) 865.

[70] G. Winterling, E. S. Koteles, and M. Cardona, Phys. Rev. Lett. 39 (1977) 1286.

[71] P. Y. Yu, Solid State Commun., 32 (1979) 29.

[72] N. Allen and E. O. Kane, Solid State Commun. 28 (1978) 965.

[73] P. Y. Yu and F. Evangelisti, Phys. Rev. Lett.

[74] D. R. Tilley, J. Phys. C: Solid St. Phys. 13 (1980) 781.

[75] A. B. Petsov, S. A. Permogorov, and A. V. Sel'kin, JETP Lett. 33 (1981) 402.

[76] E. A. Muljarov and R. Zimmermann, Phys. Rev. B 66 (2002) 235319.

[77] M. Rohlfing and S. G. Louie, Phys. Rev. B 62 (2000) 4927.

[78] L. Hedin, Phys. Rev. 139 (1965) A796.

[79] B. Arnaud and M. Alouani, Phys. Rev. B 63 (2001) 085208.

[80] A. Marini, R. Del Sole, and A. Rubio, Phys. Rev. Lett. 91 (2003) 256402.

[81] R. E. Peierls, Ann. Physik 13 (1936) 905.

[82] Robert S. Knox, *Theory of Excitons*, Supplement 5, Solid State Physics, (Academic Press, New York, 1963).

[83] Peter Y. Yu and Manuel Cardona, *Fundamentals of Semiconductors: Physics and Materials Properties* (second edition) (Springer, Berlin, 1999) p. 272.

[84] Ref. [7], Chapter 6.

[85] C. S. Ting, M. J. Frankel, and J. L. Birman, Solid State Commun. 17 (1975) 1285.

[86] K. L. Kliewer and R. Fuchs, Phys. Rev 172 (1968) 607.

[87] M. Cardona, Am. J. Phys. 39 (1971) 1277.

[88] B. B. Dasgupta and A. Bagchi, Phys. Rev. B 19 (1979) 4935.

[89] R. Fuchs and P. Halevi, in *Electromagnetic Waves, Recent Developments in Research, Vol. 1, Spatial Dispersion in Solids and Plasmas* ed. by P. Halevi (North Holland, New York, 1992), p. 1.

[90] A. Otto, Z. Phys. 216 (1968) 398.

[91] E. Kretschmann and H. Raether, Z. Naturforsch. A 23 (1968) 2135.

[92] E. Kretschmann, Z. Phys., 241 (1971) 313.

[93] J. Lagois, Solid State Commun. 39, (1981) 563.

[94] I. Balslev, Phys. Rev B 23 (1981) 3977.

[95] V. I. Sugakov and V. N. Khotyaintsev, Zh. Eksp. Teor. Fiz. 70 (1976) 1566 (Engl. Transl., Sov. Phys.-JETP 43 (1976) 817).

[96] M. F. Deigen, and M. D. Glinchuk, Fiz. Tverd. Tela 5 (1963) 3250. [Sov. Phys.-Solid State 5 (1064) 2377].

[97] S. Sakoda, J. Phys. Soc. Jpn. 40 (1976) 152.

[98] I. Balslev, Phys. Status Solidi B 88 (1978) 155

[99] L. Schultheis and I. Balslev, Phys. Rev. B 28 (1983) 2292.

[100] R. Ruppin and R. Engleman, Phys. Rev. Lett. 53 (1984) 1688; R. Ruppin, Phys. Rev. B 29 (1984) 2232.

[101] R. Zeyher, J. L. Birman, W. Brenig, Phys. Rev. B 6 (1972) 4613.

[102] K. Cho and H. Ishihara, J. Phys. Soc. Jpn. 59 (1990) 754.

[103] L. Bleckmann, O.Hunderi, W. Richter, and E. Wold, Surf. Sci. 351 (1996) 277.

[104] J. Madrigal-Melchor, F. Pérez-Rodríguez, J.A. Maytorena, and W.L. Mochán, Appl. Phys. Lett. 71 (1997) 69.

[105] A. S. Batyrev, N. V. Karasenko, and A. V. Sel'kin, Fiz. Tverd. Tela (St. Petersburg) 35 (1993 3099 [Phys. Solid State 35 (1993) 1525].

[106] F. Pérez-Rodríguez and P. Halevi, Phys. Rev. B 48 (1992) 2016.

[107] F. Pérez-Rodríguez and P. Halevi, Phys. Rev. B 45 (1992) 11854.

[108] H. Azucena-Coyotécatl, N. R. Grigorieva, B. A. Kazennov, J. Madrigal-Melchor, B. V. Novikov, F. Pérez-Rodríguez, and A. V. Sel'kin, Thin Solid Films 373 (2000) 227.

[109] F. Pérez-Rodríguez and P. Halevi, Phys. Rev. B 53 (1996) 10086.

[110] V. A. Kiselev, Solid State Commun. 43 (1982) 471.

[111] Eugene Hecht, *Optics* (Addison-Wesley, Reading, Massachusetts, 1990) Sec. 9.7.

[112] H. A. Coyotécatl, M. Palomino-Ovando, and G. H. Cocoletzi, Superlatt. and Microstruct. 26 (1999) 35.

[113] Y. Chen, A. Tredicucci, and F. Bassani, Phys. Rev. B 52 (1995) 1800.

[114] A. Fainstein, B. Jusserand, P. Senellart, J. Bloch, V. Thierry-Mieg, and R. Planel, Phys. Rev. B 62 (2000) 8199.

[115] J. Tignon, R. Ferreira, J. Wainstain, C. Delalande, P. Voisin, M. Voos, R. Houdré, U. Oesterle, and R. P. Stanley, Phys. Rev. B 56 (1997) 4068; J. Tignon, P. Voisin, C. Delalande, M. Voos, R. Houdré, U. Oesterle, and R. P. Stanley, Phys. Rev. Lett. 74 (1995) 3967.

[116] A. V. Kavokin, Phys. Rev. B 57 (1998) 3757.

[117] Stratton, Cap. 4***

[118] R. Ruppin, J. Opt. Soc. Am. 71 (1981) 755.

[119] R. Ruppin, J. Phys. Chem. Solids 50 (1989) 877.

[120] A. I. Ekimov, Al. L. Efros, and A. A. Onuschchenko, Solid State Commun. 56 (1985) 921.

[121] A. I. Ekimov, and A. A. Onushchenko, Soviet Phys. Semicond. 16 (1982) 775.

[122] T. Itoh, Y. Iwabuchi, and M. Kataoka, Phys. Status Solidi (b) 145 (1988) 567.

[123] B. G. Potter, and J. H. Simmons, Phys Rev. B, 37 (1988) 10838.

[124] M. A. Kaliteevski, S. Brand, R. A. Abram, V. V. Nikolaev, M. V. Maximov, C. M. Sotomayor Torres, and A. V. Kavokin, Phys. Rev. B 64 (2001) 115305.

[125] R. Ruppin, J. Opt. Soc. Am. B 6 (1989) 1559.

[126] N. Atenco-Analco, F. Pérez-Rodríguez, and J. Madrigal- Melchor, Rev. Mex. Fis. 48 (2002) 197.

[127] G. H. Cocoletzi, and S. Wang, Phys. Rev. B 48 (1993) 17413.

[128] I. Balslev, R. Zimmermann, and A. Stahl, Phys. Rev. B **40** (1989) 4095.

[129] The definition of $B(z,t)$ before Eq. (6) of Ref. [132] is wrong, as it is inconsistent with Eqs. (6) and (7) of that Ref.

[130] K. Henneberger, Phys. Rev. Lett. 80 (1998) 2889.

[131] M. Kira et al., Phys. Rev. B 52 (1995) 10972.

[132] H. C. Schneider, F. Jahnke, S. W. Koch, J. Tignon, T. Hasche, and D. S. Chemla, Phys. Rev. B 63 (2001) 045202.